Radiotherapy Treatment of Malignant Pleural Mesothelioma after Extrapleural Pneumonectomy

Dissertation
zur
Erlangung der naturwissenschaftlichen Doktorwürde
(Dr. sc. nat.)

vorgelegt der
Mathematisch-naturwissenschaftlichen Fakultät
der
Universität Zürich

von

Jérôme Krayenbühl
von St-Saphorin-sur-Morges (VD)

Promotionskomitee

Prof. Dr. M. Pruschy (Vorsitz, Leitung der Dissertation),
Prof. Dr. I. Ciernik, Prof. Dr. M. Hengartner, Dr. S. Klöck,

Zürich, 2014

Contents

Abstract

Malignant pleural mesothelioma (MPM) is a form of neoplasia of the cells covering the surface of the pleural cavity. The only confirmed etiological factor is asbestos. Treatment of mesothelioma is generally based on surgery, chemotherapy and/or radiotherapy.

In the last decade, different radiotherapy techniques have become available for the treatment of MPM. 3D-conformal radiotherapy (3DCRT) using photons and electrons was the main radiotherapy treatment available until the beginning of 2000. Since then, intensity modulated radiotherapy (IMRT) followed by volumetric modulated arc therapy (VMAT) and proton therapy (PT) have become available. The implementation of these new techniques for MPM is very challenging due to different reasons. First, the size of the volume to treat is usually very large, and may go up to six liters. Second, the doses to be delivered to the target are high and may easily exceed 50 Gy. Third, the target lies in close proximity to vital and sensitive organs at risk such as the heart, kidney, liver, lung and spinal cord. Fourth, changes of the patient's anatomy and morphology may occur during radiotherapy leading to a modification of the dose distribution.

In this work, I investigated these new approaches for the treatment of MPM with radiotherapy. In the first step, I did a plan optimization for IMRT by looking at the optimal number of beams, field size and beam direction needed to have the best dose distribution. In a second step, I compared the results based on the clinical outcome, such as local control, disease free survival, overall survival and dose distribution to the standard treatment used, 3DCRT. I showed that IMRT improved the dose conformity but the overall complication rates remained high. I saw major complications post-radiotherapy for 22 % of the IMRT patients. In order to improve treatment quality, I evaluated other treatment techniques, such as VMAT or PT. The results showed that VMAT as well as PT were both able to reduce the dose to healthy tissue whilst maintaining high dose conformity when compared to 3DCRT and IMRT.

I demonstrated that IMRT, VMAT and PT were able to achieve higher tumor conformity which resulted in better tumor control rates compared to 3DCRT. Technically however, I observed that tumor conformity could be affected by changes of the patient's anatomy and morphology during protracted fractionated RT. This was especially the case for MPM patients with

large air cavities in the hemithorax after removal of the lung. During radiotherapy, I showed that the volume of the cavity will decrease progressively over time in an unpredictable way. This cavity will disappear within days to months and thus will affect surrounding anatomy and modify the dose distribution. This study demonstrated that these modifications were more or less pronounced depending on the radiotherapy technique used. Modulated photon radiotherapy techniques appeared to be robust when small anatomical changes occurred, which was not the case for PT. For PT small changes of tissue density resulted in drastic dose distribution changes. Therefore adaptive radiotherapy will be required in order to take into account anatomy modifications. In order to optimize this process, image registration will be required in order to propagate the structures from one CT to an-other. In order to perform this step automatically, a colaboration with the Swiss Federal Institute of Technology Zurich was done to developp a new non-rigid automatic registration. Therefore, we compared inter- and intraobserver variability to the automatic resigstration. This study showed that inter- and intraobserver deviations were greater or similar to the variance of the population formed by deviations in contouring for the elastic region in a very large portion of the target volume. Therefore, this non rigid registration could be a big assess for adaptive RT.

In conclusion, I showed that modulated RT was able to reduce the treatment toxicity in comparison to 3DCRT and enhanced tumor control. The dose distribution was further improved with VMAT. Nevertheless, no difference was observed in respect to overall survival due to the high rate of distant metastasis. PT was able to further reduce the dose to all organs at risks in comparison to any photon techniques. However, PT was the most sensitive treatment to modifications of the anatomy, emphasizing the need for adaptive RT and replanning. A non-rigid registration algorithm was also developped. Using this tool, efficient adaptive radiotherapy can be realized by propagating structures of interest between datasets.

Zusammenfassung

Ein malignes Pleuramesotheliom (MPM) ist eine Form von Neoplasie der Zellen, welche die Oberfläche der Pleura bedeckt. Eine häufige Ursache hierfür ist Asbest. Die Behandlung von Mesotheliomen basiert in der Regel auf Chirurgie, Chemotherapie und/oder Strahlentherapie.

Innerhalb der letzten zehn Jahre wurden verschiedene Strahlentherapie-Techniken für die Behandlung von MPM verfügbar. Bis ins Jahr 2000 waren 3D-konformale Strahlentherapie (3DCRT) Techniken mit Photonen und Elektronen die weitverbreitetste Behandlungsmethode in der Strahlentherapie. Mittlerweile sind weitere Techniken wie intensitätsmodulierte Strahlentherapie (IMRT), volumen-intensitätsmodulierte Arc-Therapie (VMAT) und Protonentherapie (PT) verfügbar geworden. Die Umsetzung dieser neuen Techniken ist jedoch auf Grund von verschiedenen Gründen sehr anspruchsvoll. Erstens ist die Grösse des zu behandelten Volumens in der Regel sehr gross und kann bis zu sechs Liter fassen. Zweitens sind die an das Zielvolumen verschriebenen Dosen hoch und können leicht mehr als 50 Gy betragen. Drittens befindet sich das Zeilvolumen in der Nähe essentieller und empfindlicher Organe wie dem Herzen, der Niere, der Leber, der Lunge und dem Rückenmark. Viertens können Veränderungen der Anatomie und Morphologie des Patienten während der Strahlentherapie auftreten, welche zu einer modifizierten Dosisverteilung führen.

In dieser Arbeit, habe ich diese neue Strahlentherapie-Techniken für MPM Patienten evaluiert. Im ersten schritt habe ich die Bestrahlung Geometrie optimiert für IMRT.

Dann habe ich die IMRT und die 3DCRT verglichen im Bezug auf deren klinische Ergebnisse, wie z.B. lokale Kontrolle, krankheitsfreies Überleben, Gesamtüberleben und Dosisverteilung. Ich habe gezeigt, dass die Dosiskonformität durch die IMRT verbessert werden konnte, allerdings blieb die gesamte Komplikationsrate hoch. Schwerwiegende Post-Radiotherapeutische Komplikationen wurden in 22 % IMRT Patienten beobachtet. Um die Behandlungsqualität zu verbessern haben ich andere Behandlungstechniken, wie VMAT oder PT ausgewertet. Im Vergleich zu 3DCRT und IMRT waren VMAT sowie PT beide in der Lage die Dosis auf gesundes Gewebe zu reduzieren und dabei die hohe Dosiskonformität beizubehalten.

Ich habe gezeigt, dass IMRT, VMAT und PT in der Lage waren bessere Tumor-Konformität zu erreichen, was zu besseren Tumorkontrollraten geführt hat im Vergleich zu 3DCRT. Technisch konnte ich jedoch

beobachten, dass die Tumor-Konformität bei stark-fraktionierter Strahlentherapie durch Veränderungen der Anatomie und Morphologie des Patienten beeinflusst wird. Dies war insbesondere für MPM Patienten mit grossem Hohlraum in der Hämithorax, nach Entfernung der Lunge, der Fall. Das Volumen des Hohlraums verkleinert sich während der Strahlentherapie in unvorhersehbarer Weise, sodass der Hohlraum nach wenigen Tagen bis hin zu Monaten verwindet. Dies beeinflusst die umliegende Anatomie und verändert die Dosisverteilung. Ich zeigte, dass die Ausprägung der Veränderungen von der verwendeten Strahlentherapietechnik abhängt. Die modulierten Photonenstrahlenbehandlungstechniken scheinen gegenüber kleinen anatomischen Veränderungen robust zu sein, was jedoch für die PT nicht der Fall war. Bei der PT führten kleine Veränderungen von Gewebedichten zu drastischen Veränderungen in der Dosisverteilung. Wenn die Vorteile der Protonenstrahlgeometrie Toxizität zu minimieren ausgenutzt werden sollen, wird deshalb eine adaptive Strahlentherapie benötigt, um anatomische Veränderungen zu berücksichtigen. Um diesen Prozess zu optimieren ist eine Bildregistrierung erforderlich, damit die Strukturen von einem CT zu einem anderen übertragen werden können. Hierfür habe ich einen neuen nicht-starren Algorithmus evaluiert.

Zusammenfassend habe ich gezeigt, dass die IMRT im Vergleich zur 3DCRT in der Lage ist die Behandlungstoxizität zu reduzieren. Ausserdem konnte eine bessere Tumorkontrolle festgestellt werden. Die Dosisverteilung konnte durch VMAT weiter verbessert werden und PT konnte gegenüber allen Photonen Techniken die Dosis umliegender Risikoorgane weiter reduzieren. Die Behandlung mit PT reagierte allerdings am empfindlichsten auf Veränderungen der Anatomie, was die Notwendigkeit für adaptive RT und Umplanung verdeutlicht. Ein nicht-starrer Registrierung Algorithmus wurde ebenfalls analysiert. Mit diesem Tool kann eine effiziente adaptive Strahlentherapie durch die Weitergabe von Strukturen von Interesse realisiert werden.

Résumé

Le cancer du mésothéliome se développe dans la majorité des cas dans la région de la plévre. L'apparition du mésothéliome survient généralement après exposition à l'amiante. Ces mésothéliomes peuvent être opérés, traités par la chémotherapie ou la radiothérapie. La radiotherapie conformationnelle (3DCRT) était le principale traitement utilisant des électrons et photons pour les mésothéliomes jusqu'au début des années 2000. Durant la dernière décennie de nouvelles techniques en radiothérapie ont vu le jour pour le traitement du mésothéliome, tel que la radiothérapie conformationnelle avec modulation de l'intensité (IMRT), arc thérapie avec modulation de l'intensité (VMAT) et la protonthérapie (PT).

L'implémentation de ces nouvelles techniques n'est pas aisée pour les raisons suivantes: la taille de la région à traiter est très grande, jusqu'à 6 litres, la dose à délivrer est élevée, dépassant les 50 Gy, les nombreux organes à proximité de la tumeur et les modifications d'anatomie pouvant survenir durant le traitement.

Dans ce travail, j'ai évalué de nouvelles approches pour la radiotherapie de patients ayant un cancer du mésothéliome. Lors de la premiére étape, j'ai optimisé la géométrie du traitement avec IMRT afin d'optenir la meilleure distribution de dose possible. Dans un second temps, j'ai comparé les résultats basés sur la distribution de la dose, la survie sans maladie et sans progression de la tumeur ainsi que la survie globale à la thérapie standard, 3DCRT. J'ai pu montré que la conformité ainsi que l'homogénéité de la dose des patients traité avec IMRT étaient meilleures. Néanmoins, un taux de complications élevé suite à la radiation avec 3DCRT et IMRT à été observé. De ce fait, j'ai évalué deux autres techniques, VMAT et PT. Ces deux techniques ont permis d'améliorer la distribution de dose en comparaison à IMRT et 3DCRT en diminuant la dose aux tissus sains.

Ces techniques de radiothérapies sont capables de produire une grande conformité de dose autour de la région cible. Par contre, j'ai démontré que cette conformité sera affectée par une modification de l'anatomie du patient. Cela est spécialement le cas du traitement des mésothéliomes où une grande cavité d'air peut être présente après opération. Cette cavité d'air va disparaitre en quelques jours à quelques mois modifiant l'anatomie du patient. J'ai obervé que l'impact sur la distribution de dose sera plus ou moins importante suivant la technique utilisée. En effet, la conformité de la dose sera

modifiée dans une moindre mesure avec IMRT et VMAT, alors que la distribution de dose sera drastiquement modifiée avec PT impliquant la nécessité de faire de la radiothérapie adaptative. Afin d'optimiser le processus de la radiothérapie adaptive, il est nécessaire de pouvoir aligner les images. Pour cela, une colaboration avec l'Ecole Polythechnique Fédérale de Zurich a été faite afin de développer un algorithme utilisant une déformation non-rigide. Ce nouvel algorithme donne des résultats similaire à la ségmentation manuelle, avec l'avantage d'être automatisé.

En conclusion, j'ai montré que les traitements à modulation d'intensité permettent de réduire la toxicité du traitement et d'améliorer le contrôle de la tumeur en comparaison à 3DCRT. L'amélioration du contrôle de la tumeur n'affecte pas la survie globale du au nombre élevé de métastases se développant après traitement. Une légére amélioration de la distribution de dose est observée lorsque VMAT est utilisé au lieu de IMRT. PT est capable de réduire drastiquement la dose à tous les tissus sains par rapport aux autres techniques. Par contre, PT est la technique la plus affectée par une modification de l'anatomie impliquant la nécessité de faire de la radiotherapy adaptive. Pour cela, un algorithme a été développé qui permet la propagation automatique de structures d'un CT à un autre CT.

1 Introduction

1.1 Mesothelioma cancers

Malignant mesothelioma is a form of cancer that occurs in the layer of cells lining the mesothelium. The mesothelium is a membrane that lines several cavities including the pleura (thoracic cavity), see Fig. 1.1, peritoneum (gap between the abdominal wall and abdominal organs) and the pericardium (lines the heart and the proximal ends of the root of the pulmonary artery, aorta and vena cava).

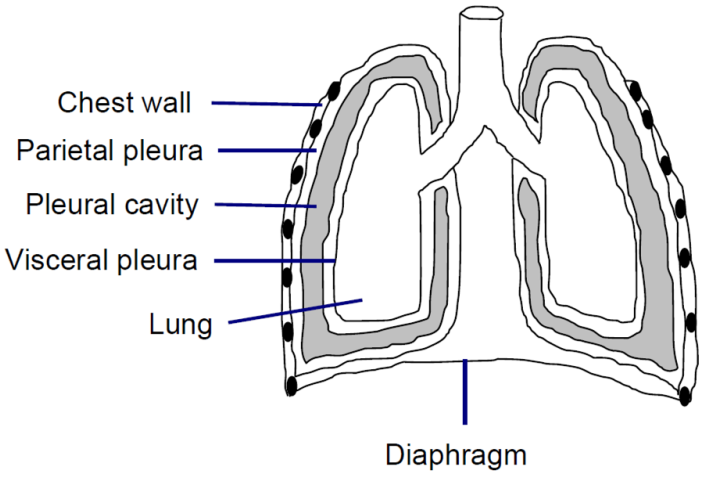

Figure 1.1: Pleural mesothelioma primary location is the pleural cavity. The pleural cavity is the gap between the parietal (outer) pleura attached to the chest wall and the visceral pleura covering the lung.

The primary location of malignant mesothelioma is in most of the cases the pleural region but can also occur more rarely in the peritoneal region. Malignant pleural mesotheliomas are generally confined to the pleural cavity which is located between the parietal pleura and the visceral pleura, see Fig. 1.1. After a period of time, typically years, the tumor metastasizes and progresses through the pleural space, including the chest wall, mediastinum, diaphragmatic and pericardial surfaces, peritoneum and lymph nodes [1].

1.2 Epidemiology of malignant pleural mesothelioma

In at least 80 % of all documented cases, malignant mesothelioma occurs after exposure to asbestos [2]. Chrysotile, amosite, and crocidolite are the three main types of asbestos that are correlated with the apparition of MPM. The risk of developing MPM as the result of occupational exposure to asbestos varies in accordance with the type of asbestos exposed to. The risk is 500 and 100 times more likely when exposed to crocidolite and amosite respectively than to chrysotile. [3]. Asbestos is considered the main cause of MPM however around 20 % of mesothelioma patients present no history of asbestos exposure [4]. However, in individual cases, it is often not clear if an exposing period was masked by the long latency time. Beside asbestos, other factors may contribute to mesothelioma. This is the case for young children with no exposure to asbestos who developed mesothelioma [5].

Since the 1950's, the number of patients diagnosed with MPM has been growing. The reason has been linked to the escalation of industrial applications of asbestos in the Western countries until the 1990's. Furthermore, better diagnostic techniques could also account to some extent for the increasing incidence of MPM. Taking into account a latency period of 30 years or more and the fact that asbestos has been banned in the late 1980's in Europe, a peak of incidence with around 9000 victims per year should be reached in Europe in 2020 [5].

The incidence rate increases with age. Indeed, for men aged between 0 and 54 years, the incidence rate was 0.1 cases per million between 2008 and 2009 in the United States [6]. The incidence rate increases to 2.3 for men aged between 55 and 64 years and to 7.2 for men aged beween 65 and 74. This goes on to increase to 15.0 for men aged between 75 and 84 years and to 21.7 for men above 85 years. For women, the same increase is observed. The incidence rate goes from 0.1 cases per million for women under 55 years to 3.0 for women above 85 years. In Europe, the incidence rates are similar to the United States , see Fig. 1.2. The difference of incidence rate with age comes mostly from the latency period and the decrease of use of asbestos in the past 30 years.

The higher incidence rate for men indicates that occupational exposure to asbestos is more relevant than environmental exposure [5]. Approximately 10 % of the people which have been exposed to a significant amount of asbestos at work will develop mesothelioma. Nevertheless, environmental exposure to asbestos has also been reported to have a direct impact on the rate of patients developing mesothelioma. Indeed, environmental exposure has also

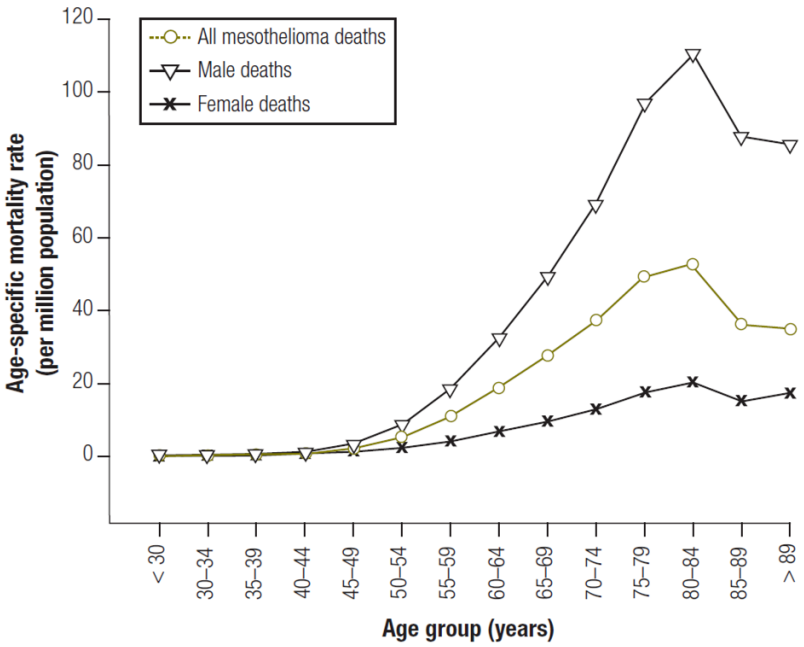

Figure 1.2: Age-specific mesothelioma mortality rate by age group and gender between 1994 and 2008 worldwide [7].

been observed in villages in Turkey where natural asbestos was present. In these villages, the mortality rate increased up to 700 cases per 100 000 people annually [8]. This was the cause of 44.5 % of all the deaths in these villages.

After banning asbestos from various applications in construction, a new category of cancerogenes rises: in the past years, nanotubes have been increasingly used in different applications. There are thousands of new materials which contain carbon nanotubes such as textiles, sports equipment and electronics. The dimension resemblance between nanotubes and asbestos has raised the question of the potential health hazards of nanotubes. Studies performed on mice with an intraperitoneal injection of carbon nanotubes resulted in inflammations and lesions within the peritoneal region. These results are similar to seen after asbestos exposure [9]. Therefore, studies hypothesize that long term response after exposure to nanotubes could lead to mesothelial injury which has been linked to the first stage of mesothelioma. Therefore, special care has to be taken with the use and fabrication of nan-

otubes devices. Otherwise a new peak of mesothelioma could appear in 30-40 years.

1.3 Asbestos

Asbestos is a term for six mineral fibers used in industry for their physical properties. All asbestos entities are formed by long fibrous crystals and are classified into two groups: the ***amphiboles*** (amosite, crocidolite, anthophyllite and actinolite) and the ***serpentine*** (chrysotile) group. The amphiboles group of minerals are formed by double chain of SiO_4, and in most cases also contains iron and/or magnesium. The serpentine group are formed by ((Mg, Fe)$_3$Si$_2$O$_5$(OH)$_4$) and can contain small amounts of other elements such as chromium, cobalt, manganese or nickel. The chrysotile accounts for 95 % of asbestos used [10].

Figure 1.3: Asbestos fibers taken with a scanning electron microscope. The size of the breathable asbestos fibers are up to 20 μm [11].

The asbestos industry began in the mid 19th century when anthophyllite was mined for use as asbestos insulation [12]. Later on, in the mid 20th century, it was used in concrete, cement pipe, heat insulation, electric wire insulation, clothes (fireproof coating), mastics, boilers and cigarette filters

[13]. Asbestos was used mainly for its inexpensive cost and for its physical properties such as fire resistance, good insulating qualities and flexibility. The mining of asbestos in the United States increased over the 20th century and reached a peak in the 1960s. At this time 136'000 tons were being produced though this was ceased in the 1990s. However worldwide asbestos production continues today with 2 million tons produced in 2012 and 200 million tons available world wide [14].

In 1960, Wagner *et al.* were the first to show a correlation between exposure to asbestos and the development of pleural mesothelioma [2]. However, it was only in the late 1980's that western industrialized countries started to ban asbestos (1989 in Switzerland, 1993 in Germany, 1997 in France). This is still not the case for developing countries, such as China, India and Russia where asbestos is commonly used.

Asbestos was a common construction material used in the last century. It now requires specialized removal at great expense which is usually left until a major renovation or demolition is performed. When buildings containing asbestos are demolished, asbestos fibers can be released in the air. This was the case when the Twin Towers collapsed in 2001 releasing 1000 - 2000 tons of asbestos in the air. The volunteers helping at ground zero as well as the people caught in the cloud released by the collapse of the towers were contaminated by asbestos and heavy metals. A survey of volunteers in 2008 reported respiratory problems in 62 % of people [15].

When asbestos is inhaled, most of the fibers are trapped in the lung and the pleural region causing irritation and inflammation. The steps that lead to mesothelioma are currently unclear. Nevertheless, current research showed that many types of DNA-interacting proteins have an affinity for asbestos [16]. These interactions may cause disturbances in the cell division and cause chromosomal aberration leading to mesothelioma. They suspect that asbestos will act as a catalyst where oxidative modification will occur. Proteins and DNA, inter alia, will be oxidatively modified by these mechanisms [16]. These modifications are linked to carcingenesis.

1.4 Symptoms of malignant pleural mesothelioma

The early symptoms of mesothelioma are similar to those of other illnesses such as the common cold or pneumonia. Therefore, the correct diagnosis of mesothelioma can be difficult and take weeks to months. A key element in the diagnosis is the history of exposure to asbestos some 20 to 50 years

prior to symptoms. Common symptoms include respiratory problems such as a reduction of the respiratory function or shortness of breath, cough, pain in the chest and fatigue can also be observed. For peritoneal mesothelioma additional symptoms can be observed such as weight loss and abdominal swelling. The radiological diagnosis of mesothelioma is generally performed with computed tomography and/or with magnetic resonance imaging. A biopsy sample establishes the definitive diagnosis.

1.5 Treatment modalities for malignant pleural mesothelioma

Currently, there are several modalities available for the treatment of MPM patients but so far no conclusive standard has been accepted. Single modality therapy and bimodality therapy has shown limited success with regard to the local control [17, 18]. Surgery alone showed no improvement in respect to survival [19]. When surgery and chemotherapy are used, a median survival rate of 19 months (vs. 13 months no treatment) was reported [12]. In the early 1990s, a trimodal approach has been propagated. It consists of chemotherapy, followed by surgery (extrapleural pneumonectomy or pleurectomy/decortication) and radiotherapy. The first trimodality approach was reported by Sugarbaker in 1991 [20]. In this study, the perioperative mortality rate was 6 % with a morbidity rate of 16 %. The survival rates were 70 % and 48 % after 1 and 2 years respectively.

1.5.1 Surgery

Currently, there are two different approaches used for MPM surgery: extrapleural pneumonectomy (EPP) and pleurectomy/decortication (P/D). For EPP, the surgeon removes the ipsilateral lung, diaphragm, pericardium and the complete pleural envelope. For P/D, the outer pleura and the parietal pleura are removed whilst sparing the lungs. During the 1970s, mortality rates of up to 30 % were observed perisurgery [21]. With the improvement of the surgical technique, patient selection and postoperative care, the mortality rate was reduced to less than 3 % [22, 23]. Nevertheless, postoperative complication rates still remain high with an overall complication rate of 60 % and major complications reported in 22 % of operated patients [19]. Post operation complications can include, inter alia, atrial fibrillation, prolonged intubation, vocal cord paralysis [22]. The optimal surgical intervention is controversial, mainly due to the small number of patients analyzed and the patient selection criteria [24].

1.5.2 Chemotherapy

Chemotherapy is the treatment of cancer with drugs that usually kill cancer cells. It stops or slow down the growth of cells that divide rapidly. The current drugs used for the treatment of MPM are cisplatin, carboplatin and pemetrexed. In the case of mesothelioma, chemotherapy alone will not cure the patient but can slow down progression and reduce the spreading of the cancer. Chemotherapy alone has failed in respect to prolongation of survival time [18].

When chemotherapy is combined with surgery, it can be given before or after the surgery. The concept of preoperative chemotherapy has been propagated by Stahel and Weder at the University Hospital Zurich and has been widely accepted [23].

1.5.3 Radiotherapy

Radiation therapy has been used as a medical therapeutic modality since the begining of the twentieth century, honored by a Nobel Prize to N.R. Finsen in 1903, only height years years after the discovery of x-rays by W. Roentgen in 1895 (Nobel Prize in 1901). Radiation therapy uses ionizing particles such as photons, electrons, protons, neutrons or heavy charged particles. These particles will interact with the cells leading to permanent damage of cellular components such as proteins or DNA. These modification of the cells can lead to there death. Ionizing radiation was first used clinically to treat skin disease either with radioactive substances, such as radium, or with conventional x-rays tubes. These x-rays tubes, which are still being used today for the treatment of skin cancer, generates x-rays up to 300 kV (orthovoltage). The advantage of these low energy x-rays is the maximal dose deposition which is given to the surface. Furthermore, the dose fall-off is strong for these low energies. Typically, for a beam having a half-value layer (HVL) of 0.1 mm of aluminium, corresponding to an energy around 20 kV, the dose remaining after 1 cm is below 10 % for an applicator having a source skin distance of 30 cm and a 10 cm round applicator [25]. This value will increase with larger HVL. For example, for a beam having a HVL of 1.0 mm of cupper, corresponding to an energy around 200kV, the dose is 95 % at 1 cm, 60 % at 5 cm and 30 % at 10 cm depth for a source skin distance of 50 cm and a 10 cm round applicator [25]. The disadvantage of orthovoltage therapy is that the beam does not penetrate deep enough to treat deep-seated tumors.

In the mid-1950's, the first cobalt machine was used to treat deep-seated tumors. The photon energies emitted from the disintegration of colbalt-60 was 1.17 MeV and 1.33 MeV. With these photons energy, skin sparing was

possible. Beside the cobalt machine, linear accelerators were also used for the treatment of deep-seated tumors. The principles of the linear accelerator were developed by Cockcroft and Walton in the 1920s (Nobel prize in 1951), and Luis W. Alvarez developed the first linear particle accelerator based in Berkley in 1947(Nobel prize 1968). The first linear accelerator used for treating cancer patients was introduced in 1956 by H. Kaplan and E. Ginzton. In the early 21st century, linear accelerators are the standard machines generating megavoltage beams for cancer treatment in the industrialized countries. Linear accelerators have the advantage of generating beams with high energies, typically between 4 MV and 22 MV. This allows better sparing of the skin and in the case of deep seated tumors better dose at depth when compared to cobalt units.

Figure 1.4: TrueBeam linear accelerator from Varian (Varian Medical System, Palo Alto, USA). The patient is positioned on the couch which can rotate around a fix point, called the isocenter, usually placed in the tumor center. The gantry and collimator can both rotate around axes through the isocenter. High energy photons from 4 MV to 22 MV as well as electrons with energy ranging from 4 MeV to 22 MeV can be generated by the same linac.

Linear accelerators, see Fig. 1.4, accelerate electrons to energies typically between 4 MeV and 22 MeV in a dedicated shaped resonator. The accelerating power is supplied by a microwave radio-frequency field. The electrons

can directly be used for patient treatment. In order to treat large volumes, the narrow electron pencil beam generated by the linac has to be broadened. Most of the linear accelerators use two scattering foils for this purpose. The first foil has a high atomic number and a homogeneous thickness in order to scatter the electrons. The second foil, which can be approximated to a cone shape, generates a homogenous energy fluence distribution. If photons needs to be generated by the linear accelerator, the electrons are accelerated and focused on a target with a high atomic-number, usually tungsten. The energy lost by the electrons is converted into bremsstrahlung radiation. The main direction of photons generated by bremsstrahlung with megavoltage energy is in the motion direction of the electrons. Therefore, a cone shaped attenuation filter (flattening filter) is placed in the beam in order to have a homogeneous energy fluence distribution. The field is then collimated by jaws and/or a multileaf collimator and blocks, see Fig. 1.5.

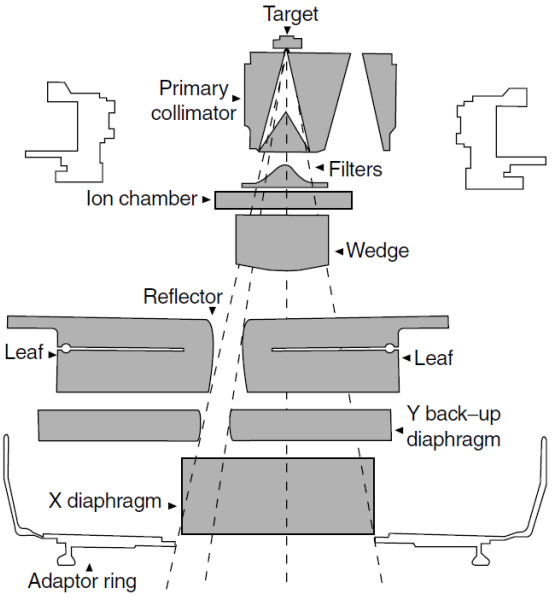

Figure 1.5: Diagram of an Elekta linac head showing the position of the primary collimators, filters, ion chamber, wedges, leaves, and the secondary collimators (X and Y back-up diaphragm) [26].

In radiotherapy, one of the goals is to achieve a sufficiently high minimal dose in the clinical target volume (CTV) while keeping the dose to the organ

at risks (OAR) as low as possible in order to avoid complication. In other words, to deliver a dose high enough to achieve a high tumor control probability (TCP) and to achieve a low normal tissue complication probability (NTCP), see Fig. 1.6. TCP and NTCP are both represented by sigmoid curves. If the two curves are close to each other, a small increase in dose will increase TCP and NTCP. If the TCP and NTCP are separated by a large gap and the TCP is on the left side of the NTCP curve, an increase in dose will increase the TCP without changing the NTCP. The gap between the TCP and NTCP curves can be affected, inter alia, by changing the sensitivity of the cells (drugs, oxygen) and by radiation and radiotherapy modalities such as photons, neutrons or charged particles. Furthermore, the energy fluence distribution of these particles can be modulated in order to improve the target dose coverage and dose conformity. By doing so, the TCP will increase and the NTCP will decrease. In all of these treatment modalities previously mentioned, a computed tomography (CT) based patient model and a linac simulation is required in order to calculate the dose distribution computer based individually which takes into account patient anatomy information.

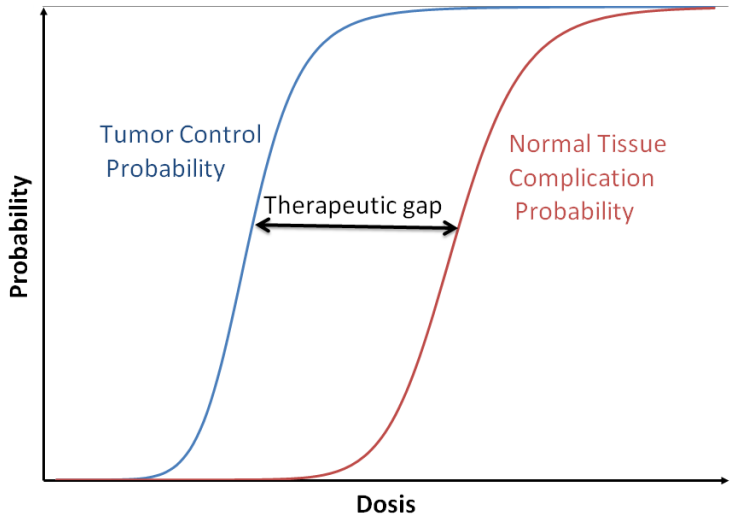

Figure 1.6: Relationship between NTCP and TCP. The goal of radiotherapy is to have a large therapeutic gap as possible. This gap will be influenced inter alia by the radiotherapy modalities.

3D-Conformal Radiotherapy and electron therapy

The 3D conformal radiotherapy (3DCRT) technique uses photons and more rarely, electrons. Photons and electrons for treatment purposes are commonly generated by a linear accelerator producing photons with energies ranging from 4 MV to 22 MV and electrons with energies ranging typically from 4 MeV to 22 MeV. Depending on beam energy, maximal dose deposition occurs at depths between 1 cm and 4 cm, see Fig. 1.7. The dose deposition of the photons after the depth of maximal dose will decrease exponentially due to absorption. Dose deposition is also dependent on the distance to the source, r, and decreases with the relationship of $1/r^2$. Therefore, the dose delivered distal from the target is not negligible, see Fig. 1.7. For electrons, a stronger dose fall-off occurs after the depth of maximal dose than photons, allowing better dose sparing of the tissue beyond the target. This fast dose fall-off for electrons is an advantage when the target lies in close proximity to the surface. When the target is beyond 6 cm, good coverage and dose homogeneity is no longer achievable with electrons.

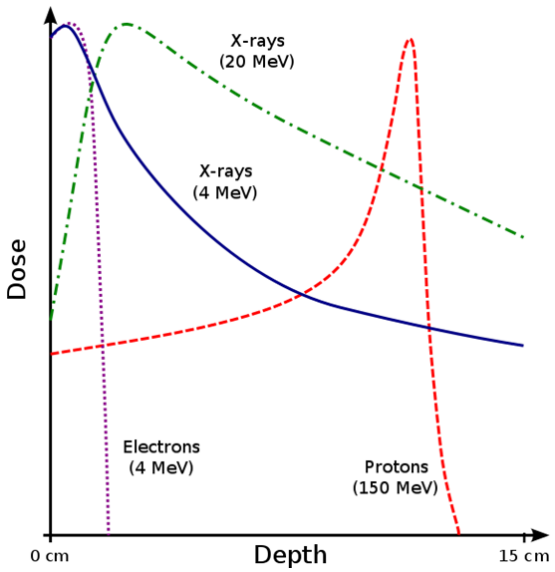

Figure 1.7: Percent depth dose curves for electrons, photons and protons. Electrons and protons shows a faster dose fall-off compared to photons [27].

In order to have good dose conformity, the electron beams are collimated

with blocks and the photon beams are collimated with a multileaf collimator (MLC), see Fig. 1.8. The beams are collimated to the projection of the tumor from the beam's eye view direction. In order to increase conformity and have a homogenous dose in the target, multiple beams from different directions are commonly used.

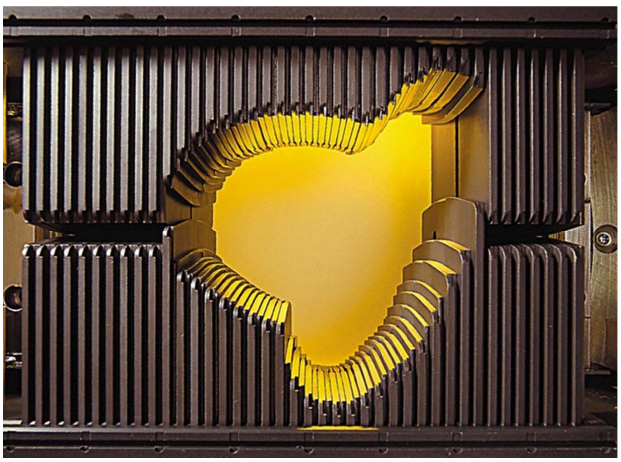

Figure 1.8: Millenium microleaf collimator from Varian. The leaf width at isocenter is 0.5 cm over the central 20 cm of the field and 1 cm on the edge of the field over 20 cm. There is a motor for each of the 120 microleaves which are able to move independently [28].

Electrons and photons fields are rarely combined in a plan due to the difficulty and the time required to match electrons and photons fields. Low dose electron isodose lines have a characteristic pear shape due to the scattering of the electrons. For photons, the energy is deposited mainly in the forward direction resulting in low energy deposition and sharp gradients laterally. Therefore, it is difficult to achieve good dose homogeneity and coverage when combining electrons and photons fields.

Intensity modulated radiotherapy

In intensity modulated radiotherapy (IMRT), the energy fluence distribution of the beam is modulated during treatment. This has the potential to create steep dose gradients between PTVs and OARs and increase the gap between NTCP and TCP curves. The fluence of the beam can be modulated using various techniques. Physical compensators modulate the beam by absorption

of the photons through compensators. This technique has important disadvantages, such as the time required for the fabrication of the compensators, the need for the therapist to enter the room and change the compensator after each field [29]. Two other techniques, step-and-shot and dynamic MLC (dMLC) methods, use a conventional multileaf collimator (MLC) to modulate the intensity, see Fig. 1.8. For the step-and-shoot method, the fluency is divided into multiple segments. In each segment, different MLC positions are defined. The beam is turned on when the MLC's are at the right position, and turned off between segments in order to allow the MLCs to move from one predefined position to the next, see Fig. 1.9. Drawbacks of this technique are, inter alia, long delivery time and the necessity of a good linearity of the linac output and profiles for segments treated with few monitor units.

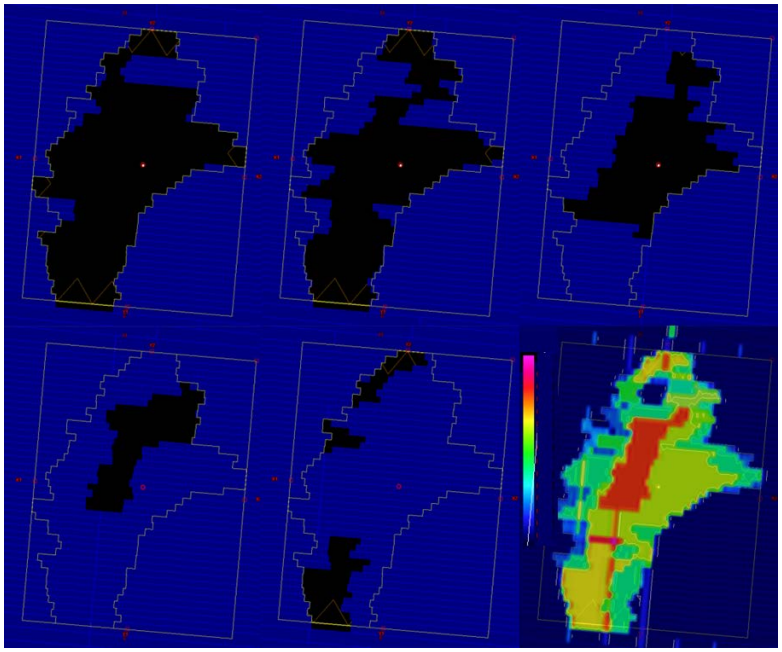

Figure 1.9: Field segments for a "step and shoot" IMRT technique (first 5 images) and the resulting dose-map fluence (last image). The dose-map fluence is in arbitrary units and the scale range from dark blue to pink (scale is displayed on the left side of the last image).

In the dMLC-sliding window method, the intensity is modulated by the

leaves which are independently moving at different velocity when the beam is on. The gap between two opposing leaves also varies during the irradiation. This gives a short delivery time, but requires a very precise MLC controller to verify the leaf positions. This is required in order to have a delivered dose distribution as close as possible to the calculated dose.

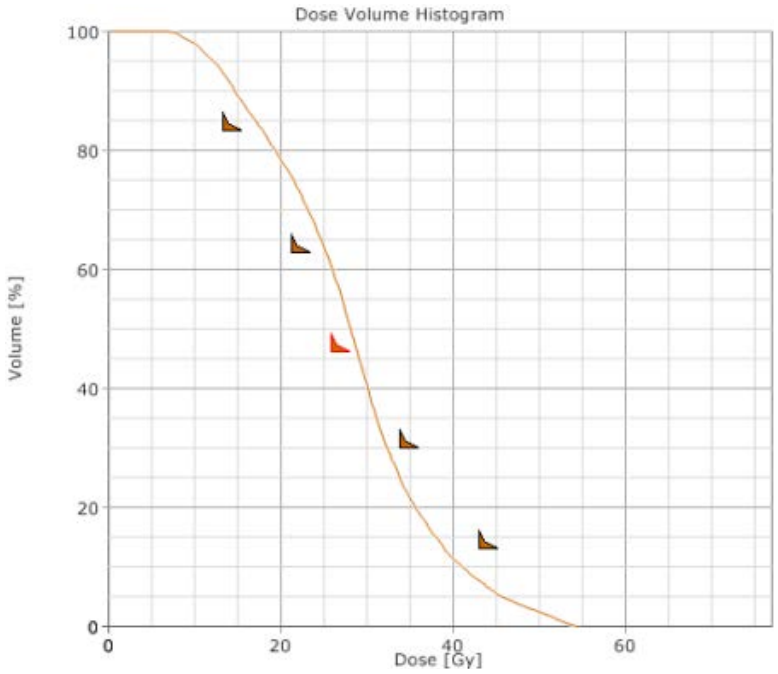

Figure 1.10: Example of dose volume constraints for organ at risks set during the inverse planning process. The planner set constraints (triangles) and the algorithm tries to fulfill the objectives. In the current example, the two constraints on the right side are achieved (the curve is on the left side of the constraints) and the three constraints on the left side are not fulfilled since the dose to the structure is higher than what is planned.

IMRT treatment plans are generated with a treatment planning system using in general inverse planning. For inverse planning, dose volume constraints are set by the planner based on clinical information. For example, target and organ at risk will have upper constraints such as "not more than x % of the volume should receive more than y Gy", see Fig. 1.10. For targets, additional lower constraints will be set such as " x % of the volume or more

should receive at least y Gy". These constraints are set during the optimization process and will be taken in an objective function. This function will be optimized in order to get as close as possible, or to achieve, all the constraints previously defined [30]. Therefore, the weight of each beamlet for every field will be optimized resulting in a fluence distribution generated by different MLC positions during the irradiation (for step-and-shoot and sliding window techniques). Today, most of the objective functions are based on dose parameters and becoming more common based on radiobiological models.

Different types of algorithms are used in the optimization and calculation process. Most of them use a fast simplified algorithm in the optimization of the objective function. This allows to optimize the plan in a reasonable time, i.e. in a couple of minutes. Therefore, for the optimization step, the pencil beam algorithm [31] may be preferred to Monte Carlo [32] due to their faster calculation time. For the dose calculation on the planning CT, more robust algorithms are preferred, such as Monte Carlo, Acuros (based on the linear Boltzmann transport equation), or collapse cone convolution. These algorithms are more suitable to take into account density inhomogeneity and display a dose distribution closer to the dose delivered when compared to simpler algorithms such as pencil beam.

Volumetric modulated arc therapy

Volumetric modulated arc therapy (VMAT), also called intensity modulated arc therapy (IMAT) or RapidArc ® (Varian Medical Systems, Palo Alto, CA, USA), is a kind of rotational IMRT where gantry angle, dose rate and MLC positions are changing during the irradiation. At each gantry angle position of an arc, a single aperture shape is formed by the MLC. No motion of the leaves is performed at a fixed gantry angle as it is the case for IMRT. During the rotation of the gantry, the speed of the gantry as well as the dose rate are modulated. This allows each leaf of the MLC to reach its position for each control point. This technique can be delivered with a C-arm shaped linac.

Some planning systems are using a direct aperture optimization (DAO) in their algorithms [33]. The aperture is optimized for each control point which corresponds to a gantry angle using an annealing algorithm. At the beginning of the optimization (for RapidArc ®), a small number of equidistant control points are used, typically five. The number of control points increases during the optimization process to reach a number of 177 control points for a full arc rotation for RapidArc®. The initial aperture shape for a new control points is interpolated between adjacent control points.

During the optimization process, random modifications of the fluence are

applied and are accepted when an improvement of the objective function is observed. These modifications have to fulfill the linac limitations such as gantry rotation speed, MLC speed and dose rate. The optimization normally stops after a given time or a given number of iterations. The algorithms used for the dose calculations are similar to those used for IMRT.

Proton therapy

Proton therapy (PT) as 3DCRT, IMRT or VMAT is an external beam radiotherapy technique which uses protons instead of photons for the treatment of cancer. The advantage of PT comes from the interaction of protons with tissue, see Fig. 1.7. There is less lateral scatter than for photons and electrons. More important is that most of the energy deposition occurs in the last few millimeters where the protons are completely stopped. The maximal dose peak is called *"Bragg peak"*. The depth of the Bragg peak depends on the proton energy. This is a big advantage in comparison to photons where megavoltage photons delivers the maximal dose between 1 cm and 4 cm depth and the beam delivers dose beyond the target which is not the case for protons. In order to cover larger volumes with good dose homogeneity with PT, different energies are combined in order to move the Bragg peak forward or backward. This results in a plateau, called the *Spread-Out Bragg Peak* (SOBP), as shown on Fig. 1.13. After the SOBP, nearly no dose is deposit, allowing the treatment of targets which are in very close proximity to critical structures. There are currently two different approaches for PT dose delivery:

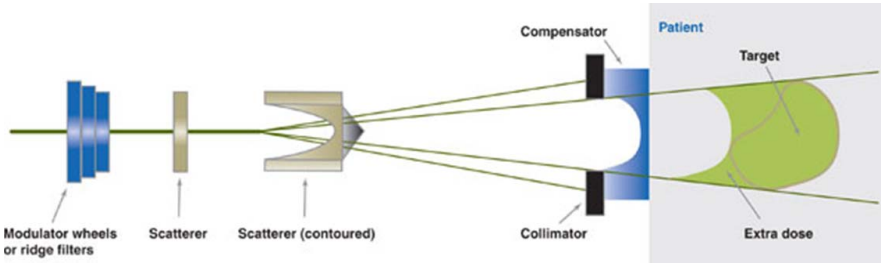

Figure 1.11: Principle of the passive spreading technique. The proton energy is modified by filters. The proton beam is then broaden by two scatterers and then collimated by a collimator and a compensator [34].

- Passive spreading also called scattering method. In this approach, the

proton beam is broadened by placing material in the beam. A single or a double scattering foil are used depending on the field size. In order to confrom the dose to the target a patient specific compensator is used, see Fig. 1.11

- Active spreading, also called spot scanning. The protons are focused by electric and magnetic fields at a given location within the tumor. By using multiple spots, it is possible to scan the dose through the entire target, treating voxel-by-voxel, see Fig. 1.12.

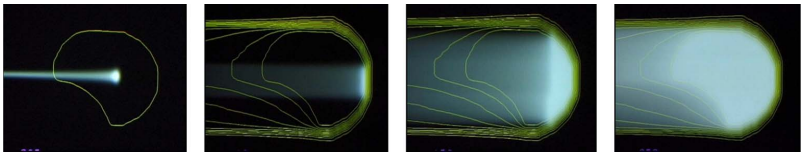

Figure 1.12: Dose distribution for a single pencil beam (first picture) to thousand pencil beams superimposed (last picture) [35].

PT can be used in similar way as the 3DCRT by using fields coming from different directions, all of them delivering a homogenous dose in the target.

The IMRT approach can also be used with protons, this technique is called intensity modulated proton therapy (IMPT). With IMPT the fluency is modulated for each spot but the combination of all the fields leads to a homogenous dose in the target and a very good sparing of the healthy tissues can be achieved. In theory, there is a clear advantage of protons over photons and electrons therapy due to the depth dose characteristics. On the other side, protons will be much more affected by patient miss-alignment and changes in the patient anatomy. This could lead to a target underdosage and/or an organ overdosage. An other disadvantage is the neutron contamination due to the proton-nuclear interaction. This neutron contamination could result in an increase of developing secondary cancer [36].

1.5.4 Photon treatment planning algorithms

Before the energy of the photons generated by a treatment machine is absorbed by the patient, a lot of interactions occur. The dose deposited at a given point in the patient can be divided in four main components [37]:

- Primary fluence. This results in around 70 % or more of the total deposited dose and is created by photons generated in the target.

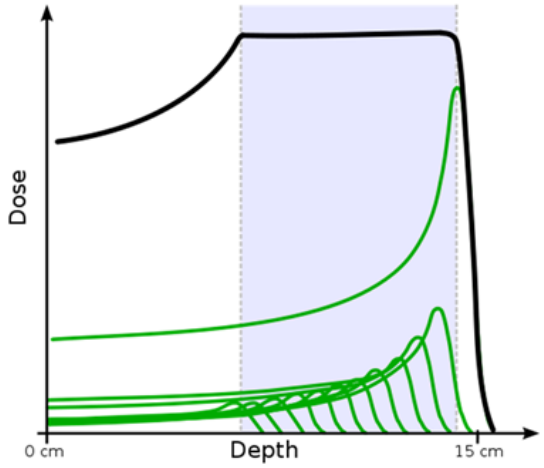

Figure 1.13: Proton dose deposition for different energies (green curves). The total dose deposited by all the proton beams are displayed in black showing a plateau in the target region (blue shaded region). After the target, a steep dose fall-off is observed with minimal dose delivered to the tissue after the target.

- Phantom scatter. This can produce up to 30 % of the total deposited dose. Scattered photons are generated by the interaction of the primary photons in a body.
- Head scatter. This typically contributes to 5 % to 10 % of the total dose. This energy is transported by photons originating in the head of the treatment machine excluding the target. These photons can be generated in the flattening filter, in the collimator system (jaws or micro-leaf collimator) or in the air column after the target.
- Contaminating charged particles present in the photon beam. There are generated in the flattening filter in photon beams. The dose deposition of these charged particles will take place in the first centimeters of the absorbing body. The depth depends on the energy of the beam.

All of these interactions which occur in the machine as well as in the patient are schematized in Fig. 1.14. These interactions are taken into account, implicitly or explicitly, depending on the sophistication of the algorithm used for dose calculation in the planning system. The dose calculations methods

are often divided into two groups. The *empirical* method also called *broad-beam* where no distinction between the type of interactions are considered. The *superposition* method on the other hand, takes into account all the different types of interactions.

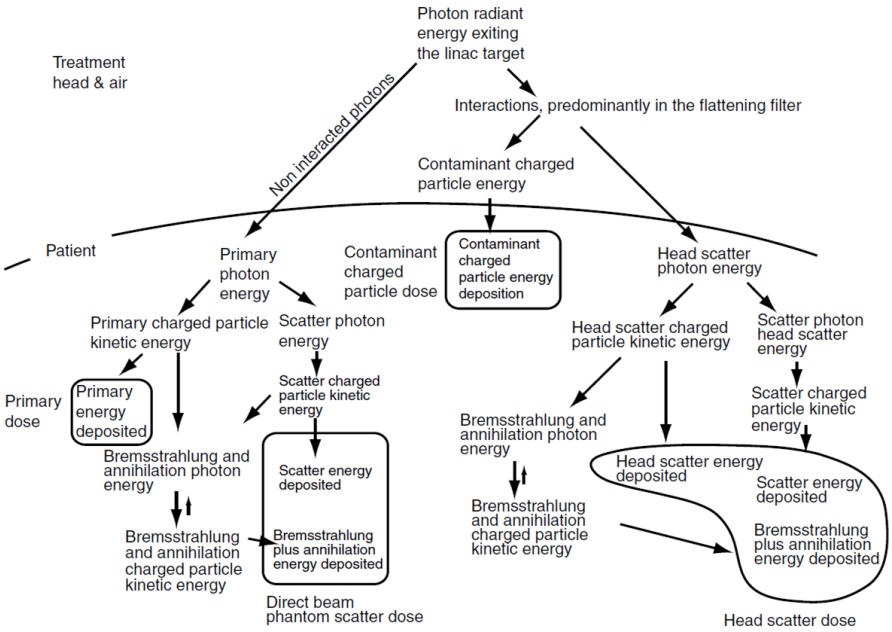

Figure 1.14: Main interactions and dose deposition of megavoltage photon beams in patients [37].

Empirical Methods

In the empirical methods two approaches can be used to calculate the dose distribution:

- Measured data under reference condition are used for the dose calculation. These data are stored in a *table* and are interpolated during the calculation process.
- Based on measured data, mathematical functions are used to fit profiles and depth-dose curves. Based on these functions a dose distribution at non reference conditions can be calculated

Correction factors are used in empirical methods to take into account differences between reference conditions and treatment conditions. For example corrections for the variation of the source skin distance, patient inhomogeneities. If a high accuracy in dose calculation is required and complex beam arrangements are used, for example in intensity modulated radiotherapy, empirical methods reach their limits. More powerful algorithms based on the superposition principle, for example, are then preferred.

Superposition methods

In the superposition methods, the dose is calculated voxel by voxel. The dose, D_P, deposited at any point P (x, y, z) can be considered as a sum of contribution of dose coming from each point P (x', y', z'), see Fig. 1.15. The main disadvantage of this approach is the large amount of computer time required to calculate the dose distribution.

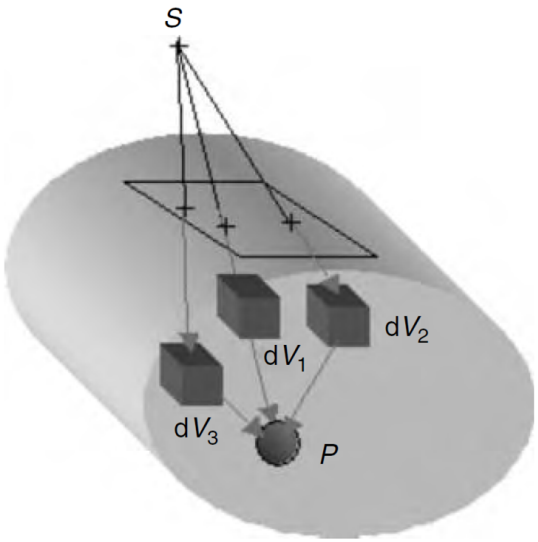

Figure 1.15: The dose at point P can be considered as the dose coming from the interaction of the primary photons interacting in the volume dV [26].

1.5.5 Planning evaluation

In the planning process, especially during inverse planning, there are contradictory objectives. These include high and uniform dose to the target on one side and low dose to the surrounding healthy tissues on the other. Furthermore, different objectives can be set for the target and the organ at risk. Therefore, there is not a unique "best plan" achievable. If a plan can be optimal for a given structure without deteriorating the other structure, such solution is called a *Pareto optimal solution.* This can be repeated for each structure leading to a set of solutions constituting the *Pareto front* [38].

In the current planning evaluation process, the Pareto front is not available, only a subset of optimal plans can be generated by the planner. Therefore, plan comparison tools are required in order to compare different plans. This can be performed by comparing the dose distribution slice by slice. This process is time consuming, and most of the time no clear answer can be given. In most cases a plan determined to be better at sparing some organs and/or delivering a better dose coverage to part of the PTVs. In combination with the isodose representation of the dose distribution, dose volume histogram (DVH) parameters are often used to describe plan quality. These DVH parameters reduce the DVH curve to a single or multiple quantitative parameter. These parameters include the mean dose, maximal dose or minimal dose to 95 % of a certain volume. This allows the comparison of 2 different plans as well as parameters able to be compared to published data. The disadvantage of this techniques comes from the loss of information when the graph is reduced to a small number of values. Thus to take into account all available parameters of the DVH and the specificity of the organs or the target structure, the equivalent uniform dose (EUD) can be used. The definition of the EUD given by Niemierko was: *"The concept of equivalent uniform dose assumes that any two dose distributions are equivalent if they cause the same radiobiological effect"* [39]. He suggested the following formula for target volumes and organs at risk:

$$EUD = \left(\frac{1}{N} \sum_{i=1}^{N} D_i^a \right)^{\frac{1}{a}} \tag{1.1}$$

Where N is the number of voxels in the structure of interest, D is the dose in the voxel i, and a is the tumor or organ parameters that describes the dose-volume effect [40]. These parameters can be calculated from published normal tissue tolerance dose [41,42]. When $a = -\infty$ the EUD is equal to the minimal dose in the structure of interest. When a increases to $+\infty$, the EUD will tend to the maximal dose in the structure of interest. In the upper graph

from Fig. 1.16, a typical lung dose volume histogram is displayed. The EUD for the lung dose volume histogram is displayed as a function of parameter a in the lower graph from Fig. 1.16. The EUD concept can be used either for target structures or for organs. The value for a is typically between 1 and 10 for organs. For targets, negative values for a are taken in order to take into account cold spots in the target and positive values are also taken in order evaluate hot spots in the target.

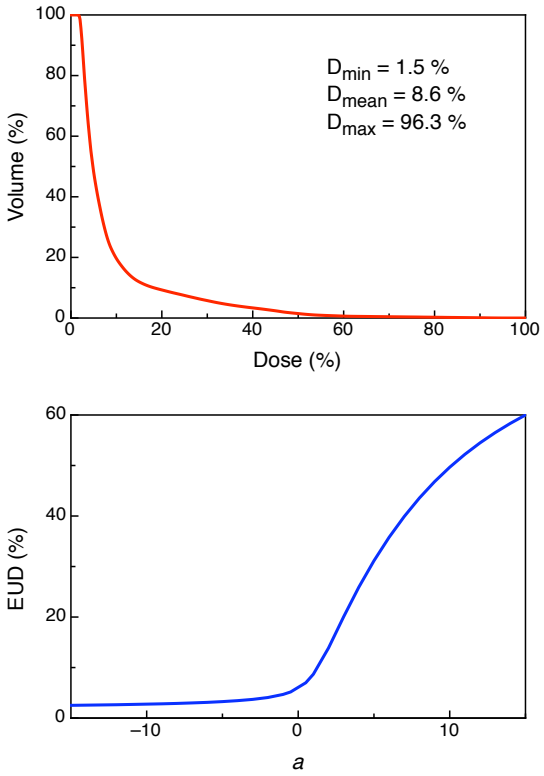

Figure 1.16: The upper picture represents a typical lung dose volume histogram for a mesothelioma patient planned with IMRT. The lower picture gives the EUD as a function of the parameter a, ranging from -15 to 15 for the graph above.

Knowing the biological equivalent dose that, if given uniformly, would lead to the same radiobiological effect, tumor control probability as well as

normal tissue complication probability can be derived from the EUD value [40, 43].

1.5.6 Adaptive radiotherapy

In radiotherapy the treatment delivery accuracy has a direct impact on the target margins [44] [1]. Furthermore, poor patient positioning could lead to target underdosage and/or overdosage of the organs at risks. Therefore treatment delivery accuracy is integral in maintaining the planned tumour control probability and normal tissue complication values. Patient positioning can be performed based on integrated imaging modalities such as cone beam computed tomography, kV of MV images. These images are then registered to the planning CT. This process can be difficult when anatomical changes occur in the patient, for example tumor shrinkage or tumor motion. This also occurs during the treatment of mesothelioma patients where change of density in the resected lung is observed after surgery [B]. Indeed, after surgery, air and/or fluid will take the place of the resected lung. The air cavity will disappear with time and will be subsequently replaced by fibrous tissue or fluid, see Fig. 1.17.

The change in the air cavity volumes can be seen on a lateral MV or kV image or more easily with a cone beam CT or conventional CT. The variation in the air cavity volume in the resected lung changes the CT density from 0 to 1 and will affect the patient external anatomy. This will change the density distribution and the radiographical path lengths in the resected lung. These changes will affect the absorption of the photons and particles used during radiotherapy leading to a change in the dose distribution [B]. Therefore *adaptive radiotherapy* is required in order to modify the original plan to take into account changes in patient anatomy. Adaptive radiotherapy is the adaptation of the treatment plan on changes in the patient geometry, anatomy and morphology during the radiotherapy treatment in order to improve radiation treatment success [46]. These modifications are performed in order to take into account in changes in patient anatomy, modification of the tumor size or change in tumor location. Therefore, on-line and off-line approaches can be used in order to assess these changes. With the on-line approach, an adaptive plan is performed based on a cone beam CT taken prior to radiotherapy treatment. This approach is currently used only for small tumors such as those in the prostate [47] due to technical issues (maximum size of the cone beam CT in the cranial-caudal direction is currently limited

[1] A margin around the tumor is applied to take into account the accuracy of the delivery among other things. The volume treated will be the tumor and the margin volume in order to ensure that the wished dose is delivered in the tumor.

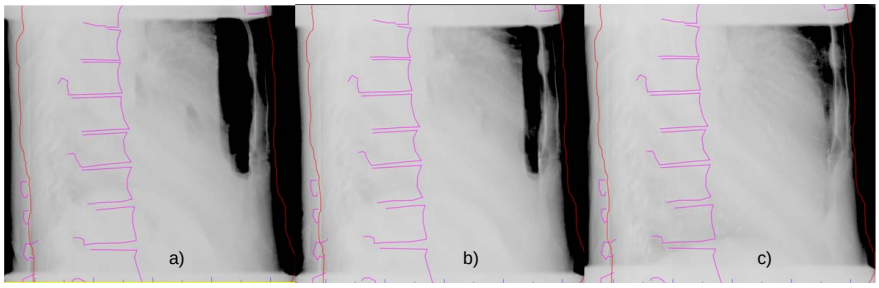

Figure 1.17: Variation of air cavities during radiotherapy treatment. These three images have been taken with a kV imager from 90 degrees. The left image has been taken on the first day of radiotherapy treatment. Image *b* was taken at fraction 12, 16 days after the first radiotherapy treatment. Image *c* was acquired on the last day of treatment, 31 days after the first radiotherapy treatment. The purple structure in the middle of the picture represents the vertebra column. The black structure on the chest wall represents the air cavity.

to 20 cm) and the time required for reoptimization which is correlated to the target size. For large tumors, such as mesothelioma, the off-line approach is the only one currently available for adaptive radiotherapy. In this approach, conventional CT will be required due to the dimension of the tumor, up to 40 cm in the cranial-caudal direction.

Image registration

In adaptive radiotherapy, planning CT and online acquired cone beam CT are registered in order to verify the patient positioning as well as a modification in patient anatomy before starting the treatment. After the registration process, volume propagation can be performed from one set of images to the other set. Several publications have presented different approaches for registration. Here, only a short summary will be presented [48,49]. Following the classification formulated by Elsen *et al.* [50], registration algorithms can be either *extrinsic* or *intrinsic*. In the extrinsic registration, the patient datasets are matched based on artificial markers. These markers can be non-invasive such as skin markers, or invasive, such as a stereotactic frame screwed into the patients skull. The extrinsic registration is a fast and easy method. This approach is mostly used for rigid registration such as cranial stereotaxy. The non-rigid registration approach often fails due to the lack of deformation

information coming from the markers. Indeed, a very high number of markers would be needed in order to obtain enough information on the deformation. The intrinsic registration uses the patient's image structures such as the body contour, anatomy landmarks, pixel intensities and bone structures.

There are three main types of intrinsic registration. They can be based on:

- Landmarks. Registration with landmarks can be separated in two groups: anatomical or geometrical. The anatomical landmarks are based on locatable anatomical structures. The geometric landmarks are points derived from various shapes such as curvatures minima or extrema. This registration is often used for rigid registration due to the lack of deformation information.

- Segmentation. In the segmentation registration, anatomic structures, in most cases, surfaces, are taken from both data sets for registration. This registration can either use a rigid registration or deformable model. This approach is often used for head registration which relies on the skin surface from the different image modalities [49]. This allows an easy and quick registration.

- Voxel properties. In this registration method, the grey value of the images are taken in order to register two sets of images. In this approach, no data reduction is requested as it the case for the segmentation registration. This kind of registration can either be used for rigid or deformable models. The main drawback of this registration is the high computer power/memory required [49].

For all these types of registration, the nature of the transformation can differ, be it rigid, affine, projective or curved. In rigid transformation the two image sets will be moved in order the keep the objects as close to each other while keeping the shape and geometrical correlation of the objects unchanged. Therefore, only translations and rotations are allowed. In the affine registration, the objects are segmented and a straight line in the first image is mapped onto a straight line in the second image [50]. The parallelism is preserved in this method. A projective transformation is an affine registration where the parallelism is not preserved. In other words, the transformation maps lines to lines. In the curved registration, also called elastic registration, the object is segmented and a straight line in the first image is mapped onto curved lines in the second image, see Fig. 1.18.

Transformations are called global when the transformation is applied to an entire data set and local if each subsection of the data set has its own transformation, see Fig. 1.18.

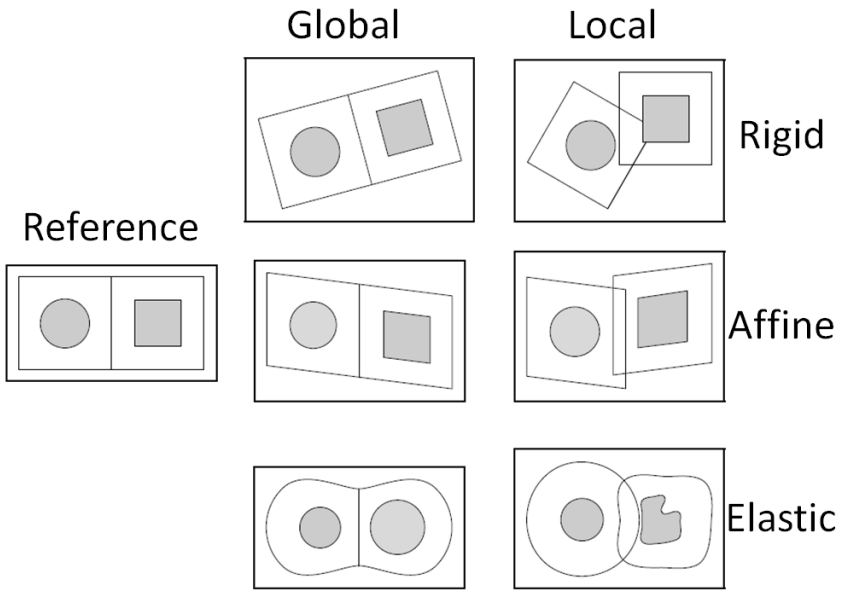

Figure 1.18: Example of different types of registration [49]. In the rigid registration, only translation and rotation transformation are allowed. For the affine registration, objects are segmented and straight lines are mapped to straight lines. For the elastic registration, straight lines are mapped to curved lines. The registration is called global when the transformation is applied to the entire data set and local if each subsection has his own transformation.

1.6 Aims of this study

Currently there are no standard procedures for the treatment of MPM patients. Different studies are currently running to show what are the benefits from the different modality combinations. For example we are investigating the benefit of radiotherapy in the tri-modality approach [51] [2], in the Swiss group of clinical cancer research (SAKK)[3]. Nevetherless, there is not yet a general agreement on which treatment modality should be used. The goal from this PhD thesis was to compare different external beam radiotherapy treatment techniques, such as 3DCRT, IMRT, VMAT and PT, for the treatment of MPM patients after EPP. This was performed based on clinical data,

[2] Tri-modality treatment is the combination of neoadjuvant chemotherapy surgery and radiotherapy.

[3] *J. Krayenbuehl* is the responsible medical physicist for this national study

planning comparison and plan robustness. A non-rigid algorithm was also developed for the purpose of adaptive radiotherapy.

In more details, chapter 2 and chapter 5 gives an evaluation of the possibility to treat MPM patient with IMRT. Evaluations of patient clinical data such as local control, disease free survival, overall survival have been done for 3DCRT and IMRT in chapter 5. Furthermore, an evaluation of optimal 3DCRT and IMRT plans has been performed in chapter 2. The dosimetric advantages of both techniques were assessed based mainly on dose volume histogram parameters.

A feasibility study on the use of proton therapy (PT) and volumetric modulated arc therapy (VMAT) has also been performed. The results are presented in chapter3, 4 and 5. These two techniques were compared to IMRT in respect to dose distribution and treatment time. Also for consideration is the instability of tissue density in the ipsilateral hemithorax following an EPP procedure. The EPP will leave variable air cavities which are subsequently replaced by fibrous tissue, see chapter 3 and 4. These air cavities variations will affect the anatomy and the density of the ipsilateral lung resulting in a modification of the dose distribution. The dynamic of volume decrease has been evaluated and the results are presented in chapter 3 and 4. The modification of the dose distribution due to the modification of patient anatomy was performed for the targets and the organs at risk. This evaluation has been done based on the equivalent uniform dose (chapter 3) and dose volume parameters (chapter 4) for IMRT, VMAT and PT.

In order to take into account the deformation of the patient anatomy during the treatment, adaptive radiotherapy can be used. Images have to be registered in order to propagate volumes from one set of images to another set of images. This volume propagation was evaluated using a new approach using non-rigid registration. In order to validate this algorithm, a comparison between automatic segmentation (affine and non-rigid registration) and manual segmentation was performed. This validation was performed on prostate cancer patients due technical reasons (size of the target, computation time and accessibility to control CTs). The results from this study are presented in chapter 6.

Bibliography

[1] A Ahamad, C W Stevens, W R Smythe, A A Vaporciyan, R Komaki, J F Kelly, Z Liao, G Starkschall, and K M Forster. *Intensity-modulated radiation therapy: a novel approach to the management of malignant pleural mesothelioma.* Int J Radiat Oncol Biol Phys **55**(3), 768–775 (2003)

[2] J C Wagner, C A Sleggs, and P Marchand. *Diffuse pleural mesothelioma and asbestos exposure in the North Western Cape Province.* Br J Ind Med **17**, 260–271 (1960)

[3] J T Hodgson. *The Quantitative Risks of Mesothelioma and Lung Cancer in Relation to Asbestos Exposure.* Ann occup Hyg **44**(8), 565–601 (2000)

[4] F Montanaro. *Pleural mesothelioma incidence in Europe evidence of some deceleration in the increasing trends.* Cancer Causes and Control **14**, 791–803 (2003)

[5] J Peto, A Decarli, C La Vecchia, F Levi, and E Negri. *The European mesothelioma epidemic.* Br J Cancer **79**(3-4), 666–672 (1999)

[6] SEER. *SEER Cancer Statistics Review 1975-2008.* National Cancer Institute (2011)

[7] V Delgermaa, K Takahashi, E K Park, G Vinh Le, T Haraa, and T Sorahan. *Global mesothelioma deaths reported to the World Health Organization between 1994 and 2008.* Bull World Health Organ **89**, 716–724 (2011)

[8] Y B Izzettin and P Grandjean. *Prospective Study of Mesothelioma Mortality in Turkish Villages With Exposure to Fibrous Zeolite.* J Natl Cancer Inst , 414–417 (2006)

[9] C A Poland. *Carbon nanotubes introduced into the abdominal cavity ofmice show asbestoslike pathogenicity in a pilot study.* Nature Nanotechnology **3**, 423–428 (2008)

[10] A H Smith. *Chrysotile Asbestos is the Main Cause of Pleural Mesothelioma.* American College of Chest Physicians **30**, 252–266 (1966)

[11] *http : //serc.carleton.edu/research*$_e$*ducation/geochemsheets/techniques/SEM.html.* **28.07.2012**, 28.07.2012

[12] J H Betts. *A review of the history of mining, mineral collecting and minerals found in the five boroughs of New York City.* Rocks and Minerals magazine **84**(3), 204–252 (2009)

[13] A Tossavainen and K Antti. *Global Use of Asbestos and the Incidence of Mesothelioma.* International Journal of Occupational and Environmental Health (January/March), 22–25 (2004)

[14] L V Robert. *Mineral Commodoty Summaries.* US Geological Survey **703**, 1–198 (2013)

[15] M Farfel, L DiGrande, R Brackbill, and et al. *An Overview of 9 11 Experiences and Respiratory and Mental Health Conditions among World Trade Center Health Registry Enrollees.* J Urban Health **85**(6), 880–909 (2008)

[16] H Nagai. *Asbestos surface provides a niche for oxidative modification.* Japanese Cancer Association **102**(12), 2118–2125 (2011)

[17] K Antman. *Malignant Mesothelioma: Prognostic Variables in a Registry of 180 Patients, the Dana-Farber Cancer Institute and Brigham and Women's Hospital Experience Over Two Decades, 1965-1985.* Journal of Clinical Oncology **6**(1), 147–153 (1988)

[18] D J Sugarbaker and J G Garcia. *Multimodality Therapy for Malignant Pleural Mesothelioma.* American College of Chest Physicians **112**, 272–275 (1997)

[19] D J Sugarbaker. *Extrapleural Pneumonectomy in the Multimodality Therapy of Malignant Pleural Mesothelioma.* Annals of surgery **224**(3), 288–296 (1996)

[20] D J Sugarbaker, E C Heher, T H Lee, G Couper, S Mentzer, J M Corson, J J Collins, R Shemin, R Pugatch, L Weissman, and K H Antman. *Extrapleural pneumonectomy, chemotherapy, and radiotherapy in the treatment of diffuse malignant pleural mesothelioma.* J Thorac Cardiovasc Surg **102**, 10–15 (1991)

[21] E G Butchart, T Ashcroft, W C Barnsley, and M P Holden. *Pleuropneumonectomy in the management of diffuse malignant mesothelioma of the pleura.* Thorax **31**, 15–24 (1976)

[22] D J Sugarbaker. *Prevention, early detection, and management of complications after 328 consecutive extrapleural pneumonectomies.* General Thoracic Surgery , 138–146 (2004)

[23] W Weder, P Kestenholz, C Taverna, S Bodis, D Lardinois, M Jerman, and R A Stahel. *Neoadjuvant chemotherapy followed by extrapleural pneumonectomy in malignant pleural mesothelioma.* J Clin Oncol **22**(17), 3451–3457 (2004)

[24] R M Flores. *Extrapleural pneumonectomy versus pleurectomy decortication in the surgical management of malignant pleural mesothelioma: Results in 663 patients.* General Thoracic Surgery , 620–626 (2008)

[25] M Cohen, D E A Jones, and D Greene. *Central Axis Depth Dose Data for Use in Radiotherapy.* British Journal of Radiotherapy **11**, 8–17 (1972)

[26] P Mayles, A Nahum, and J C Rosenman. *Handbook of radiotherapy phyisics.* (2007)

[27] Cern. $http://lasciencepourtous.cafe-sciences.org/articles/tag/cern/$.

[28] $http://varian.mediaroom.com/image-gallery.$, 08.05.2013

[29] S X Chang, T J Cullip, K M Deschesne, E P Miller, and J G Rosenman. *Compensators: An alternative IMRT delivery technique.* Journal of applied clinical medical physics **5**(3), 15–36 (2004)

[30] S Webb. *The physical basis of IMRT and inverse planning.* Br J Radiology **76**, 678–689 (2003)

[31] A Brahme. *Optimization of stationary and moving beam radiation therapy techniques.* Radiother Oncol **12**(2), 129–140 (1988)

[32] J Steel. *Prognostic factors in mesothelioma.* Seminar Oncology **29**(1), 36–40 (2002)

[33] K Otto. *Volumetric modulated arc therapy: IMRT in a single gantry arc.* Med Phys **35**(1), 310–317 (2008)

[34] $http://medicalphysicsweb.org/cws/article/opinion/42793.$, 28.05.2010

[35] $http://radmed.web.psi.ch/asm/gantry/scan/n_scan.html.$, 08.05.2013

[36] C Z Jarlskog and H Paganetti. *Sensitivity of different dose scoring methods on organ-specific neutron dose calculations in proton therapy.* Physics in Medicine and Biology **53**, 4523–4532 (2008)

[37] A Ahnesjo and M M Aspradakis. *Dose calculations for external photon beams in radiotherapy.* Phys. Med. Biol. **44**, 99 – 155 (1999)

[38] R O Ottosson, P E Engstrom, D Sjostrom, Behrens C F, A Karlsson, T Knoos, and C Ceberg. *The feasibility of using Pareto fronts for comparison of treatment planning systems and delivery techniques.* Acta Oncol **48**(2), 233–237 (2009)

[39] A Niemierko. *Reporting and analyzing dose distributions: Aconcept of equivalent uniform dose.* Med Phys **24**, 103 – 110 (1997)

[40] Q Wu, R Mohan, A Niemierko, and R Schmidt-Ullrich. *Optimization of intensity-modulated radiotherapy plans based on the equivalent uniform dose.* Int J Radiat Oncol Biol Phys **52**(1), 224–235 (2002)

[41] B Emami. *Tolerance of normal tissue to therapeutic irradiation.* Int J Radiat Oncol Biol Phys **21**, 109–122 (1991)

[42] M T Milano, L S Constine, and P O Okunieff. *Normal Tissue Tolerance Dose Metrics for Radiation Therapy of Major Organs.* Radiother Oncol **17**(2), 131–140 (2007)

[43] L B Marks. *Use of NormalTissueComplicationProbability Models in the Clinic.* Int J Radiat Oncol Biol Phys **76**(3), 10–19 (2010)

[44] M Van Herk. *Errors and margins in radiotherapy.* Semin Radiat Oncol **14**(1), 52–64 (2004)

[45] J Krayenbuehl, M Hartmann, A J Lomax, S Kloeck, E B Hug, and I F Ciernik. *Proton therapy for malignant pleural mesothelioma after extrapleural pleuropneumonectomy.* Int J Radiat Oncol Biol Phys **78**(2), 628–634 (2010)

[46] D Yan, F Vicini, F Wong, and A Martinez. *Adaptive radiation therapy.* Phys Med Biol **42**(1), 123–132 (1997)

[47] T Li. *On-Line Adaptive Radiation Therapy Feasibility and Clinical Study.* Journal of Oncology , 1–12 (2010)

[48] A Andronache. *Multi-Modal Non-Rigid Registration of Volumetric Medical Images.* Swiss Federal Institute of Technology Zurich (2006)

[49] J B A Maintz and M A Viergever. *A survey of medical image registration.* Medical Image Analysis **2**(1), 1–36 (1998)

[50] P A van den Elsen, E D Pol, and M A Viergever. *Medical Image Matching - A Review with Classification.* IEEE engineering in medicine and biology , 26–39 (1993)

[51] R Stahel, W Weder, I Ciernik, H Moch, and K Ribi. *Protocol SAKK 17/04. Neoadjuvant chemotherapy and extrapleural pneumonectomy of malignant pleural mesothelioma (MPM) with or without hemithoracic radiotherapy. A randomized multicenter phase II trial.* Swiss group for clinical research (2005)

List of publications

[I] Journal Publications

[A] **J Krayenbuehl**, S Oertel, J B Davis and I F Ciernik
Combined photon and electron three-dimensional conformal versus intensity-modulated radiotherapy with integrated boost for adjuvant treatment of malignant pleural mesothelioma after pleuropneumonectomy
Int J Radiat Oncol Biol Phys **24**, S1493-S1599 (2007)

[B] **J Krayenbuehl**, M Hartmann, A Lomax, S Kloeck, E B Hug and I F Ciernik
Proton therapy for malignant pleural mesothelioma after extrapleural pleuropneumonectomy
Int J Radiat Oncol Biol Phys **78**, 628-634 (2010)

[C] **J Krayenbuehl**, O Riesterer, S Graydon, P Dimmerling, S Kloeck and I F Ciernik
Volumetric modulated arc therapy for malignant pleural mesothelioma after extrapleural pneumonectomy
J App Clin Med Phys **14** (2013)

[D] A Andronache, **J Krayenbuehl**, G Szekely and I F Ciernik
Hirarchical enhanced non-rigid registration for target volume correction and propagation for adaptive external beam radiotherapy of carcinoma of the prostate
J App Clin Med Phys, 222-230 (2013)

[E] **J Krayenbuehl**, P Dimmerling, I F Ciernik and O Riesterer
Clinical Outcome of Postoperative Highly Conformal versus 3D Conformal Radiotherapy in Patients with Malignant Pleural Mesothelioma
Radiation Oncology, in press (2014)

[II] Conference Publications

[1] **J Krayenbuehl**, J B Davis, I F Ciernik
Evaluation of two treatment techniques for mesothelioma
ESTRO 2006, Leipzig

[2] **J Krayenbuehl**, I F Ciernik, G Kunz, J B Davis, A J Lomax
Proton radiotherapy versus 3DCRT and IMRT for malignant pleural mesothelioma
SASRO 2007, Aarau

[3] **J Krayenbuehl**, J B Davis, I F Ciernik
Evaluation of mesothelioma air cavities after extrapleural Pleuropneumonectomy
SASRO 2008, Lausanne

[4] **J Krayenbuehl**, G Kunz, M Hartmann , E B Hug, A J Lomax, I F Ciernik
Evaluation of air cavities after extrapleural pleuropneumectomy in mesothelioma patient during IMRT or PT
SASRO 2009, PSI

[5] **J Krayenbuehl**, G Kunz, M Hartmann, A J Lomax, E B Hug, I F Ciernik
Adjuvant proton vs. photon therapy for malignant pleural mesothelioma after extrapleural pleuropneumectomy
8th Day of Clinical Research of University Hospital Zurich, 2009, Zurich

[6] P Dimmerling, D R Zwahlen, **J Krayenbuehl**, C Glanzmann, G Studer, I F Ciernik, O Riesterer
Extrapleural pneumonectomy in patients with malignant pleural mesothelioma
SASRO, 2010, Bern

[7] P Dimmerling, D R Zwahlen, **J Krayenbuehl**, C Glanzmann, G Studer, I F Ciernik, O Riesterer
Intensity Modulated Radiotherapy After Extrapleural Pneumonectomy in Patients with Malignant Pleural Mesothelioma
ESTRO, 2010, Barcelona

[8] **J Krayenbuehl**, S Kloeck, I F Ciernik, O Riesterer
Intensity modulated radiotherapy and volumetric modulated arc radiotherapy for malignant pleural mesothelioma
SASRO, 2011, Geneva

[9] **J Krayenbuehl**, S Kloeck, I F Ciernik, O Riesterer
Intensity modulated radiotherapy and volumetric modulated arc radiotherapy for malignant pleural mesothelioma
10th Day of Clinical Research of University Hospital Zurich, 2011, Zurich

[10] **J Krayenbuehl**, A Andronache, G Szekely, I F Ciernik
Hierarchical enhanced non-rigid registration for target volume correction and propagation for adaptive external beam radiotherapy of carcinoma of the prostate
10th Day of Clinical Research of University Hospital Zurich, 2011, Zurich

[11] **J Krayenbuehl**, M Hartmann, O Riester, T J Lomax, S Kloeck, E B Hug, I F Ciernik
Protonentherapie, intensitaetsmodulierte Strahlentherapie oder volumetrisch modulierte Bogenbestrahlung zur postoperativen Radiotherapie nach extrapleuraler Pleuropneumektomie des Mesothelioms
17. Jahrestagung der Deutschen Gesellschaft fuer Radioonkologie, 2011, Wiesbaden

[12] **J Krayenbuehl**, M Hartmann, O Riester, T J Lomax, S Kloeck, E B Hug, I F Ciernik
Evaluation of different external radiotherapy techniques for the treatment of Malignant Pleural Mesothelioma after Extrapleural Pleuropneumonectomy
11th Day of Clinical Research of University Hospital Zurich, 2012, Zurich

[13] **J Krayenbuehl**, M Hartmann, O Riester, T J Lomax, S Kloeck, E B Hug, I F Ciernik
Evaluation of different external radiotherapy techniques for the treatment of Malignant Pleural Mesothelioma after Extrapleural Pleuropneumonectomy
3rd European Lung Cancer Conference, 2012, Geneva

[14] M Feigen, C Kelsey, V Mehta, J Cho, P Giraud, M A Mahe, M Scorsetti, S Tonoli, F Sterzing, **J Krayenbuehl**, A M Allen
International survey of radiation toxicity following hemithoracic intensity-modulate radiotherapy in patients with malignant pleural mesothelioma
3iMig, 2012, Boston

[15] **J Krayenbuehl**, M Hartmann, O Riester, T J Lomax, S Kloeck, E B Hug, I F Ciernik
Evaluation of different external radiotherapy techniques for the treatment of Malignant Pleural Mesothelioma after Extrapleural Pleuropneumonectomy
ASTRO 54th annual meeting, 2012, Boston

[16] **J Krayenbuehl**, M Hartmann, O Riester, T J Lomax, S Kloeck, E B Hug, I F Ciernik
Intensity Modulated Radiotherapy After Extrapleural Pneumonectomy in Malignant Pleural Mesothelioma Patients
ESTRO, 2013, Geneva

[17] **J Krayenbuehl**, A Androache, G Szekely, IF Ciernik
Hierarchical enhanced non-rigid registration for target volume correction and propagation for adaptive external beam radiotherapy of carcinoma of the prostate
ESTRO 2013, Geneva

[18] P Dimmerling, **J Krayenbuehl**, I F Ciernik, O Riesterer
Clinical outcome after treatment with highly-conformal modulated beam radiotherapy of patients with operable malignant pleural mesothelioma
SASRO, 2013, Davos

Acknowledgements

I wish to express my gratitude to all of you who contributed to the completion of this work:

First, I would like to express my gratitude to Prof. Dr. Martin Pruschy for giving me the possibility to do a PhD at the University of Zurich and taking care of the administrative work.

I would like to thank Prof. Dr. Ilja Ciernik for his support, enthusiasm and inspiring discussion. It was for me a successful and stimulating collaboration. Thanks for the great job with this project.

Many thanks go to Dr. Stephan Klöck for being a great supervisor, who gave valuable support during the last three years.

I would like to than Dr. Adrian Andronache and Prof. Gabor Szekely for the fruitful collaboration on the image registration.

I would like to thank Prof. Dr. Michael Hengartner for accepting to be the co-examiner of my thesis.

Thanks to all the past and present members of the Radiation and Oncology team for the nice working atmosphere.

Last but not least, I would like to thank my wife Axelle who supported me and proof-reading my manuscripts. Without her, it would have been, for sure, much harder to finish this work.

Curriculum Vitae

Personal data

Name	Krayenbühl
First names	Jérôme
Date of birth	11.4.1975
Nationality	Swiss
Citizen	St-Sulpice (VD)

Education

1991–1994	High school in Lausanne Diplôme général scientifique
1994–1995	Cours de mathématiques spéciales, EPFL
1995–2001	Studies of Physics at the University of Lausanne
March 2001	Graduation with a Diploma in Physics (Master of Science) at the Institute of Condensed Matter at the Laboratory of Physics of Living Matter
2001–2002	Teaching certificate, Lausanne
2004–2006	Master of Advanced Studies in Medical Physics, ETHZ
2010–2013	PhD Student at the Faculty of Science (MNF), University of Zurich
January 2014	Ph.D. examination

Working Experience

2001–2003	Science and Math teacher, Moudon
2003–2007	Medical physicist at University Hospital Zurich
2007–2008	Medical physicist at Cantonal Hospital Chur
2008–2014	Medical physicist at University Hospital Zurich

Zurich, January 2014 Jérôme Krayenbühl

1 Combined photon and electron three-dimensional conformal versus intensity-modulated radiotherapy with integrated boost for adjuvant treatment of malignant pleural mesothelioma after pleuropneumonectomy

J. Krayenbuehl[1], S. Oertel[1], J.B. Davis[1], I.F. Ciernik[1, 2]

[1] Department of Radiation Oncology, Zurich University Hospital, Zurich, Switzerland

[2] Oncology Institute of Southern Switzerland, Ospedale San Giovanni e Valli, Bellinzona, Switzerland

Status of the manuscript: published in *International Journal of Radiatiation, Oncology, Biology and Physics* 2007 Dec 1;69(5):1593-9 (2007)

Author contribution J. Krayenbuehl: planning, data analysis and interpretation of all data, manuscript drafting, revision and editing.

1.1 Abstract

The optimal technique for postoperative radiotherapy (RT) after extrapleural pleuropneumonectomy (EPP) of malignant pleural mesothelioma (MPM) remains debated.

The data from 8 right-sided and 9 left-sided consecutive cases of MPM treated with RT after radical EPP were reviewed. Of the 17 patients, 8 had been treated with three-dimensional (3D) conformal RT (3D-CRT) and 9 with intensity-modulated RT (IMRT) with 6-MV photons. The clinical outcome and adverse events were assessed. For comparative planning, each case was replanned with 3D-CRT using photons and electrons or with IMRT. Homogeneity, doses to the organs at risk, and target volume coverage were analyzed.

Both techniques yielded accepteble plans. The dose coverage and homogeneity of IMRT increased by 7.7 % for the first planning target volume and 9.7 % for the second planning target volume, ensuring $\geq$ 95 % of the prescribed dose compared with 3D-CRT ($p < 0.01$). Compared with 3D-CRT, IMRT increased the dose to the contralateral lung, with an increase in the mean lung dose of 7.8 Gy and an increase in the volume receiving 13 Gy and 20 Gy by 20.5 % and 7.2 %, respectively ($p < 0.01$). A negligible dose increase to the contralateral kidney and liver was observed. No differences were seen for the spinal cord and ipsilateral kidney. Two adverse events of clinical relevant lung toxicity were observed with IMRT.

Intensity-modulated RT and 3D-CRT are both suitable for adjuvant RT. IMRT improves the planning target volume coverage but delivered greater doses to the organs at risk. Rigid dose constraints for the lung should be respected.

1.2 Introduction

The role of radiotherapy (RT) for palliative treatment of malignant pleural mesothelioma (MPM) is well established [1, 2]. RT is effective for pain control in the case of thoracic wall invasion and is used for the prevention of malignant seeding after invasive procedures [3, 4]. The role of RT within the setting of radical multimodal therapy is less well defined, although the thoracic relapse rates after extrapleural pleuropneumonectomy (EPP) of MPM are high and adjuvant treatment is warranted. In recent years, adjuvant RT has been advocated as a part of postoperative therapy, and various techniques with different field geometries and dose schedules have been used [5, 6]. More recently, neoadjuvant therapy with preoperative chemotherapy

has been added to the treatment concept and has shown promising results in specialized institutions [7].

The best-documented multimodal potentially curative approach to MPM is pleuropneumonectomy, combined with chemotherapy and RT (trimodality approach) in selected patients with early disease stages. The survival rate of a large series of 176 patients after surgery was 38 % at 2 years and 15 % at 5 years, with a median survival of 19 months [5]. More recently, preoperative chemotherapy followed by EPP has been investigated, and its feasibility has been reported in a multicenter trial [7, 8]. The benefit of preoperative chemotherapy, however, will remain difficult to prove unless randomized trials are initiated. In some cases, operable disease might progress during chemotherapy, rendering subsequent resection more difficult. In our experience, the overall treatment time resulting from combined chemotherapy followed by surgery and the protracted therapy-associated stress on patients have made postoperative RT potentially more difficult and more challenging [9]. The radiation oncologist has to decide whether full coverage of the hemithorax can be proposed or a treatment volume limited to the initial tumor region is sufficient and feasible after chemotherapy and EPP in each case. There is little doubt that preoperative chemotherapy can jeopardize the benefits from RT because of cumulative toxicity and treatment-related asthenia. Furthermore, no standard for either chemotherapy or RT exists. In particular, the acceptable size of the target volumes, dose constraints, and radiation techniques should be considered before implementation of RT in multimodal settings.

We evaluated two RT techniques that were used in our center for the purpose of RT after chemotherapy and surgery for MPM: three-dimensional (3D) conformal RT (3D-CRT), used until 2004, and intensity-modulated RT (IMRT). With both planning techniques, the entire ipsilateral hemithorax was defined as the clinical target volume (CTV2), with a high-risk area represented by the macroscopically resected tumor (CTV1).

1.3 Methods and materials

For this retrospective treatment planning study, we reviewed the clinical records of all patients (n = 17) diagnosed with MPM between 2000 and 2006 who were treated with chemotherapy followed by EPP and RT. All patients had presented with Stage cT1-T3 N0-N1 M0. Mediastinal staging was done using computed tomography (CT) and positron emission tomography/CT. Mediastinoscopy was performed in all patients to exclude mediastinal involvement; patients with mediastinal involvement did not qualify for EPP.

The performance status before RT was Eastern Cooperative Oncology Group score of ≤ 2 in all patients. Lung function before RT was assessed, and the requirements for RT was a forced expiratory volume in 1 s of >1 L. In brief, chemotherapy consisted of three cycles of pemetrexed 500 mg/m^2 and cisplatin 75 mg/m^2, repeated after 21 days for a total of three cycles. Surgery was done as described previously [7]. In brief, EPP yielded complete resection of all macroscopic tumor, and resection of invaded areas with suspected microscopic spread of the thoracic wall, diaphragm, or pericardium was accomplished in each case. Reconstruction of the diaphragm was done in 11 patients. Of the 17 patients, 8 were treated with a conventional photon technique (mean dose 53 Gy) and 9 with IMRT (mean dose, 55.9 Gy). All cases were retrospectively replanned with IMRT or the conventional electron-photon technique to compare the two techniques [10, 11]. The patient group consisted of 2 women and 15 men. At diagnosis, the median age was 60 years (range, 46 - 66 years).

The patients were immobilized in the supine position using a body cast and wing board, with their arms extended above their heads to grab a T-bar. The planning CT scan was based on 3-mm CT slices with no gap. Two CTVs were defined, from which the planning target volumes (PTVs) were derived. CTV2 was defined as the field of surgery, including the entire preoperative pleural and pulmonary structures and the surgical scars. CTV1 was defined as the area at risk of residual postoperative microscopic disease or the area of greatest risk of intrathoracic relapse, as determined by the surgeon. After complete resection (R0 or R1), no macroscopic tumor was visible on the postoperative radiographs. Thus, no gross tumor volume was available. The CTVs were defined by the risk of relapse. CTV2 covered low-risk areas (< 50 Gy), and CTV1 covered high-risk areas, resulting in high-dose areas (> 50 Gy). A working CTV2 (wCTV2) was established first. The wCTV2 covered the inner border of the thoracic cavity, the diaphragm, and the mediastinum and surgical channels and was outlined using computerassisted 3D contouring. With respect to the mediastinum, the ipsilateral hilar, subcarinal, lower and upper ipsilateral paratracheal, and prevascular and retrotracheal lymph nodes were included in the wCTV2. The para-aortic and subaortic lymph nodes were included for left-sided disease or if nodal involvement had been documented in right-sided disease. The paraesophageal lymph nodes and lymph nodes of the pulmonary ligament were not included in the wCTV2, unless microscopic contamination was suspected. The wCTV2 was expanded to the final CTV2 with a margin of 0.4 - 0.5 cm. CTV1 was defined by the areas of macroscopic tumor and, after detailed review of the CT scans with the surgeon, included the areas of increased risk of relapse and macroscopic disease, which might have been perceived differently during surgery than on

the preoperative CT scans. The CTVs were expanded to the PTV, respecting internal target movement variability and setup variability. The PTVs were used for RT planning. The PTV2 margins were 1.2 - 1.5 cm in the caudal direction, 1.0 cm in the cranial direction, 0.6 cm in the dorsal direction, 1.2 cm in the anterior direction, and 0.8 cm in the lateral direction. The PTV1 margins respected the localization of the CTV1. If the CTV1 was located in the upper one-half of the hemithorax, breathing movements were assumed to be less prominent than for CTV2s located in the lower hemithorax or adjacent to the diaphragm. The PTV margins for CTV1 in the upper hemithorax were 1.0 - 1.2 cm in the caudal direction, 0.8 - 1.0 cm in the cranial direction, 0.6 cm in the dorsal direction, 1.0 cm in the anterior direction, and 0.7 - 0.8 cm in the lateral direction. If the CTV1 was located in the lower hemithorax, the PTV margins were 1.2 cm in the caudal direction, 1.0 cm in the cranial direction, 0.6 cm in the dorsal direction, 1 cm in the anterior direction, and 0.8 cm in both lateral directions. An example of a series of three coronal views of a representative case is shown in Fig. 1.1.

1.3.1 Three-dimensional CRT

The treatment plan of the 3D-CRT patients included 25 x 1.8 Gy to the PTV1 and PTV2 followed by 7 x 1.8 Gy only to the PTV1. The ipsilateral kidney (or liver, respectively) was shielded during the entire treatment from the posteroanterior (anteroposterior and posteroanterior, respectively) direction. The heart was shielded with a block after 19.8 Gy. When any point of the spinal cord reached a dose of 45 Gy, the spinal cord was shielded. The target volumes shielded because of dose limitations to the organs at risk (OARs), regions under the ipsilateral kidney (or the liver in the case of right-sided disease), retrocardiac space, and spinal cord were treated with electrons as described previously by Kutcher et al. [12]. To compensate for the blocked areas, electron fields were used. The electron energy range was 9 - 16 MeV, and the photon energy was 6 or 18 MV. The electron fields accounted for block transmission. The gantry angle used for the electrons and photons fields was 0°and 180°, respectively. With this beam configuration, we obtained the best compromise between target coverage and myelin avoidance. In 2 patients with left-sided disease, the PTV1 was dorsally and laterally located, and customized gantry angles were used for the last seven fractions (from 45 Gy to 57.6 Gy). The photon beams angles used in these 2 cases were 190°and 45°for the first case and 200°and 40°for the second case. No electron fields were used in these 2 cases, because the OARs were out of the fields. The dose calculation for electrons and photons was performed on Pinnacle (Philips Medical Systems) for a linear accelerator (Clinac 2100C, Varian Medical

Systems, 80 multileaf collimator). The 3D-CRT plans were not delivered as calculated in the present study. All patients were treated without electron fields, and the corresponding clinical results have been previously reported [7].

1.3.2 Intensity-modulated RT

Five radiation beams were used in the optimized IMRT plans for each patient. The beam angles were patient-specific and ranged from 170°to 30°for left-sided tumors and 330°and 200°for right-sided tumors. The angles between two consecutive beams ranged from 45°to 70°. An example of a gantry set used for a right-sided tumor was 170°, 220°, 280°, 330°, and 20°, and for a left-sided tumor was 345°, 30°, 80°, 140°, and 195°. The gantry angles used for the left sided tumor were used for the treatment of the targets displayed in Fig. 1.1. The red structure represents the PTV1 and the green structure the PTV2. The treatment of the IMRT patients was planned using 26 x 1.75 Gy (45.5 Gy) to the PTV2, including a simultaneously integrated boost of 26 x 2.15 Gy (55.9 Gy) to the PTV1.

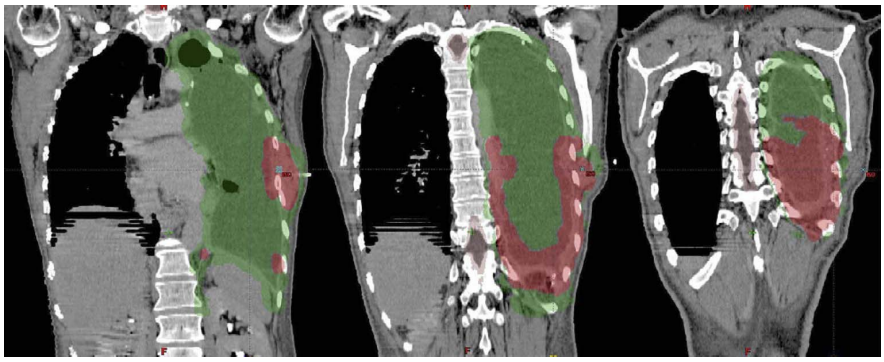

Figure 1.1: Target volume definition. Areas of previous macroscopic tumor involvement and areas causing surgical difficulties during radical resection were treated with additional integrated or sequential boost, planning target volume 1 (PTV1) (red). PTV2 (green) represents areas of previous pleural extension.

Dose calculation and optimization were done using an inverse treatment planning system, (HELIOS, Eclipse, version 7.3.2, Varian Medical Systems). Treatment was delivered using a 6-MV linear accelerator (Clinac 6EX, Varian

Medical Systems, 120 leaf Millennium multileaf collimator) using the sliding-window technique.

Before the first session, quality assurance is routinely done. Quality assurance is done using three different modalities: (1) film dosimetry, (2) ionization chamber measurements; and (3) software verification. For film dosimetry, the film (Kodak EDR2 Film, Eastman Kodak, Rochester, NY) was placed horizontally at the isocenter under 5 cm equivalent water. The gantry angle was set to 0°. A γ evaluation was performed for each single field with an acceptance level of 5 % and 3 mm with our treatment planning system. For the ionization chamber measurements, a PTW Farmer chamber, 0.6 cm^3 was used, and the measurements were done at the isocenter in a cylindrical water equivalent phantom. A deviation of less than 5 % per beam with our treatment planning system was accepted. Finally, the dose at the isocenter was verified with an independent software program (RadCalc, LifeLine Software, Tyler, TX) for each field. A deviation of less than 5 % per beam with our treatment planning system was accepted. An overall error of dose delivery inaccuracy of less than 3 % was requested. All plans had to fulfill these criteria before the first treatment session.

1.3.3 Dose-volume constraints

The dose - volume constraints are listed in Table 1.1. The dose constraints applied were calculated to 2 Gy/d equivalent dose, respecting an $\frac{\alpha}{\beta}$ ratio of 3. The maximal dose to any part of the spinal canal was kept at < 50 Gy. The mean dose given to the heart was limited to < 40 Gy, and the maximal heart volume receiving 45 Gy was kept to < 30 %. The maximal mean lung dose allowed was 15 Gy, and not >10 % of the lung volume could receive > 20 Gy. The mean dose to the liver was not allowed to be $> 3\ 0$ Gy. The maximal mean dose to the kidneys allowed was 12 Gy, and the volume receiving > 15 Gy was kept at < 20 %.

1.3.4 Plan comparision

For the comparison of the treatment plans, the dose - volume histograms (DVHs) were normalized, so that the mean dose of PTV1 was equal to 55.9 Gy (2.15 Gy for 26 fractions). IMRT and 3D-CRT were compared using DVH parameters after normalization for a single dose prescription.

Normal tissue	Constraints
Spinal cord	
Maximal dose (Gy)	< 50
Liver	
Mean dose (Gy)	< 30
Kidney	
Mean dose (Gy)	< 12
V15 (%)	< 20
Lung	
Mean dose (Gy)	< 15
V20 (%)	< 10
Heart	
Mean dose (Gy)	< 40
V45 (%)	< 30

Table 1.1: IMRT optimization parameters. *Abbreviations*: IMRT = intensity-modulated radiotherapy; V_{15}, V_{20}, V_{45} = volume of organ receiving dose of $\geq$15, $\geq$20, $\geq$45 Gy, respectively.

1.3.5 Statistical analysis

Statistical analysis was performed using a paired t-test. The t-test and p value were calculated with the software StatView (version 5.0.1) (SPSS Inc., Chicago, IL). A p - value of < 0.05 was accepted as significant.

1.4 Results

The percentage of the PTVs receiving < 95 % and the percentage receiving > 105 % of the prescribed dose were assessed for 3D-CRT and IMRT. The mean dose for all structures was assessed. The percentage of the kidney (or heart) receiving > 15 Gy (or 45 Gy), the percentage of the lung receiving > 13 and 20 Gy, and the maximal dose to the spinal cord were evaluated Table 1.2. The reported values were averaged for the 17 MPM patients from the present study. Dose delivery to the PTV was improved using IMRT. Dose homogeneity was also improved with IMRT. The volume covered by the 95 % isodose was increased by 7.7 % for PTV1 ($p = 0.01$) and by 9.7 % for PTV2 ($p < 0.01$). The volume covered by the 105 % isodose was reduced with IMRT compared with 3D-CRT by 17.6 % for PTV1 ($p = 0.01$) and 27.4 % for PTV2 ($p =$ NS).

Parameter	3D-CRT	IMRT	Mean difference	p*
PTV1 receiving 95% of prescribed dose (%)	88.3 ± 11.2	96 ± 2.9	7.7	< 0.01*
PTV1 receiving 105% of prescribed dose (%)	21.3 ± 23.2	3.7± 4.8	17.6	0.02*
PTV2 receiving 95% of prescribed dose (%)	85 ± 5.9	94.7 ± 3.8	9.7	< 0.01*
PTV2 receiving 105% of prescribed dose (%)	45.2 ± 15	27.8 ± 22.6	27.4	0.08
Maximal dose to spinal cord (Gy)	42.9 ± 4.6	40.1 ± 4.0	2.8	0.13
Mean dose to contralateral kidney (Gy)	0.5 ± 0.5	4.1 ± 1.7	3.6	< 0.01*
Contralateral kidney receiving V15 (%)	0.2 ± 0.7	1.0 ± 3.4	0.8	0.46
Mean dose to ipsilateral kidney (Gy)	11.0 ± 5.7	11.4 ± 5.7	0.4	0.8
Ipsilateral kidney receiving V15 (%)	38 ± 22	25 ± 19	13	0.08
Mean dose to liver (Gy)	5.2 ± 6.5	13.2 ± 6.7	8	< 0.01*
Mean dose to heart (Gy)	17.1 ± 10.5	26.2 ± 6.2	9.1	< 0.01*
Heart receiving V45 (%)	1.0 ± 1.9	1.6 ± 2.0	0.6	0.3
Mean dose to lung (Gy)	1.2 ± 0.9	9.0 ± 1.4	7.8	< 0.01*
Lung receiving V13 (%)	0.8 ± 1.1	21.3 ± 10.6	20.5	< 0.01*
Lung receiving V20 (%)	0.5 ± 0.7	7.7 ± 5.6	7.2	< 0.01*

Table 1.2: DVH details for all 17 patients for 3D-CRT and IMRT plans. *Abbreviations*: DVH = dose - volume histogram; 3D - CRT = three - dimensional conformal radiotherapy; PTV = planning target volume; V13 = volume receiving ≥13 Gy; other abbreviations as in Table 1.1. Data presented as mean ± standard deviation. ∗ Statistically significant ($p < 0.05$); 3D - CRT vs. IMRT, paired t - test).

An example of the dose distribution at the level of the isocenter for the 3D-CRT and IMRT plans is shown in Fig. 1.2. On these two slices, IMRT displayed better coverage of the PTV2 (green structure). The heart dose and lung dose were slightly larger than with 3D-CRT. Fig. 1.3 and Fig. 1.4 show the mean DVH average for all the MPM patients for 3D-CRT (plain line) and IMRT (dotted line). The DVHs were normalized to 55.9 Gy at 100 % of the mean dose to the PTV1. A better coverage of the PTVs was observed with IMRT, but a lower dose to the liver, lung, and contralateral kidney (or heart) was achieved with 3D-CRT.

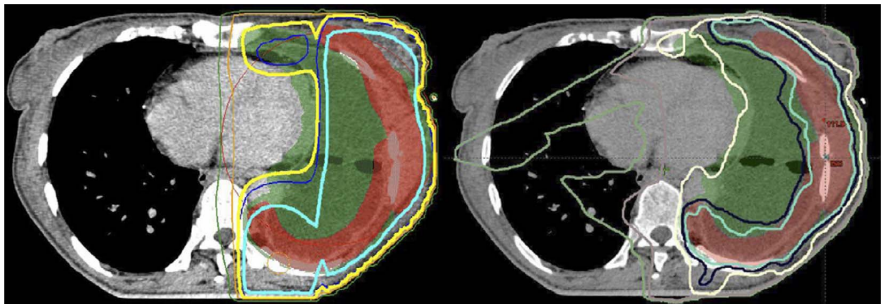

Figure 1.2: Isodose distribution of representative transverse slice (planning target volume 1 (PTV1) in red and PTV2 in green) for (Left) three-dimensional conformal radiotherapy (3D - CRT) and (Right) intensity-modulated radiotherapy (IMRT). Gantry angles for IMRT beams were 345°, 30°, 80°, 140°, and 195°. Beam angle for 3D - CRT was 0°and 180°for photons and electrons, respectively. Green, brown, blue, and cyan isodose lines represent 20 %, 50 %, 90 %, and 95 % of prescribed dose (55.9 Gy for IMRT and 57.6Gy for 3D - CRT), respectively. Yellow isodose line represents 95 % of prescribed dose to PTV2 dose (45.5 Gy for IMRT and 45 Gy for 3D - CRT).

1.4.1 Organs at risk

Both techniques were able to keep the maximal spinal cord dose to less than its tolerance limits. A non significant reduction of 2.8 Gy to the maximal dose was achieved with IMRT compared with 3D-CRT (p = NS), as indicated in Table 1.2. The maximal spinal cord dose was kept to < 47 Gy for each patient with both techniques.

The mean contralateral dose delivered to lung tissue was increased by

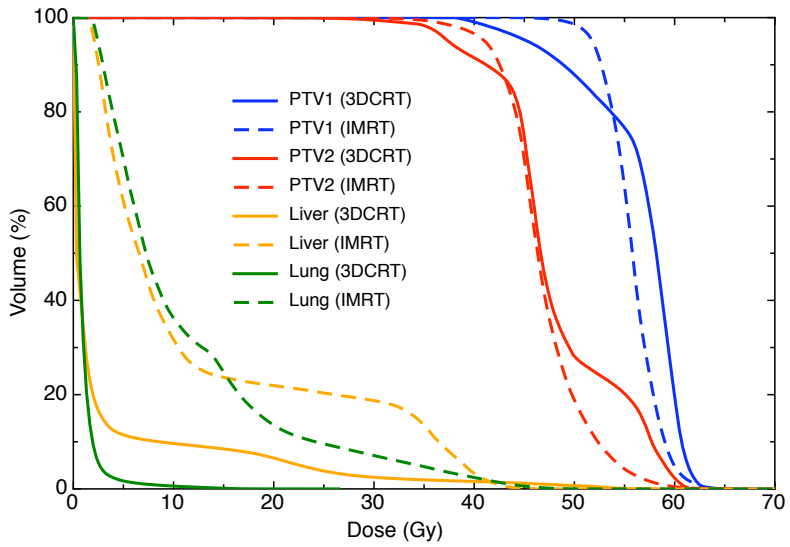

Figure 1.3: Mean dose - volume histogram (DVH) of planning target volume 1 (PTV1) (blue), PTV2 (red), liver (orange), and lung (green). DVHs normalized to 55.9 Gy at 100 % of mean dose to PTV1. Solid lines represent three-dimensional conformal radiotherapy (3D - CRT) plans, and dotted lines represent intensity-modulated radiotherapy (IMRT) plans.

7.8 Gy ($p < 0.01$) and the volume receiving a dose > 13 Gy (or > 20 Gy) increased by 20.5 % (or > 7.2 %) with IMRT ($p < 0.01$, or $p < 0.01$).

The mean heart dose increased with IMRT compared with 3D-CRT by 9.1 Gy, from 17.1 Gy to 26.2 Gy ($p < 0.01$). No difference was observed for the heart volume receiving a dose > 45 Gy (Table 1.2).

The mean dose delivered to the contralateral kidney was reduced with 3D-CRT by 3.6 Gy from 4.1 Gy to 0.5 Gy ($p < 0.01$). No difference in dose delivery > 15 Gy to the contralateral kidney was observed for 3D-CRT and IMRT, nor was the difference in the mean dose or the volume of the ipsilateral kidney receiving a dose > 15 Gy significant.

1.4.2 Patient outcome and toxicities

The clinical outcome of all 17 patients, treated with 3DCRT using photons before February 2005 and with IMRT after February 2005 was analyzed. At follow-up, 6 patients had died (mean time between treatment onset and

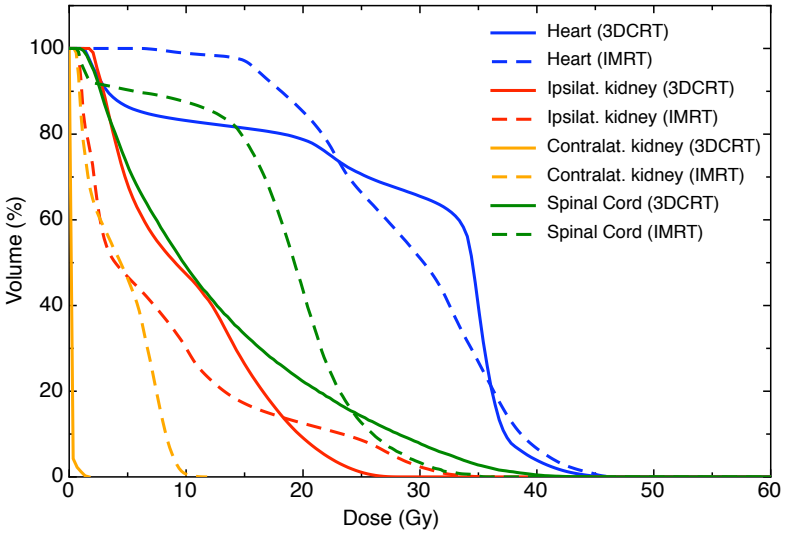

Figure 1.4: Mean dose - volume histogram (DVH) of heart (blue), ipsilateral kidney (red), contralateral kidney (orange), and spinal cord (green) for three-dimensional conformal radiotherapy (3D - CRT) (solid lines) and intensity-modulated radiotherapy (IMRT) (dotted lines).

death, 22.5 months). All had experienced disease recurrence before death. Six additional patients experienced local failure. Local failure occurred after a mean of 18 months (range, 14 - 29 months). Adverse events exceeding Common Toxicity Criteria Grade 2 were observed in 2 patients, both of whom had received IMRT.

One patient developed pneumonitis 2 weeks after RT was completed. He was admitted to the intensive care unit and received oxygen for 5 days. He had recovered completely within the next 2 weeks. The mean dose to the lung was 8 Gy, comparable to the mean lung dose in all IMRT patients (Table 1.2). However, the volume of the pleural cavity receiving > 50 Gy was six times larger than average.

A second patient with severe post-RT toxicity was admitted to the hospital with suspected pneumonitis 1 week after the end of RT. The mean lung dose had been 10 Gy compared with a mean dose of 6.9 ± 1.4 Gy in the whole cohort of patients treated with IMRT without complications. He died after 3 weeks of cardiopulmonary failure. The autopsy revealed chronic empyema

and consolidative bacterial pneumonia, as well as residual mesothelioma in the mediastinal region. The event was scored as a lung-associated adverse event, Common Toxicity Criteria Grade 5.

The volume receiving $\leq$ 5 Gy (V5) in Patient 1 was 61 % and was 92 % in Patient 2. The volume receiving $\leq$ 20 Gy (V20) was 4.7 % in Patient 1 and 3.9 % in Patient 2. In contrast to the V20, the V5 in Patient 2 significantly exceeded the mean values (6.8 % $\pm$ 4.6 % for V20, range, 0.5 - 17 %; and 58 % $\pm$ 20 % for V5, range, 44 - 88 %) of the IMRT patients without complications. The PTV2 in both patients was comparable to that in the whole cohort; however, the high-dose area (PTV1) was significantly greater in Patient 1 (Table 1.3).

Parameter	Patient 1 (post-IMRT lung toxicity CTC Grade 4)	Patient 2 (post-IMRT lung toxicity CTC Grade 5)	No lung toxicity after IMRT* (n = 7)
V5 (Gy)	61	92	58 ± 20
V20 (Gy)	4.7	3.9	6.8 ± 4.6
Mean dose to contralat. lung (Gy)	7.8	9.8	6.9 ± 1.4
PTV1 (cm^3)	3'215	387	471 ± 462

Table 1.3: DVH parameters of IMRT patients with and without lung toxicity. *Abbreviations*: CTC = Common Toxicity Criteria; other abbreviations as in Table 1.1 and Table 1.2

1.5 Discussion

Continuously improving technology have led to improved dose conformity and increasing interest in integrating RT in the treatment concepts of MPM [13, 14]. Because IMRT is an optimal technical approach for treating concave regions with many critical and radiation-sensitive tissue structures in close proximity to the targeted region, it seems especially well suited for the treatment of MPM, especially because greater conformity has the potential to improve the effect of RT [15]. However, more recently, IMRT for MPM has come into discredit after the report of high rates of pneumonitis after EPP. In a recently published series, 46 % of the patients died of pneumonitis within a median of 1 month [16]. Thus, a prudent and well-optimized treatment design with the most appropriate technology seems to be essential in the treatment of MPM patients with ionizing RT. How to optimize and define dose-volume constraints to target volumes and OARs continues to be debated, and the contralateral lung is of special concern if IMRT should remain an option for postoperative RT for MPM.

The major advantage of 3D-CRT is that protection of contralateral lung tissue is easy, because no photon beams penetrate the contralateral lung. Comparing the mean dose and lung V5 and V20, 3D-CRT performs better than IMRT. However, whether the greater dose delivered to the contralateral lung necessarily results in a proportional increase in the risk of pneumonitis remains to be proved.

In the present comparative technique study, the statistical analysis and clinical follow-up, at least to some extent, have helped to judge the role of IMRT. The pneumonitis rate for IMRT after EPP in our series seemed quite high, with lung-associated toxicities in 2 (22 %) of 9 patients. These observations and the reported incidence of 10 % of lung toxicity for patients treated to a mean lung dose of < 15 Gy reported by others highlight the need for rigorous dose constrains [17, 18]. A recent report analyzing pneumonitis incidents after IMRT showed that adherence to constraints that generally considered only the mean and maximal dose to the OARs might not be enough and that the V5 might be a better predictor of pneumonitis than the mean lung dose or the lung V20 [19]. As shown in Table 1.3, we did not observe large differences in the V20 or mean dose between the 2 IMRT patients with lung-associated toxicities and the other 7 IMRT patients. However, in the patient who developed pneumonitis, the volume receiving the simultaneous integrated boost was significantly greater (3,215 cm^3 vs. 766 cm^3). The patient who died of cardiopulmonary failure had had a significantly greater V5 of 92 % compared to a mean V5 of 58 % $\pm$ 20 % in the IMRT group without complications. Wang et al. [20] proposed a cutoff of 40 % in their series to

avoid lung toxicity. In present series, a cutoff of 50 - 60 % seems acceptable. As indicated by the case of Patient 1, the total volume of the hemithorax receiving > 50 Gy must also likely be weighed to properly estimate the lung toxicity.

Although the present numbers were too low to allow a definite conclusion, taking into account observations from other investigators, we propose redefining the OAR constraints for IMRT to minimize the incidence of pneumonitis after IMRT. We recommend maintaining the mean lung dose as a value for reporting and decision making and propose to limit it to 10 Gy to lung tissue for IMRT. The V20 should be kept $\leq$ 10 %, if possible, and the V5 should be $\leq$ 60 % and, if feasible, $\leq$ 50 %.

In the present series, all patients were treated with IMRT using a simultaneous integrated boost technique. This approach allowed us to deliver > 2 Gy/d to defined subregions of PTV2. More information and controlled clinical experience concerning the tolerance of large volumes treated with a simultaneous integrated boost is needed. At this point, we suggest reducing the PTV1 (the volume that received $\leq$ 54 Gy in our series) to $\leq$ 750 cm^3. We estimate that by implementing these stringent constraints, serious lung toxicities can be maintained at < 5 % and the incidence of fatal pneumonitis counterbalanced [16].

The balance between toxicity and efficacy seems to be a determinant for MPM treatment, because improved local tumor control after PEE is a prerequisite for better survival rates. Thus, "cold and hot spots" represent a problem inherent to 3D-CRT. Matching of photons and electrons is difficult, and poor matching would result in > 20 % dose inhomogeneity in the junction area. In addition, because the spinal cord is blocked when the dose to it reaches 45 Gy, insufficient dose delivery to the superior mediastinum has been observed [21], resulting in underdosage to critical areas [11, 12]. Assuming that homogenous high dose delivery reduces the risk of local relapse, IMRT should be the preferential initial approach for adjuvant RT after EPP. Three-dimensional conformal RT should only be used if IMRT techniques exceed the toxicity constraints. Moreover, IMRT allows one to also escalate the dose to the area of greatest risk with the best conformity using an simultaneously integrated or sequential boost.

1.6 Conclusion

Both 3D-CRT and IMRT might be adequate techniques for the treatment of MPM. In the present study, 3D-CRT and IMRT were both able to keep the maximal and mean doses in the OARs to less than the reported critical

levels. However, after preoperative chemotherapy and EPP, the dose constraints must be reduced to respect the specific case. An individualized use of techniques respecting patient- and disease-specific features is the key for optimal use of RT. Still, IMRT seems to be the superior technique to deliver greater doses with better dose homogeneity, even though the larger doses to the OARs, especially in the contralateral lung, must be taken into consideration. Currently, we recommend constraints for the lung of 5 Gy delivered to $\leq$ 60 %, with $\leq$ 50 % preferable, if possible, and a mean total lung dose of $\leq$ 13 Gy, with <10 Gy, preferable, if possible.

Bibliography

[1] C W Stevens, K M Forster, W R Smythe, and D Rice. *Radiotherapy for mesothelioma.* Hematol Oncol Clin North Am **19**(6), 1099–1115 (2005)

[2] F M Kong, L Zhao, and J A Hayman. *The role of radiation therapy in thoracic tumors.* Hematol Oncol Clin North Am **20**(2), 363–400 (2006)

[3] L de Graaf-Strukowska, J van der Zee, W van Putten, and S Senan. *Factors influencing the outcome of radiotherapy in malignant mesothelioma of the pleura–a single-institution experience with 189 patients.* Int J Radiat Oncol Biol Phys **43**(3), 511–516 (1999)

[4] C Boutin, F Rey, and J R Viallat. *Prevention of malignant seeding after invasive diagnostic procedures in patients with pleural mesothelioma. A randomized trial of local radiotherapy.* Chest **108**(3), 754–758 (1995)

[5] D J Sugarbaker, R M Flores, M T Jaklitsch, W G Richards, G M Strauss, J M Corson, M M DeCamp, S J Swanson, R Bueno, J M Lukanich, E H Baldini, and S J Mentzer. *Resection margins, extrapleural nodal status, and cell type determine postoperative long-term survival in trimodality therapy of malignant pleural mesothelioma: results in 183 patients.* J Thorac Cardiovasc Surg **117**(1), 54–63 (1999)

[6] L R Holsti, S Pyrhonen, M Kajanti, M Mantyla, K Mattson, P Maasilta, and L Kivisaari. *Altered fractionation of hemithorax irradiation for pleural mesothelioma and failure patterns after treatment.* Acta Oncol **36**(4), 397–405 (1997)

[7] W Weder, P Kestenholz, C Taverna, S Bodis, D Lardinois, M Jerman, and R A Stahel. *Neoadjuvant chemotherapy followed by extrapleural pneumonectomy in malignant pleural mesothelioma.* J Clin Oncol **22**(17), 3451–3457 (2004)

[8] J Steel. *Prognostic factors in mesothelioma.* Seminar Oncology **29**(1), 36–40 (2002)

[9] I Opitz, P Kestenholz, D Lardinois, M Muller, V Rousson, D Schneiter, R Stahel, and W Weder. *Incidence and management of complications after neoadjuvant chemotherapy followed by extrapleural pneumonectomy for malignant pleural mesothelioma.* Eur J Cardiothorac Surg **29**(4), 579–584 (2006)

[10] S Yajnik, K E Rosenzweig, B Mychalczak, L Krug, R Flores, L Hong, and V W Rusch. *Hemithoracic radiation after extrapleural pneumonectomy for malignant pleural mesothelioma.* Int J Radiat Oncol Biol Phys **56**(5), 1319–1326 (2003)

[11] V Gupta, B Mychalczak, L Krug, R Flores, M Bains, V W Rusch, and K E Rosenzweig. *Hemithoracic radiation therapy after pleurectomy/decortication for malignant pleural mesothelioma.* Int J Radiat Oncol Biol Phys **63**(4), 1045–1052 (2005)

[12] G J Kutcher, C Kestler, D Greenblatt, H Brenner, B S Hilaris, and D Nori. *Technique for external beam treatment for mesothelioma.* Int J Radiat Oncol Biol Phys **13**(11), 1747–1752 (1987)

[13] C W Stevens, P F Wong, D Rice, M Jeter, K Forster, and X R Zhu. *Treatment planning system evaluation for mesothelioma IMRT.* Lung Cancer **49**(Suppl 1), 75–81 (2005)

[14] M W Munter, C Thieke, A Nikoghosyan, S Nill, and J Debus. *Inverse planned stereotactic intensity modulated radiotherapy (IMRT) in the palliative treatment of malignant mesothelioma of the pleura: the Heidelberg experience.* Lung Cancer **49**(Suppl 1), 83–86 (2005)

[15] A Ahamad, C W Stevens, W R Smythe, A A Vaporciyan, R Komaki, J F Kelly, Z Liao, G Starkschall, and K M Forster. *Intensity-modulated radiation therapy: a novel approach to the management of malignant pleural mesothelioma.* Int J Radiat Oncol Biol Phys **55**(3), 768–775 (2003)

[16] A M Allen, M Czerminska, P A Janne, D J Sugarbaker, R Bueno, J R Harris, L Court, and E H Baldini. *Fatal pneumonitis associated with intensity-modulated radiation therapy for mesothelioma.* Int J Radiat Oncol Biol Phys **65**(3), 640–645 (2006)

[17] S L Kwa, J V Lebesque, J C Theuws, L. B Marks, M T Munley, G Bentel, D Oetzel, U Spahn, M V Graham, R E Drzymala, J A Purdy, A S Lichter, M K Martel, and R K Ten Haken. *Radiation pneumonitis as a function of mean lung dose: an analysis of pooled data of 540 patients.* Int J Radiat Oncol Biol Phys **42**(1), 1–9 (1998)

[18] D Oetzel, P Schraube, F Hensley, G Sroka-Perez, M Menke, and M Flentje. *Estimation of pneumonitis risk in three-dimensional treatment planning using dose-volume histogram analysis.* Int J Radiat Oncol Biol Phys **33**(2), 455–460 (1995)

[19] E D York, A Jackson, and K E Rosenzweig. *Correlation of dosimetric factors and radiation pneumonitis for non-small-cell lung cancer patients in a recently completed dose escalation study.* Int J Radiat Oncol Biol Phys **63**, 692–699 (2005)

[20] S L Wang, Z Liao, and A A Vaporciyan. *Investigation of clinical and dosimetric factors associated with postoperative pulmonary complications in esophageal cancer patients treated with concurrent chemoradiotherapy followed by surgery.* Int J Radiat Oncol Biol Phys **64**, 692–699 (2006)

[21] M F Chan, C S Chui, Y Song, C Burman, E Yorke, C Della-Biancia, K E Rosenzweig, and K Schupak. *A novel radiation therapy technique for malignant pleural mesothelioma combining electrons with intensity-modulated photons.* Radiother Oncol. **79**(2), 218–223 (2006)

1 Proton therapy for malignant pleural mesothelioma after extrapleural pleuropneumonectomy

J. Krayenbuehl[1], M. Hartmann[2], A. J. Lomax[2], S. Kloeck[1], E. B. Hug[2], I.F. Ciernik[3, 4]

[1] Department of Radiation Oncology, Zurich University Hospital, Zurich, Switzerland
[2] Center for Proton Radiation Therapy, Paul Scherrer Institute, Villigen, Switzerland
[3] Center for Clinical Research, University of Zurich, Zurich, Switzerland
[4] Department of Radiotherapy and Oncology, Dessau Municipal Hospital, Dessau, Germany

Status of the manuscript: published in *International Journal of Radiatiation, Oncology, Biology and Physics, 2010 Oct 1;78(2):628-34 (2010).*

Author contribution J. Krayenbuehl: IMRT and PT planning, data analysis and interpretation of all data, manuscript drafting, revision and editing.

1.1 Abstract

To perform comparative planning for intensity-modulated radiotherapy (IMRT) and proton therapy (PT) for malignant pleural mesothelioma after radical surgery.

Eight patients treated with IMRT after extrapleural pleuropneumonectomy (EPP) were replanned for PT, comparing dose homogeneity, target volume coverage, and mean and maximal dose to organs at risk. Feasibility of PT was evaluated regarding the dose distribution with respect to air cavities after EPP.

Dose coverage and dose homogeneity of the planning target volume (PTV) were significantly better for PT than for IMRT regarding the volume covered by $> 95\%$ (V95) for the high-dose PTV. The mean dose to the contralateral kidney, ipsilateral kidney, contralateral lung, liver, and heart and spinal cord dose were significantly reduced with PT compared with IMRT. After EPP, air cavities were common (range, 0 - 850 cm^3), decreasing from 0 to 18.5 cm^3/day. In 2 patients, air cavity changes during RT decreased the generalized equivalent uniform dose (gEUD) in the case of using an a value of < -10 to the PTV2 to < 2 Gy in the presence of changing cavities for PT, and to 40 Gy for IMRT. Small changes were observed for gEUD of PTV1 because PTV1 was reached by the beams before air.

Both PT and IMRT achieved good target coverage and dose homogeneity. Proton therapy accomplished additional dose sparing of most organs at risk compared with IMRT. Proton therapy dose distributions were more susceptible to changing air cavities, emphasizing the need for adaptive RT and replanning.

1.2 Introduction

Malignant pleural mesothelioma (MPM) is an increasing health problem; it has a high mortality rate, with a median survival of only 19 months and survival rates at 2 and 5 years of 38% and 15%, respectively [1–3]. Multimodal strategies have been proposed owing to the inability of any single modality to achieve satisfactory long-term survival rates. Currently, the combination of surgery, radiotherapy (RT), and pre- or postoperative chemotherapy achieves best results if patients present with an adequate performance status [4–7]. Definitive local control of MPM with ionizing radiation remains a major challenge owing to the large C-shaped clinical target volume (CTV) and the proximity to kidneys, spinal cord, liver, heart, and contralateral lung. Conventional RT has shown its limitations, primarily due to the poor ra-

diation tolerance of neighboring normal organs (organs at risk, OARs) [8], and intensity-modulated RT (IMRT) has been evaluated for postoperative RT [4, 9, 10]. However, the size of the target volumes has resulted in considerable risks of toxicity to the lung. We have previously established the feasibility and appropriateness of IMRT, achieving good planning target volume (PTV) coverage in comparison with three-dimensional conformal RT (3D-CRT) [11]. Intensitymodulated RT is a valid treatment option as long as dose to the healthy, contralateral lung tissue can be minimized. Because of its beam characteristics, proton therapy (PT) has promising features for postoperative RT, potentially minimizing toxicity to neighboring OARs.

In this study, we compared postoperative IMRT with PT, to define potential advantages of each technique. A dosimetric evaluation based on dose - volume histogram (DVH) analysis and dose - volume parameters was performed. The goal was to define the benefit of PT compared with IMRT and to estimate the technical feasibility of treating MPM with postoperative PT. After extrapleural pleuropneumonectomy (EPP), the ipsilateral hemithorax contains variable amounts of air cavities, which subsequently are replaced by fibrous tissue. Special consideration was given to changes of the air cavities during the postoperative RT period. Their impact on dose coverage of the target volumes was estimated, and the accuracy of the two techniques was defined.

1.3 Methods and Materials

Eight consecutive patients diagnosed with MPM and treated with preoperative chemotherapy followed by EPP and IMRT between October 2004 and June 2006 at the Zurich University Hospital (Zurich, Switzerland) were retrospectively replanned with PT. The group consisted of 1 female patient and 7 male patients; 4 patients presented with right-sided MPM and 4 patients with left-sided MPM. The median age was 58 years (range, 48 - 66 years). The clinical results of these 8 patients have been reported previously. For the purpose of the present analysis, all target and nontarget structures were maintained as originally planned [11]. Two CTVs were defined [11]. The first, CTV1, defined the boost volume covering the postoperative areas with possible microscopic disease by means of submacroscopic spread not resected or not accessible to resection, the area of highest risk for relapse as defined by the surgeon, or areas of positive margins according to pathology report, and the area of preoperative macroscopic tumor. The second, CTV2, was determined by the field of surgery including the entire preoperative pleural and pulmonary structures and scars, including the drainage sites. The

PTV1 (respectively PTV2) was constructed using the automated region expansion tools from CTV1 (respectively CTV2 without CTV1) by adding an additional margin of 5 to a maximum 10 mm in all three spatial directions.

PT treatment

Since 1996 PT has been routinely used for deep-seated tumors at Paul Scherrer Institute (Villigen, Switzerland). Details of beam delivery, treatment planning system, and procedures have been published previously [12]. Dose calculation and optimization were performed using the planning algorithm based on spot scanning [13].

All patients were planned with two fields. The first covered the PTV1 and PTV2 (45.5 Gy in 26 fractions) and the second covered only the PTV1, applied as an integrated boost (55.9 Gy total dose in 26 fractions). Fractionation was the same as for IMRT. Beam angles were patient specific and were chosen to optimize the coverage of the target and the avoidance of OARs.

IMRT treatment

Seven radiation beams (6 MV) were used. The superior portion of the PTV was treated with only three to four beams that did not pass through the contralateral lung tissue, as recommended by Allen et al. [14]. The remaining beams were restricted superiorly at the inferior level of the heart for the left-sided cases and at the level of the liver for the right-sided cases. Intensity-modulated RT patients were planed with 26 x 1.75 Gy (45.5 Gy) to PTV2, including a simultaneously integrated boost of 26 x 2.15 Gy (55.9 Gy) to PTV1. Calculation and optimization were performed using an inverse treatment planning system (HELIOS, Eclipse V8.5 with AAA 8.2.23 algorithm; Varian Medical Systems, Palo Alto, CA). Treatments were delivered on a 6-MV photon linear accelerator (Clinac 6EX; Varian Medical Systems) equipped with a 120 dynamic multileaf collimator using the sliding windows with a dose rate of 300 monitor units per minute.

Dose - volume constraints

The maximum dose to any part to of the spinal canal was kept below 50 Gy. The mean dose given to the heart was limited to < 40 Gy, and the maximum heart volume receiving 45 Gy was kept to < 30 %. The mean contralateral lung dose was limited to ≤ 8.5 Gy, in accordance with our previous observations that patients receiving 6.9 ± 1.4 Gy did not experience any pneumonitis as compared with patients with pneumonitis with a mean

dose of 8.8 Gy (11). Not more than 10 % of the contralateral lung volume was allowed to receive a dose $\geq$ 20 Gy. The mean dose to the liver was not permitted to exceed 30 Gy. The mean dose to the kidneys was restricted to $\leq$ 12 Gy, and the volume of kidney receiving more than 15 Gy was kept to $<$ 20%.

Plan comparison

Dose - volume histograms were calculated for the PTVs and OARs for each plan. For comparison purposes DVHs were normalized to the mean dose of the PTV1 (55.9 Gy over 26 fractions). Target dose distribution was evaluated according to the volume covered by 95 % (V95) and 105 % (V105) of the prescribed dose. The doses to OARs were evaluated according to mean dose and organ-specific tolerance levels, such as the volume covered by 15 Gy (V15) for kidneys, dose to 2 % volume of the spinal cord (D2), V45 for heart, and V5, V13, and V20 for contralateral lung [3, 15, 16].

Air cavities

Air cavity changes within the ipsilateral hemithorax after pleuropneumonectomy were measured as a function of time on various postoperative diagnostic CT scans and the RT planning CT. Optimized plans with air cavities $>$ 100 cm ^{3} were used to evaluate the effect of the variation of the air cavities on the dose distribution by overwriting the density of the air cavity to 1 and recalculating the dose distribution. Evaluation of the variation of DVH parameters was performed for PT and IMRT [17] for 2 patients: 1 with the largest and 1 with the smallest air cavity measured on the planning CT. The generalized equivalent uniform dose (gEUD) was also calculated for both techniques and for each structure [18].

Statistics

Statistical analysis was performed using a paired t test. The t - test and the p - value were calculated with StatView 5.0.1 software. A p - value of < 0.05 was accepted as significant.

1.4 Results

An example of comparative treatment planning is shown in Fig. 1.1. Intensity-modulated RT and PT covered the PTV1 and PTV2 by 95% of the prescribed dose. The lung and the two kidneys received a larger dose

with IMRT compared with PT. Fig. 1.1 also shows a rapid dose fall-off outside the PTVs for the PT plan.

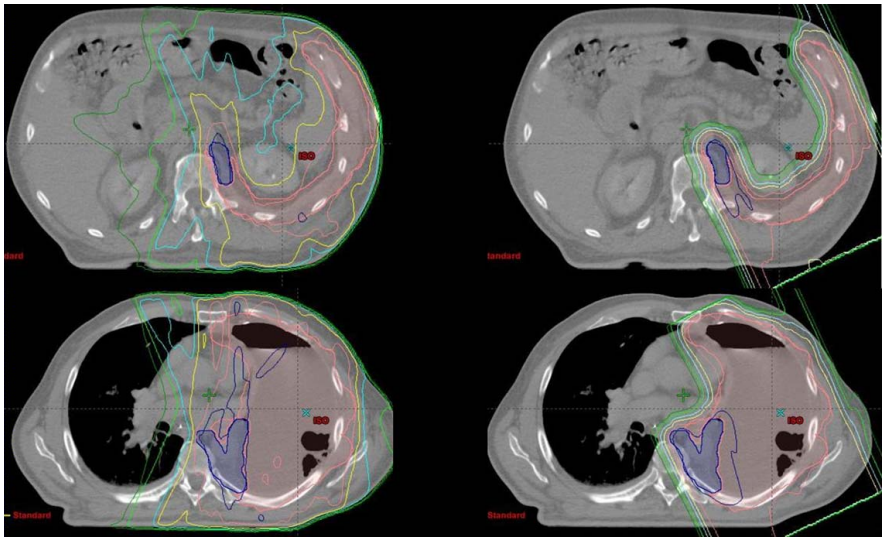

Figure 1.1: Dose distribution in transverse planes for protons (right) and intensity-modulated radiotherapy (left) at the axial level of kidney (top) and lung (bottom). Curves are shown for the entire treatment to a total dose of 55.9 Gy to Planning Target Volume 1 (PTV1) (blue structure) and 45 Gy to PTV2 (pink structure). The dark blue and pink isodose lines represent 95 % the prescribed dose to PTV1 (55.9 Gy) and PTV2 (45.5 Gy). The yellow, cyan, light green, and dark green isodose lines represent 30 Gy, 20 Gy, 10 Gy, and 5 Gy, respectively.

Parameter	IMRT	PT	Mean difference	p
V95 (PTV1) (%)	95.4 ± 1.3	97.0 ± 1.2	1.6	0.04*
V105 (PTV1) (%)	4.0 ± 2.6	3.2 ± 2.0	-0.8	0.2
V95 (PTV2) (%)	92.0 ± 5.7	95.7 ± 2.1	3.7	0.43
V105 (PTV2) (%)	30.2 ± 22.4	31.2 ± 27.5	1	0.13
Dmean (liver) (Gy)	13.2 ± 8.1	3.7 ± 4.0	-9.5	0.01*
D2 (spinal cord) (Gy)	35.5 ± 4.8	28.3 ± 2.9	-7.2	0.03*
Dmean (contralateral kidney) (Gy)	2.7 ± 1.2	0.1 ± 0	-2.6	< 0.01*
V15 (contralateral kidney) (%)	0 ± 0	0 ± 0	0	-
Dmax (contralateral kidney) (Gy)	12.1 ± 4.7	0.2 ± 0	-11.9	< 0.01*
Dmean (ipsilateral kidney) (Gy)	11.8 ± 5.3	7.0 ± 4.0	- 4.8	0.02*
V15 (ipsilateral Kidney) (%)	27.6 ± 15.1	17.4 ± 10.6	-10.2	0.07
Dmean (heart) (Gy)	25.0 ± 6.7	6.0 ± 4.6	-19.0	< 0.01*
V45 (heart) (%)	6.8 ± 6.0	2.1 ± 3.2	-4.7	0.5
Dmean (lung) (Gy)	4.6 ± 0.7	0.4 ± 0.4	-4.2	< 0.01*
V5 (lung) (%)	27.5 ± 9.1	1.5 ± 2.1	-26.0	< 0.01*
V13 (lung) (%)	7.1 ± 2.1	0.7 ± 1.0	-6.4	< 0.01*
V20 (lung) (%)	2.9 ± 1.7	0.5 ± 0.8	-2.4	< 0.01*

Table 1.1: Dose-volume histogram parameters: comparison of IMRT and PT. *Abbreviations*: IMRT = intensity-modulated radiotherapy; PT = proton therapy; PTV = planning target volume; V15, V20, V45 = volume of the organ receiving a dose of 15, 20, 45 Gy or more; D2 = dose to 2 % volume of the respective organ; Mean dose - volume histogram parameters averaged over 8 patients. * Significant ($p < 0.05$).

Target volumes

The average DVHs of IMRT and PT plans for targets and OARs are shown in Table 1.1 and Fig. 1.2. The DVHs were normalized to 55.9 Gy at 100% of the mean dose to PTV1. The DVH graphs for PTV1 are steeper with PT than with IMRT, reflecting improved dose conformity and dose homogeneity to the targets. When expressed as the parameter V95, the difference reached significance only for PTV1 ($p = 0.04$). Indeed, V95 for PTV2 was 95.7 % for PT and 92.0 % for IMRT (p = NS). For PTV1, V95 was 97.0 % for PT and 95.4 % for IMRT ($p = 0.04$). The V105 for PTV1 was 3.2 % for PT and 4.0 % for IMRT, and for PTV2 (p = NS) was 31.2 % for PT and 30.2 % for IMRT (p = NS).

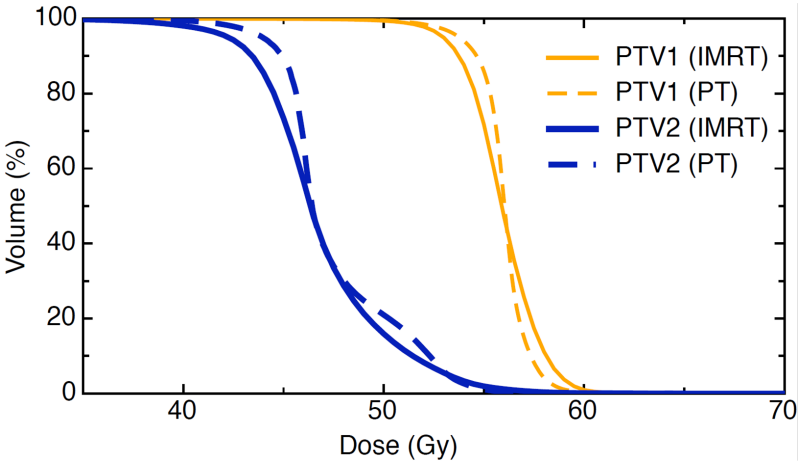

Figure 1.2: Dose - volume histogram for Planning Target Volume 1 PTV1) and PTV2 for intensity-modulated radiotherapy (IMRT, solid lines) and proton therapy (PT, dotted lines). The dose - volume histograms have been normalized to 55.9 Gy at 100 % of the mean dose to PTV1.

Organs at risk

Comparison data for OAR are summarized in Table 1.1 and Fig. 1.3. Both IMRT and PT were able to keep the maximum spinal cord dose below tolerance limits. A reduction by 7.2 Gy of the dose to 2 % of the spinal cord volume was achieved with PT in comparison with IMRT ($p = 0.03$). The volume of spinal cord receiving a dose between 0 and 40 Gy was reduced to

a greater extent with PT compared with IMRT (Fig. 1.3).

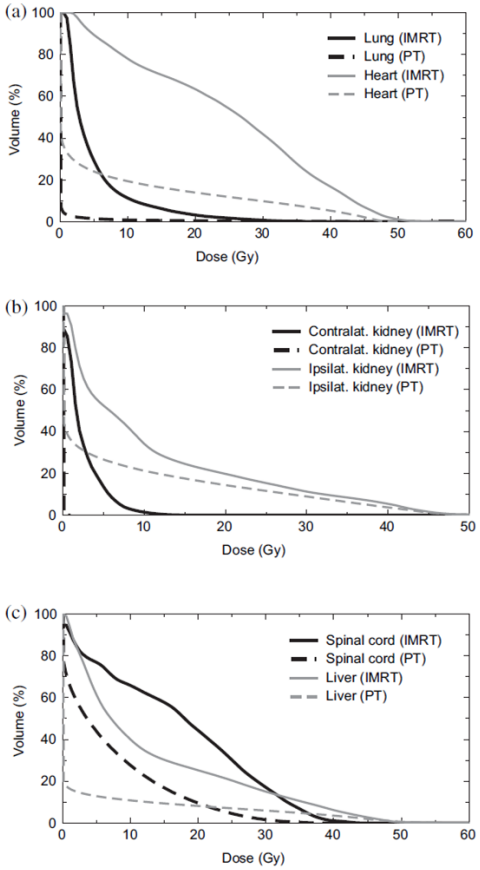

Figure 1.3: (a - c) Dose - volume histogram of the contralateral lung, spinal cord, liver, heart and the kidneys for intensity-modulated radiotherapy (IMRT, solid lines) and proton therapy (PT, dotted lines).

The mean dose to the residual lung for IMRT was 4.6 Gy, 5.1 Gy for left-sided tumor and 4.1 Gy for right-sided tumor (Fig. 1.3 a). The mean lung dose decreased by 4.2 Gy with PT to 0.4 Gy (0.5 Gy for left-sided tumors and 0.3 Gy for rightsided tumors) compared with IMRT. The lung volume receiving a dose > 5 Gy, > 13 Gy, or > 20 Gy decreased by a factor of 18 (from 27.5 % to 1.5 %, V5), 10 (from 7.1 % to 0.7 %, V13), and 6 (from 2.9

% to 0.5 %, V20) with PT compared with IMRT ($p < 0.01$).

Dose - volume histograms for the heart are displayed in Fig. 1.3 a. The mean dose delivered to the heart decreased with PT by a factor of 4.2 in comparison with IMRT, from 25.0 Gy to 6.0 Gy (textitp < 0.01). The dose to the heart for leftsided tumors was 30.4 Gy for IMRT and 9.7 Gy for PT and for right-sided tumors was 19.5 Gy (IMRT) and 2.3 Gy (PT). The part of the heart receiving a dose > 45 Gy was located in close proximity to PTV. No differences were observed on the heart volume receiving a dose > 45 Gy (2.1 % for PT and 6.8 % for IMRT). However, PT spared to a greater extent the heart volume at all levels below 45 Gy.

The mean liver dose was 6.7 Gy for left-sided tumors and 19.7 Gy for right-sided tumors for IMRT. The mean liver dose decreased by a factor of 3.6 with PT, from 13.2 Gy to 3.7 Gy (7.1 Gy for left-sided tumor and 0.3 Gy for right-sided tumor) ($p = 0.01$). Eighty percent of the liver volume (D80) received < 1 Gy with PT, whereas D80 increased to 26.5 Gy for IMRT (Fig. 1.3 c).

The dose to the contralateral kidney was minimal with PT (mean dose of 0.1 Gy), whereas IMRT delivered a mean dose of 2.7 Gy ($p < 0.01$). The maximal contralateral dose was reduced by a factor of 37, from 7.5 Gy for IMRT to 0.2 Gy with PT. The mean dose to the ipsilateral kidney was decreased by a factor of 1.7, from 11.8 Gy for IMRT to 7.0 Gy with PT ($p = 0.02$). A decrease by 10.2 % of the ipsilateral kidney volume, from 27.6 % with IMRT to 17.4 % with PT receiving a dose >15 Gy, was observed with PT ($p =$ NS) (Table 1.1).

Air cavities

An example of air cavity changes after EPP on a transverse and sagittal section is displayed in Fig. 1.4. The variation of air cavity volumes in the operated hemithorax as a function over time between surgery and postoperative CTs is displayed in Fig. 1.5 for all patients. The points have been fitted with an exponential function:

$$V = 684exp(-\frac{t}{30.7}) \tag{1.1}$$

were V is the volume in cm^3, t is the number of days from the operation. The median time between the operation and the RT planning CT was 68 days (range, 54 - 293 days). A median period of 18 days (range, 13 - 22 days) was observed between the dedicated planning CT and the first RT treatment. Air cavity changes regressed with time from surgery. After 80 days a mean air cavity of 50 cm^3 was observed, and after 100 days the mean of

the volume of the air cavities was 26 cm^3. All air cavities resolved within 293 days, although the dynamics of the air cavities depended on the individual patient. The fastest volume changes of the air cavity were observed in Patient 8, with a reduction of 222 cm^3 within 12 days (18.5 cm^3/day).

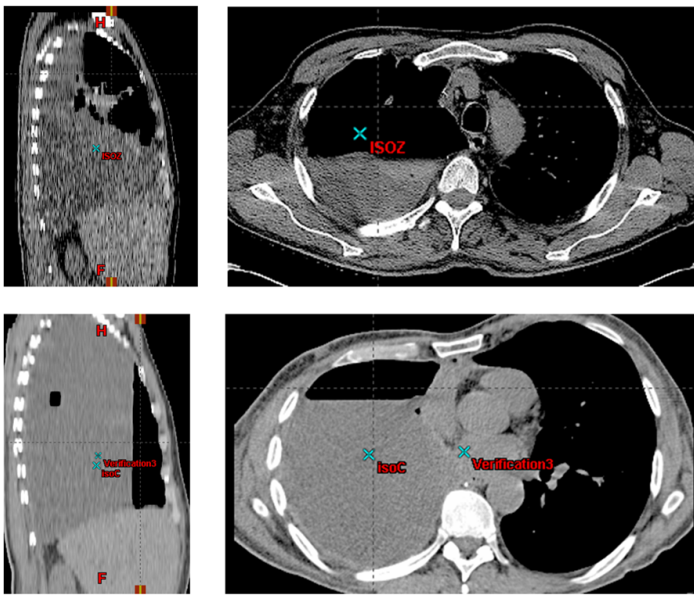

Figure 1.4: Computed tomography of a right-sided malignant pleural mesothelioma patient 7 days (top) and 47 days (bottom) after extrapleural pleuropneumonectomy. Initial air cavity of 850 cm^3 on Postoperative Day 7 was reduced to 340 cm^3 by Day 47. Right: transverse image planes; left: sagittal planes.

The influence of the variation of the cavities on the dose distribution was studied in detail for 2 patients, representing either the smallest or largest air cavity on planning CT. The size of the initial air cavity was 380 cm^3 in Patient 1 and 160 cm^3 in Patient 4 (Fig. 1.5). The mean dose to PTV1 and PTV2 decreased by < 1 Gy for both patients and both techniques. The volume covered by 95 % of the prescribed dose decreased by 0.2 % for PT and 1.6 % for IMRT for PTV1 and by 3.2 % for PT and 0.4 % for IMRT for PTV2 for Patient 4. The difference of the mean dose to liver, contralateral lung, and kidneys, as well as the maximum dose to the spine, was within 0.5 Gy for PT and IMRT.

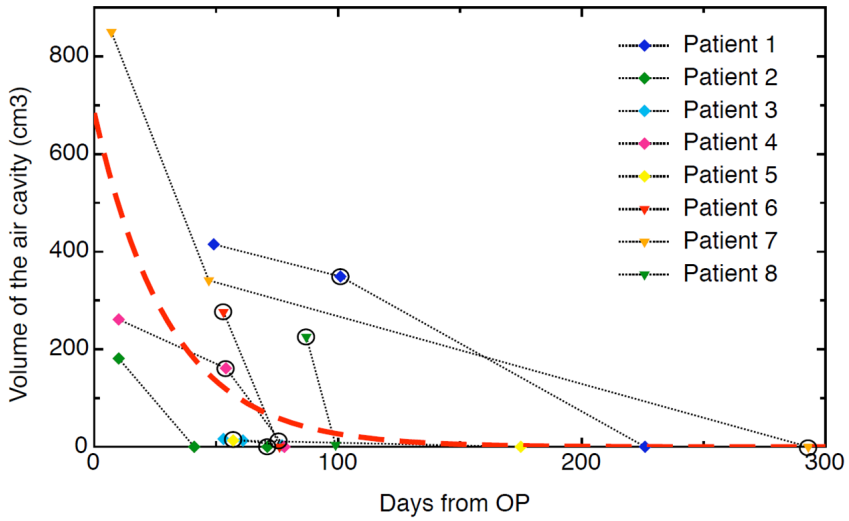

Figure 1.5: Variation of the air cavity size as a function of time. Day 0 = date of surgery (extrapleural pleuropneumonectomy). Points with a circle represent the CT scan used for the radiotherapy treatment. The averaged extrapolated data are shown with the interrupted red line.

In contrast to the V95 % evaluation of the target volumes, gEUD analysis proved more sensitive for pinpointing underdosed PTV2, especially for small cold spots. The gEUD is a function depending on the parameter a, which is a tumor parameter that describes the dose volume effect. For $a = 0$, the EUD is equal to the geometric mean dose. When $a = -\infty$, the EUD is equal to the minimal dose. Because the actual value of a to calculate the gEUD to the target volumes is unknown, we evaluated the gEUD for a values from -1 to -20 for PT. The gEUD for IMRT was hardly affected by the changes and IMRT of tissue densities (air cavity). For PT, the gEUD dropped to $<$ 2 Gy for Patients 1 and 4, compared with 40 Gy for IMRT (Fig. 1.6). The gEUD was also calculated for PTV1 and the OARs for PT and IMRT. No significant difference was observed when comparing plans with or without cavities if air cavities were avoidable using an optimal beam arrangement.

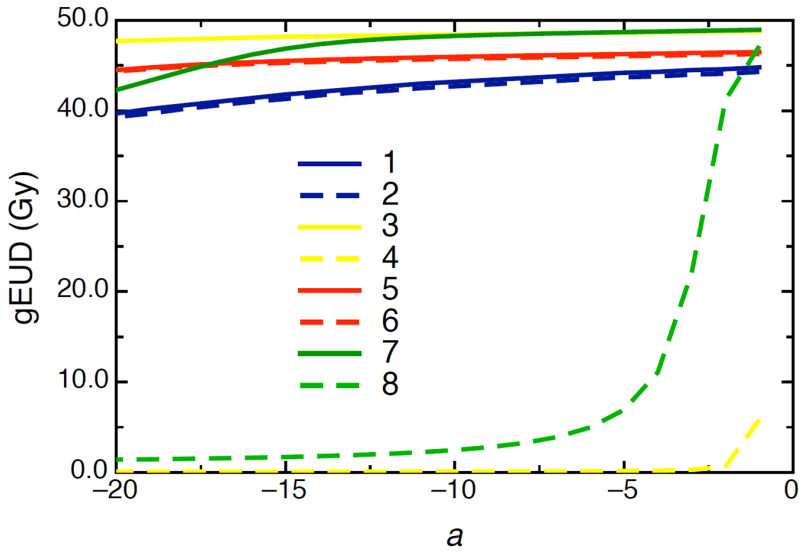

Figure 1.6: Generalized equivalent uniform dose (gEUD) for Planning Target Volume 2 (PTV2) as a function of the parameter a for a patient with and without air cavity. The gEUD for the PTV2 without air cavities (solid lines) and with air cavities (dotted lines) for Patient 1 (blue and yellow curves) and Patient 4 (red and green curves). The blue and red curves are for intensity-modulated radiotherapy (IMRT), and the yellow and green curves are for proton therapy (PT). 1 = Patient 1 with air cavity planned with IMRT; 2 = Patient 1 without air cavity planned with IMRT; 3 = Patient 1 with air cavity planned with PT; 4 = Patient 1 without air cavity planned with PT; 5 = Patient 4 with air cavity planned with IMRT; 6 = Patient 4 without air cavity planned with IMRT; 7 = Patient 4 with air cavity planned with PT; 8 = Patient 4 without air cavity planned with PT.

1.5 Discussion

Significant improvements in dose conformity have been achieved with IMRT. In 2003 preliminary data on IMRT for the treatment of MPM after EPP were reported, and better local control than with conventional techniques was suggested [4]. Others have indicated a limitation of IMRT in MPM patients due to the risk of pneumonitis [11, 19]. Severe lung complications in MPM patients after IMRT, including radiation-related deaths from pneumonitis in 10 % or more of patients treated with IMRT, have been reported [11, 19, 20].

Even with optimized IMRT, the contralateral lung will always receive an exit dose, resulting in low dose to a large volume of lung, and helical tomotherapy has been recently reported to result in low mean dose delivered to the contralateral lung [21]. Excessive dose to the contralateral lung rarely occurs with 3D-CRT [11,22]. However, both techniques have their limitations: dose coverage is improved with IMRT compared with 3D-CRT at the expense of a higher dose to OARs [11].

Proton therapy is able to accomplish both goals, namely target coverage and low dose to OARs. Protons, unlike photons, deposit most of their energy at a specific energy-dependent depth (Bragg peak). Furthermore, scatter from the irradiated cavity to healthy lung tissue can be reduced with protons up to a factor of 10, especially if using spot scanning technology [23]. Intensity-modulated RT and PT beam angles were chosen specifically to limit dose. However, the contralateral lung dose remained significant for IMRT at a mean of 4.6 Gy; PT kept this value to < 1 Gy because of the lack of exit dose. The reduction in contralateral lung dose achieved with PT is expected to significantly reduce any risk of pneumonitis [15,16,20] compared with IMRT [11,19]. Furthermore, the exact dose in the lowdose region may be underestimated for IMRT owing to inaccuracy of the treatment planning system to adequately simulate the microleaf collimator. Dose underestimation for the healthy lung has been reported as high as 25 % for V5 and 7 % for V10 for MPM patients [24]. Taking into account inaccuracies, the difference between PT and IMRT could be even larger than reported here. Proton therapy improved target dose coverage for all patients; this difference was statistically significant for PTV1. Proton therapy also performed consistently better for each OAR. Both IMRT and PT were safe for the spinal cord, keeping D2 to < 40 Gy for each patient. Proton therapy reduced the D2 of the spinal cord by 7.2 Gy. Dose reduction to the spinal cord, without compromising the dose in the target volumes, could be especially useful if incomplete resection is suspected at the vertebro-pleural recess. Side effects during or afterward might be reduced or the dose saved in case of salvage. Another aspect of dose reduction in nontarget tissues is dose escalation to the target structures.

We investigated the impact of postoperative air in the chest after EPP. Air volume changes during RT were considerable, and alterations in patient anatomy and modified target coverage and dose given to OARs need to be considered [25–27]. The difference of dose to the targets between the plans with and without air cavities showed reduced target coverage, a decrease of V95 by 1.6 % and 0.2 % for PTV1 and 0.4 % and 3.2 % for PTV2 for IMRT and PT, respectively. The gEUD to the target changed only for PTV2. The values of gEUD with filled air cavities had a significant reduction of dose to

PTV2, reducing dose to < 2 Gy. This reduction is due to the quality of the proton dose fall-off. When the air cavities are replaced by liquid over time, the depth of the dose maximum (Bragg peak) is pulled upstream, removing the dose downstream, in the deepest part of the target. Alternatively, avoiding air cavities along the proton beam track is likely to avoid underdosage, and flexible gantry angles potentially improve on dose delivery. However, it is important to compensate for anatomic changes and to reassess all air cavities with adaptive planning to ascertain proper dose delivery. Although photons as provided by multiangle IMRT are subject to loss of dose to target volumes in the presence of air - liquid surfaces, the impact is far less prominent than with singleangle proton beams. The difference of dose, as well as the gEUD, to the OARs did not seem to be relevant (<0.5 Gy) when air cavities were replaced with liquid. To avoid these dose variations, a delay of 100 days between EPP and the RT CT would decrease by 75 % the number of patients with residual air cavities. However, a prolonged delay of starting RT after EPP would likely reduce the chance for successful tumor control [28]. Therefore, repetitive on- or off-line replanning (e.g., using an on-board cone-beam CT system to evaluate air cavities periodically and adapt treatment) is recommended [29, 30].

1.6 Conclusion

Proton therapy seems to be a superior technique to minimize the dose to all OARs and to result in better coverage of the target volumes. Clinical validation is mandatory. The major drawback is that protons seem highly sensitive to changing air cavities, requiring follow-up CTs during treatment to evaluate changes of cavities. Beam angle adaptation and replanning might be necessary to ascertain optimal dose delivery.

Bibliography

[1] J C Wagner, C A Sleggs, and P Marchand. *Diffuse pleural mesothelioma and asbestos exposure in the North Western Cape Province.* Br J Ind Med **17**, 260–271 (1960)

[2] J Peto, A Decarli, C La Vecchia, F Levi, and E Negri. *The European mesothelioma epidemic.* Br J Cancer **79**(3-4), 666–672 (1999)

[3] D J Sugarbaker, R M Flores, M T Jaklitsch, W G Richards, G M Strauss, J M Corson, M M DeCamp, S J Swanson, R Bueno, J M Lukanich, E H Baldini, and S J Mentzer. *Resection margins, extrapleural nodal status, and cell type determine postoperative long-term survival in trimodality therapy of malignant pleural mesothelioma: results in 183 patients.* J Thorac Cardiovasc Surg **117**(1), 54–63 (1999)

[4] A Ahamad, C W Stevens, W R Smythe, A A Vaporciyan, R Komaki, J F Kelly, Z Liao, G Starkschall, and K M Forster. *Intensity-modulated radiation therapy: a novel approach to the management of malignant pleural mesothelioma.* Int J Radiat Oncol Biol Phys **55**(3), 768–775 (2003)

[5] W Weder, P Kestenholz, C Taverna, S Bodis, D Lardinois, M Jerman, and R A Stahel. *Neoadjuvant chemotherapy followed by extrapleural pneumonectomy in malignant pleural mesothelioma.* J Clin Oncol **22**(17), 3451–3457 (2004)

[6] M F Chan, C S Chui, Y Song, C Burman, E Yorke, C Della-Biancia, K E Rosenzweig, and K Schupak. *A novel radiation therapy technique for malignant pleural mesothelioma combining electrons with intensity-modulated photons.* Radiother Oncol. **79**(2), 218–223 (2006)

[7] G L Ceresoli, C Gridelli, and A Santoro. *Multidisciplinary treatment of malignant pleural mesothelioma.* Oncologist **12**(7), 850–863 (2007)

[8] Baldini. *Patterns of failure after trimodality therapy for malignant pleural mesothelioma.* Ann Thorac Surg **63**, 334–338 (1997)

[9] K M Forster, W R Smythe, G Starkschall, Z Liao, T Takanaka, J F Kelly, A Vaporciyan, A Ahamad, L Dong, M Salehpour, R Komaki, and

C W Stevens. *Intensity-modulated radiotherapy following extrapleural pneumonectomy for the treatment of malignant mesothelioma: clinical implementation.* Int J Radiat Oncol Biol Phys **55**(3), 606–616 (2003)

[10] M W Munter, C Thieke, A Nikoghosyan, S Nill, and J Debus. *Inverse planned stereotactic intensity modulated radiotherapy (IMRT) in the palliative treatment of malignant mesothelioma of the pleura: the Heidelberg experience.* Lung Cancer **49**(Suppl 1), 83–86 (2005)

[11] J Krayenbuehl, O Susann, J B Davis, and I F Ciernik. *Combined Photon and Electron 3D-Conformal versus Intensity Modulated Radiotherapy with an Integrated Boost for Adjuvant Treatment of Malignant Pleural Mesothelioma following Pleuropneumonectomy.* Int J Radiat Oncol Biol Phys **69**(5), 1593–1599 (2007)

[12] E Pedroni, R Bacher, H Blattmann, and et al. *The 200-MeV proton therapy project at the Paul Scherrer Institute: Conceptual design and practical realization.* Med Phys **22**, 37–53 (1995)

[13] A J Lomax, M Goitein, and J Adams. *Intensity modulation in radiotherapy: photons versus protons in the paranasal sinus.* Radiother Oncol **66**(1), 11–18 (2003)

[14] A M Allen, D Schofield, F Hacker, L E Court, and M Czerminska. *Restricted field IMRT dramatically enhances IMRT planning for mesothelioma.* Int J Radiat Oncol Biol Phys **69**(5), 1587–1592 (2007)

[15] E D York, A Jackson, and K E Rosenzweig. *Correlation of dosimetric factors and radiation pneumonitis for non-small-cell lung cancer patients in a recently completed dose escalation study.* Int J Radiat Oncol Biol Phys **63**, 692–699 (2005)

[16] S L Wang, Z Liao, and A A Vaporciyan. *Investigation of clinical and dosimetric factors associated with postoperative pulmonary complications in esophageal cancer patients treated with concurrent chemoradiotherapy followed by surgery.* Int J Radiat Oncol Biol Phys **64**, 692–699 (2006)

[17] A Niemierko. *Reporting and analyzing dose distributions: Aconcept of equivalent uniform dose.* Med Phys **24**, 103 – 110 (1997)

[18] Q Wu, R Mohan, A Niemierko, and R Schmidt-Ullrich. *Optimization of intensity-modulated radiotherapy plans based on the equivalent uniform dose.* Int J Radiat Oncol Biol Phys **52**(1), 224–235 (2002)

[19] A M Allen, M Czerminska, P A Janne, D J Sugarbaker, R Bueno, J R Harris, L Court, and E H Baldini. *Fatal pneumonitis associated with intensity-modulated radiation therapy for mesothelioma.* Int J Radiat Oncol Biol Phys **65**(3), 640–645 (2006)

[20] D C Rice, W R Smythe, Z Liao, T Guerrero, J Y Chang, M F McAleer, M D Jeter, A Correa, A A Vaporciyan, H H Liu, R Komaki, K M Forster, and C W Stevens. *Dose-Dependent Pulmonary Toxicity After Postoperative Intensity-Modulated Radiotherapy for Malignant Pleural Mesothelioma.* Int J Radiat Oncol Biol Phys , 350–357 (2007)

[21] F Sterzing, G Sroka-Perez, and K Schubert. *Evaluating target coverage and normal tissue sparing in the adjuvant radiotherapy of malignant pleural mesothelioma: Helical tomotherapy compared with step-and-shoot IMRT.* Radiother Oncol **86**, 251–257 (2008)

[22] V Gupta, B Mychalczak, L Krug, R Flores, M Bains, V W Rusch, and K E Rosenzweig. *Hemithoracic radiation therapy after pleurectomy/decortication for malignant pleural mesothelioma.* Int J Radiat Oncol Biol Phys **63**(4), 1045–1052 (2005)

[23] X G Xu, B Bednarz, and H Paganetti. *A review of dosimetry studies on external-beam radiation treatment with respect to second cancer induction.* Phys Med Biol **53**, 193–241 (2008)

[24] S Y Jang, H H Liu, and R Mohan. *Underestimation of low-dose radiation in treatment planning of intensity-modulated radiotherapy.* Int J Radiat Oncol Biol Phys **71**, 1537–1546 (2008)

[25] J L Barker, A S Garden, and Ang. K K. *Quantification of volumetric and geometric changes occurring during fractionated radiotherapy for head-and-neck cancer using an integrated CT/linear accelerator system.* Int J Radiat Oncol Biol Phys **59**, 960–970 (2004)

[26] E K Hansen, M K Bucci, and J M Quivey. *Repeat CT imaging and replanning during the course of IMRT for head-and-neck cancer.* Int J Radiat Oncol Biol Phys **64**, 355–362 (2006)

[27] J C O'Daniel, A S Garden, and D L Schwartz. *Parotid gland dose in intensity-modulated radiotherapy for head and neck cancer: Is what you plan what you get?* Int J Radiat Oncol Biol Phys **69**, 1290–1296 (2007)

[28] C Choan, S Dahrouge, and R Samant. *Radical radiotherapy for cervix cancer: The effect of waiting time on outcome.* Int J Radiat Oncol Biol Phys **2005**, 1071–1077 (2005)

[29] K Nakagawa, H Yamashita, and K Shiraishi. *Verification of intreatment tumor position using kilovoltage cone-beam computed tomography: A preliminary study.* Int J Radiat Oncol Biol Phys **69**, 970–973 (2007)

[30] J Pouliot, A Bani-Hashemi, and J Chen. *Low-dose megavoltage cone-beam CT for radiation therapy.* Int J Radiat Oncol Biol Phys Med Biol **61**, 552–560 (2005)

1 Intensity modulated radiotherapy and volumetric modulated arc therapy for malignant pleural mesothelioma after extrapleural pleuropneumonectomy

J. Krayenbuehl[1], O. Riesterer[1], S. Graydon[1], P. Dimmerling[1], S. Kloeck [1], I.F. Ciernik[2, 3],

[1] Department of Radiation Oncology, Zurich University Hospital, Zurich, Switzerland
[2] Center for Clinical Research, University of Zurich, Zurich, Switzerland
[3] Department of Radiotherapy and Oncology, Dessau Municipal Hospital, Dessau, Germany

Status of the manuscript: published in *Journal of Applied Clinical Medical Physics*, 14 (4), 2013.

Author contribution J. Krayenbuehl: planning, data analysis and interpretation of all data, manuscript drafting, revision and editing. The evaluation of the optimal beam geometry for volumetric modulated arc plans was performed by *S. Graydon*.

1.1 Abstract

Radiotherapy reduces the local relapse rate after pleuropneumonectomy of malignant pleural mesothelioma (MPM). The optimal treatment technique with photons remains undefined. Comparative planning for intensity-modulated radiotherapy (IMRT) and volumetric-modulated arc therapy (VMAT) was performed. Six MPM patients with significant postoperative intrathoracic air cavities were planned with IMRT and VMAT. A dose comparison for the targets and organ at risks (OAR) was performed. Robustness was assessed in respect to the variation of target dose with change in volume of air cavities. VMAT reduced the dose to the contralateral lung by reducing the volume covered by 13 Gy and 20 Gy by a factor 1.8 and 2.8, in respect to IMRT ($p = 0.02$). Dose distribution with VMAT was the most stable technique in regard to postsurgical air cavity variation. For IMRT, V90, V95, and the minimal target dose decreased by 40 %, 64 %, and 12 % compared to 29 %, 47 %, and 7 % with VMAT when air cavity decreased. Two arcs compared to one arc decreased the dose to all the organs at risk (OAR) while leaving PTV dose coverage unchanged. Increasing the number of arcs from two to three did not reduce the dose to the OAR further, but increased the beam-on time by 50 %. Using partial arcs decreased the beam-on time by 43 %. VMAT allows a lower lung dose and is less affected by the air cavity variation than IMRT. The best VMAT plans were obtained with two partial arcs. VMAT seems currently the most suitable technique for the treatment of MPM patients when air cavities are remaining and no adaptive radiotherapy is performed.

1.2 Introduction

Malignant pleural mesothelioma (MPM) is an aggressive tumor with a high mortality rate and a survival rate of 38 % after two years and 15 % after five years [1]. The role of RT after extrapleural pneumonectomy (EPP) is to reduce local failure [2,3]. The dose to the hemithorax is typically limited to 45 Gy with a boost to 55 Gy [2, 4] due to the adjacent dose limiting structures, such as the lung, kidney, spinal cord, liver, and heart. However, the tumor control rates after EPP, chemotherapy, and radiotherapy remains poor [5]. In order to enhance tumor control, dose escalation is an option if dose conformity is improved (e.g., proton therapy has been proposed for dose escalation due to the low dose delivered to the contralateral lung, heart, and kidney) [5]. However, access to proton therapy (PT) remains limited and proton techniques are hampered by postsurgical air cavities. After EPP, the

ipsilateral hemithorax contains variable amounts of air, which subsequently are replaced by fibrous tissue. These cavities decrease over time, reducing drastically the dose to the target for PT which would decrease tumor control and counteract any potential benefit of an eventual dose escalation.

In this study, an evaluation of a new RT technique, volumetric-modulated arc therapy (VMAT) was performed for the treatment of MPM patients. The optimal number of arcs and degree of rotation were evaluated for the treatment of MPM patients with VMAT. Postoperative IMRT and VMAT were compared in order to define potential advantages of each technique: dosimetric benefit and treatment time. Another goal was to evaluate the dose variation of VMAT and IMRT in respect to the variation of air cavities in the resected lung, and to evaluate for which air cavity variation adaptive planning is required. This was evaluated in respect to the change of dose in the target.

1.3 Methods and materials

etween 2004 and 2011, 16 patients diagnosed with MPM were treated with external radiotherapy at the Zurich University Hospital, Switzerland. All of these patients received preoperative chemotherapy followed by extrapleural pleuropneumonectomy (EPP) and modulated radiotherapy. Six of 16 patients had air cavities exceeding 100 cm^3 when the treatment planning computer tomography (CT) was performed and were selected for the present study. All CTs have been performed in supine head-first position. Five patients were male and one female. Five patients presented with right-sided MPM and one patient with left-sided MPM. Two of these six patients were treated with VMAT and four patients were treated with IMRT. All patients were planned with IMRT and VMAT, two patients prospectively and four patients retrospectively. The comparison between IMRT and VMAT was based on dose distribution, treatment time, and robustness of the techniques in respect to the effect of variation of the air cavity on the dose distribution.

Target volume definition was obtained as described previously in detail [5]. All patients were planned and treated with 26 x 1.75 Gy (45.5 Gy) to the planning target volume two (PTV2) including a simultaneously integrated boost of 26 x 2.15 Gy (55.9 Gy) to the PTV1. Due to the difficulty of the algorithm to optimize correctly the dose in air cavity, a PTV2* was defined for evaluation purpose only as PTV2 without air cavity.

1.3.1 IMRT and VMAT treatment

The technique used for IMRT was described previously [3] and followed the recommendation from Allen [6].

The VMAT plans were performed with two clockwise arcs of 205°ranging from 180°to 25°for right-sided tumors and from 335°to 180°for left-sided tumors. The isocenter was placed in the middle of the PTV2. The partial-arc technique was used in order to avoid entrance dose to the contralateral lung. The collimator angles were set to 355°and 5°.

The patient with the PTV volume closest to the mean PTV volume of all six MPM patients was chosen to assess the optimal number of arcs and the rotation angle required to treat MPM patients. Plans with one, two, or three full arcs (360°) or partial arcs (205°) were performed in order to assess the optimal number of arcs and gantry rotation. When one arc was used, the collimator angle was set to 5°. If a second arc was added (respectively a third arc), the collimator angle was set to 355°(respectively 10°).

1.3.2 Dose calculation and delivery

Calculation and optimization were performed for IMRT and VMAT using an inverse treatment planning system (HELIOS, Eclipse V8.9 with AAA 8.9.08 algorithm, Varian Medical System, Palo Alto, CA). One patient was calculated with Acuros XB (Varian Medical System) in order to quantify the dose distribution difference between one of the most advanced algorithm (Acuros) and AAA, the algorithm used clinically [7]. Treatments were delivered on a 6 MV photon linear accelerator (Trilogy, Varian Medical Systems) equipped with a Millennium multileaf collimator with 120 leaves. Patient positioning was verified with either cone-beam CT (CBCT) or with two orthogonal kV images.

Pretreatment dose verification was performed with a cylindrical PMMA phantom having two perpendicular planes of 1069 diodes (Delta4; ScandiDos Inc., Uppsala, Sweden). The verification of the plan had to reach a gamma score of 95 % (3 % dose difference, 3 mm distance to agreement) before patient irradiation. .

1.3.3 Dose volume constraints, plan and treatment comparison

The dose constraints chosen were published previously [3] and are summarized in Table 1.1. DVHs were calculated for the PTVs and OARs for each

plan. Target dose distributions were evaluated according to the volume covered by 80 %, (V80), 85 % (V85), 90 % (V90), 95 % (V95) and 105 % (V105) of the prescribed dose and to the minimal dose (D99) and maximal dose (D1). The dose to OARs were evaluated according to mean dose, and organ-specific tolerance levels such as the volume covered by 15 Gy (V15) for kidneys, maximal dose to the spinal cord (D1), and V5, V13, and V20 for contralateral lung [1, 8, 9].

The treatment time, as well as the number of monitor units needed for one fraction, were evaluated for IMRT and VMAT.

1.3.4 Air cavities

Air cavity volume changes within the ipsilateral hemithorax following pleuropneumonectomy were measured as a function of time on various postoperative control computed tomographies (CT), RT planning-CT. and CBCT [3]. The air cavity volumes ranged from 150 cm^3 to 1276 cm^3. The axial, sagittal, and coronal views from the patients are displayed on Fig. 1.1. The evaluation of the variations of D1, D99, V80, V85, V90, V95, V100, and V105 with decrease of the air cavity volumes for the PTV1 and PTV2* were performed for IMRT and VMAT. Therefore, the dose distribution calculated on the planning CT was recalculated on all control CTs. When cone-beam CTs or lateral images where available, the resected lung density of the planning study was modified in respect to these images. The effect of the air cavity decrease on the OARs was small as observed in this study and also on a previous study [3]. Therefore, the OAR dose fluctuation and air cavity variation are not reported in this study.

1.3.5 Statistics

Statistical analysis was performed using a paired t-test. A p-value of < 0.05 was accepted as significant.

1.4 Results

The dose distribution calculated with AAA or Acuros, showed similar results. Indeed, V90, V95, as well as the mean dose for the targets and air cavities, where within 1 %. Therefore, all data presented were calculated with the algorithm, AAA, used clinically.

A typical dose distribution for IMRT and VMAT are displayed in the axial, sagittal, and coronal view for one patient on Fig. 1.2. IMRT and VMAT

covered PTV1 with the 95 % of the prescribed dose, but the PTV2* was partially underdosed with IMRT. The dose to the spinal cord, contralateral lung, and heart is equivalent for this patient. A larger posterior dose from the PTV1 is observed for IMRT. This "hot spot" results from the intersection of the three dorsal fields.

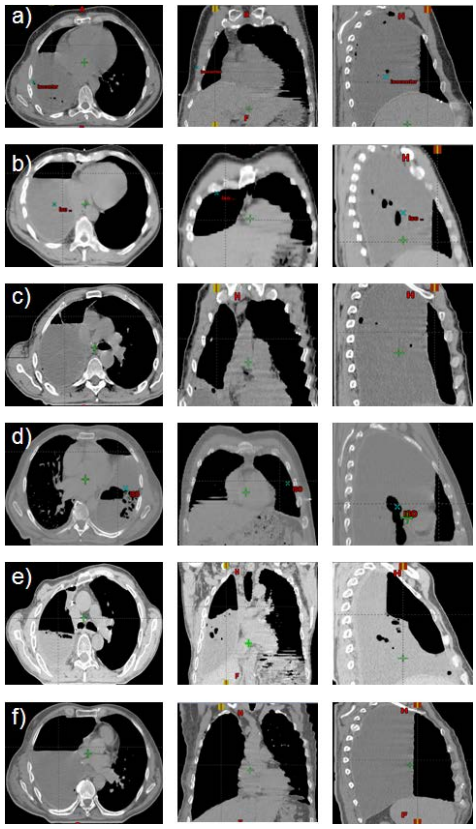

Figure 1.1: Air cavities remaining in the resected lung at the date of the planning CT in the axial (left images), coronal (middle images) and sagittal (right images) view. Five patients had a right sided MPM (a, b, c, e and f) and one patient had a left sided MPM (d). The volume of the air cavities are 150 cm^3 (a), 225cm3 (b), 243 cm^3 (c), 276 cm^3 (d), 379 cm^3 (e) and 1276 cm^3 (f).

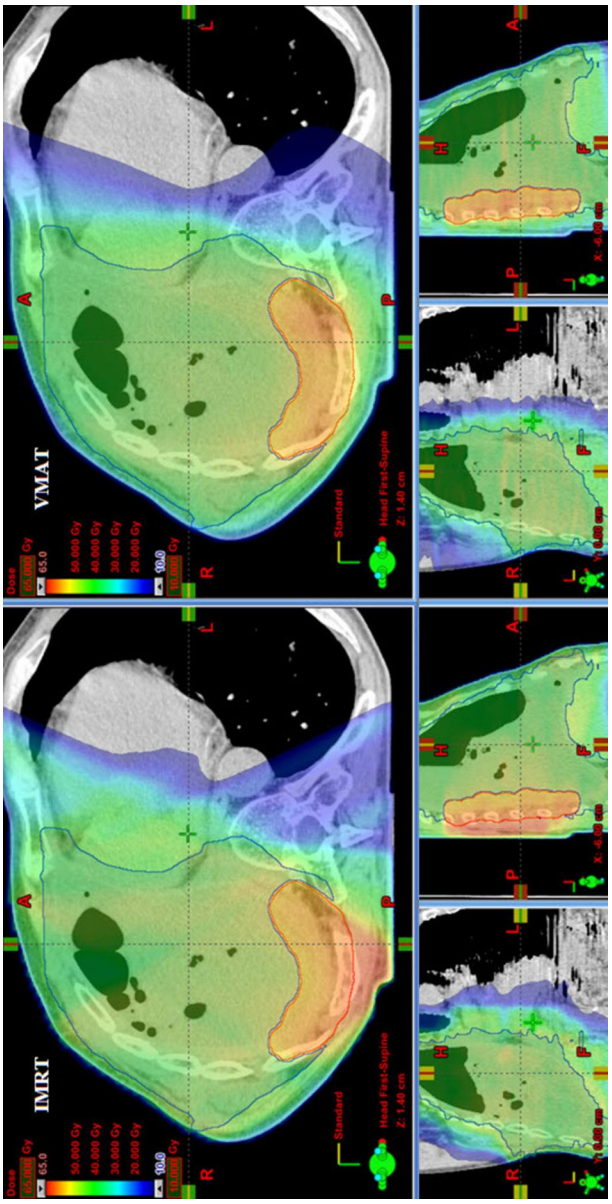

Figure 1.2: Typical dose distribution in axial sagittal and coronal planes for IMRT (left side) and VMAT (right side). Dose distribution is shown for the entire treatment to a total dose of 55.9 Gy to the PTV1 (red structure) and 45 Gy to the PTV2 (green structure) for the patient having the PTV1 volume closest to the mean PTV1 volume of all six MPM patients. The volume of the air cavities was 379 cm^3.

1.4.1 Target volumes

DVH parameters for IMRT and VMAT plans for targets and OARs are summarized in Table 1.1. These parameters where calculated for VMAT using two partial arcs of 205°. The dose distribution was normalized to 55.9 Gy at 100 % of the mean dose to the PTV1. The difference in dose homogeneity, minimal dose and maximal dose in the PTV1 for IMRT and VMAT was small and not significant. Indeed, the mean difference for V95, V105, D1, and D99 was within 1.8 % (p not significant). Regarding the PTV2*, VMAT increased the V95 by 0.5 % and decreased V105 by 1.8 % (p not significant). V80, V85, and V90 for PTV2* were always larger than 98 % for each IMRT and VMAT plans. Therefore, these values were not displayed on Table 1.1.

	Objectives	IMRT	VMAT	p-test
V_{95} (PTV1) (%)		94.7 ± 2.1	94.2 ± 1.3	0.39
V_{105} (PTV1) (%)		4.5 ± 3.5	6.3 ± 2.0	0.49
D_{99} (PTV1) (%)	95	90.9 ± 2.8	91.4 ± 1.3	0.13
D_1 (PTV1) (%)	107	106.7 ± 1.8	106.8 ± 0.7	0.18
V_{95} PTV2* (%)	95	94.8 ± 3.0	95.3 ± 2.4	0.38
V_{105} PTV2* (%)	10	20.1 ± 9.0	18.3 ± 8.8	0.21
Mean lung dose (Gy)	8.5	5.2 ± 0.9	4.6 ± 1.5	0.23
Lung V_5 (%)	50	32.4 ± 18.3	40.8 ± 13.6	0.23
Lung V_{13} (%)	20	6.1 ± 1.8	3.3 ± 1.4	0.02
Lung V_{20} (%)	10	2.5 ± 1.2	0.9 ± 1.1	0.02
Contralateral kidney mean dose (Gy)	12	3.6 ± 1.2	3.8 ± 1.8	0.47
Contralateral kidney V_{15} (%)	20	0 ± 0	0 ± 0	-
Ipsilatateral kidney mean dose (Gy)	12	12.4 ± 6.1	11.9 ± 6.8	0.25
Ipsilateral kidney V_{15} (%)	20	28.2 ± 18.6	31.5 ± 20.0	0.06
Spinal Cord Dmax (Gy)	50	43.0 ± 3.2	44.1 ± 4.0	0.42
Liver mean dose (Gy)	24	14.8 ± 6.4	14.6 ± 7.9	0.19

Table 1.1: Dose objectives and mean dose volume histogram results from six IMRT and corresponding VMAT plans, respectively *Abbreviation*: V_x (%) = volume receiving > x % of prescribed dose, D_x (%) = dose received by x % of volume. Significant ($p < 0.05$)

1.4.2 OAR

Comparison data for OAR are summarized in Table 1.1. Both, IMRT, and VMAT were able to keep the dose to the OAR below the constraints fixed in Table 1.1, except for the ipsilateral kidney. The mean dose and V15 for the ipsilateral kidney, which is surrounded by the target, could not be kept below 12 Gy and 20 %.

The mean ipsilateral kidney dose and V15 were 12.4 Gy and 28.2 Gy (respectively) for IMRT, and 11.9 % and 31.5 % (respectively) for VMAT (p = 0.25 and 0.06). It was not possible to keep these values below our objectives of 12 Gy and 20 % due to the target surrounding the ipsilateral kidney. For the contralateral kidney, both techniques were able to keep the mean dose far below the constraints of 12 Gy (3.6 Gy for IMRT and 3.8Gy for VMAT, p = 0.47), and V15 was kept at 0 % for IMRT and VMAT. The contralateral lung V5 increased by 8.4 % with VMAT in respect to IMRT, but the mean dose, as well as V13 and V20 to the contralateral lung, were reduced by 0.6 Gy, 2.7 %, and 1.6 % (respectively) with VMAT. The difference reached significance only for V13 and V20 (p = 0.02). The maximal spinal cord dose as well as the mean liver dose for IMRT and VMAT were very close to each other and the difference was not significant (p = 0.42 and 0.19).

1.4.3 MU and Treatment time

The mean number of monitor units was drastically reduced from IMRT to VMAT by a factor 4.2 from 2080 ± 414 MU for IMRT to 485 ± 82 MU for VMAT in order to deliver 2.15 Gy (p<0.01). The time required to deliver the plan was around 10 minutes for IMRT and 4 minutes for VMAT. The beam-on time for VMAT depends on the number of monitor units, dose rate, gantry angle rotation, and gantry rotation speed. For all the plans performed with VMAT, the gantry rotation speed was always at its maximal speed, 4.8°/s, and the dose rate was modulated accordingly. Therefore, in our case, the monitor units were not affecting the treatment time for the delivery of the VMAT plans, but only the gantry rotation angle determined the beam-on time.

1.4.4 Air cavities

Air cavities on the planning CT are displayed in Fig. 1.1. The initial air cavity measured on the planning CT ranged from 150 cm^3 to 1275 cm^3. The air cavity remaining after EPP shrinks with time to disappear completely. The volume decrease can reach 220 cm^3 in 12 days [3]. The decrease of V80, V85,

V90, V95, V100, V105, D1, and D99 in planning situation with air cavities are displayed on Fig. 1.3 and Fig. 1.4. IMRT and VMAT were not affected by the change of the air cavity volumes in respect to V80. V85 decreased only for IMRT when the air cavity variation was larger than 880 cm^3. A decrease up to 10.2 % for V85 was observed when the air cavity volume decreased by 1276 cm^3. IMRT (respectively VMAT) V90 decreased when a variation larger than 310 cm^3 (respectively 610 cm^3) was observed. The decrease of V90 was up to 40.3 % for IMRT and 9.4 % for VMAT. A reduction of V95 for IMRT and VMAT was observed for air cavity variation > 200 cm^3. The decrease of V95 could reach 64.4 % for IMRT and 29.2 % for VMAT. A decrease $>$ 28 % for V95 is observed for IMRT in comparison to VMAT for air cavity reduction larger than 311 cm^3. Concerning PTV2, similar results as for PTV1 have been observed when air cavity shrinks. V80 (respectively V85) was not affected by a change of air cavity for IMRT (respectively VMAT). Decrease larger than 20 % of V100 was observed when air cavity decreases by 300 cm^3 and 600 cm^3 for IMRT and VMAT, respectively.

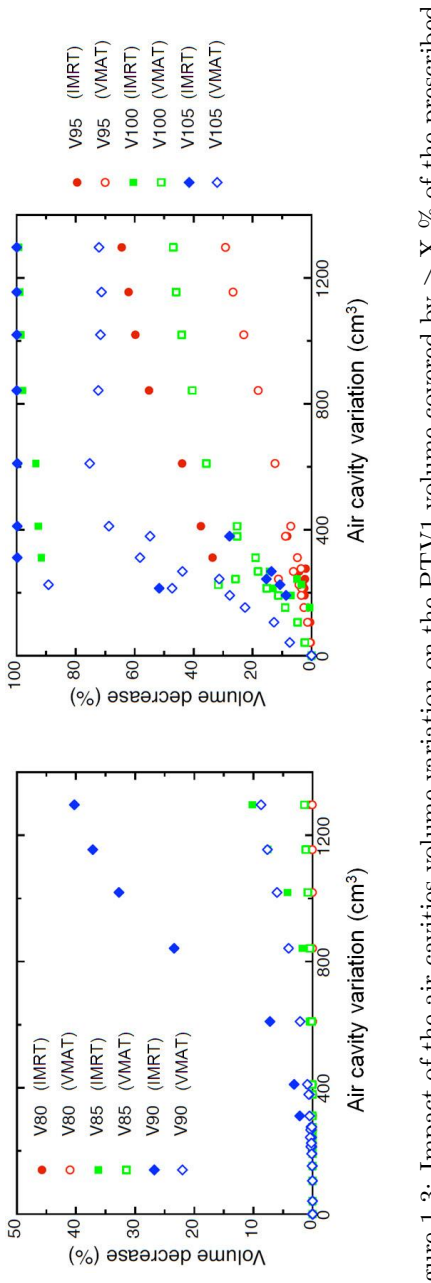

Figure 1.3: Impact of the air cavities volume variation on the PTV1 volume covered by > X % of the prescribed dose (Vx). Data are derived from 6 MPM patients with air cavities larger than 100 cm^3.

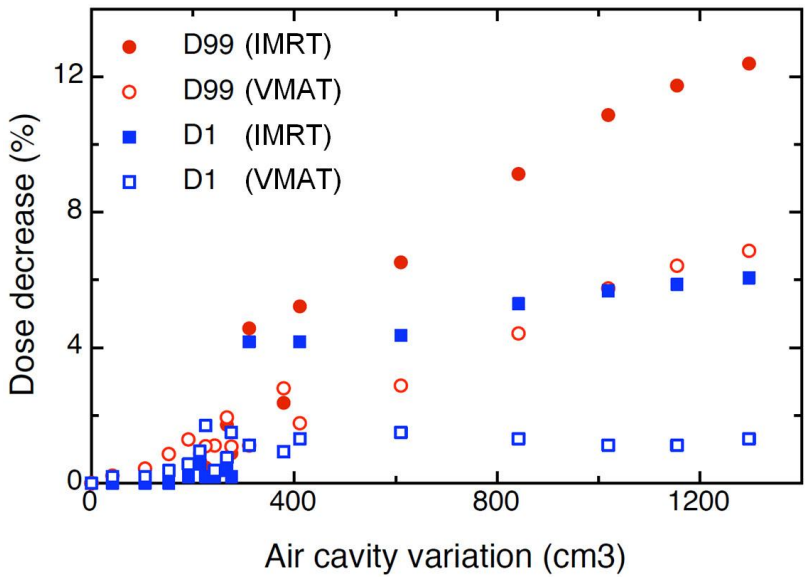

Figure 1.4: Impact of the air cavities volume variation on the minimal and maximal dose of PTV1 for IMRT and VMAT. The PTV1 minimal dose (D99), respectively maximal dose (D1) is defined as dose received by 99 %, respectively 1 %, of the PTV1 volume. Data are derived from 6 MPM patients with air cavities larger than 100 cm^3.

A decrease of V100 and V105 was observed for IMRT and VMAT even for small volume shrinking (150 cm^3). This decrease reached 100 % for IMRT when the air cavity volume decreases by 310 cm^3 for V105 and 842 cm^3 for V100. For VMAT, a maximal decrease of 47 % for V100 and 72 % for V105 was observed.

The minimal dose and the maximal dose in the PTV1 as a function of the variation of the air cavities are displayed in Fig. 1.4. The minimal dose for IMRT decreased up to 12.4 % and up to 6.9 % for VMAT. The decrease of the maximal dose was more pronounced for IMRT with a decrease up to 6.1 % and 1.7 % for VMAT.

1.4.5 Optimal number of arcs for VMAT plans

DVH parameters and monitor units for plans performed with one, two, and three partial and full arcs are displayed in Table 1.2. These parameters have been calculated for the patient having the PTV volume closest to the mean

PTV volume. When one arc is used, a full rotation showed better results than a partial rotation. Indeed, the V95 for the PTV1 was increased from 93.3 % to 95.6 % and V105 was decreased by 4.5 % with the full-arc rotation. All OARs had a lower dose with the full-rotation arc, except for the maximal dose to the spinal cord. If two arcs are used instead of one arc, V95 and V105 for the PTV were slightly improved and the dose to all OARs was drastically reduced. The same observation was seen for the dose to the left and right kidneys, liver, heart, and maximal dose to the spinal cord. The difference between two arcs of 205°and two arcs of 360°was very small, with a small improvement for the partial arcs in respect to the lung dose. If the number of arcs is increased from two to three, there is a small benefit for V95 for the PTV1. For the OAR, slight deviation was observed between two and three partial- or full-arc rotation.

	1 partial arc	1 full arc	2 partial arc	2 full arc	3 partial arc	3 full arc
V_{95} PTV1 (%)	93.3	95.6	94.5	95.1	95.1	95.6
V_{105} PTV1 (%)	6.6	2.1	2.2	1.8	2.0	1.9
V_{95} PTV2 (%)	95.8	96.0	96.5	96.4	97.4	97.4
D_{mean} ipsi. kidney (Gy)	10.8	10.6	6.4	6.0	6.6	6.2
V_{15} ipsi. kidney (%)	27.7	23.2	8.5	8.4	12	9.3
D_{mean} contr. kidney (Gy)	8.7	8.5	6	6.1	5.9	5.3
V_{15} contr. kidney (%)	8.6	5	0	0	0	0
D_{mean} lung (Gy)	8.4	8.4	4.8	5.1	4.7	5.0
V_5 lung (%)	87.1	87.1	30.3	36.1	29	33.3
V_{13} lung (%)	12.1	10.8	1.5	2.1	1.8	2
V_{20} lung (%)	0	0	0	0	0	0
D_{mean} liver (Gy)	20.4	20.5	16.8	16.7	16.8	16.8
D_{mean} heart (Gy)	17.7	16.4	11	11.4	10.8	12.2
D_{mean} myelon (Gy)	37.4	41.3	35.4	36.8	34	36.3
Monitor units	251	298	513	638	563	708

Table 1.2: DVH parameters and monitor units for plans performed with 1, 2 and 3 partial and full arcs. The values are calculated for one patient with the PTV1 volume closest to the mean PTV1 volume from all six MPM patients. *Abbreviation*: V_x (%) = volume receiving > x % of prescribed dose, D_x (%) = dose received by x % of volume. Significant ($p < 0.05$)

The number of monitor units increased with the gantry rotation angle. The monitor units ranged from 251 for a partial arc (205°rotation) to 708 for three full rotations (3 x 360°). The difference of beam-on time between the partial-arcs rotation and full-arc rotation was always 43 % in favor of the partial-arc rotation. Indeed, the gantry rotation speed was always at its maximal velocity, 4.8°/s, during the rotation of the arcs for each plan. Therefore, the treatment time was not affected by the number of monitor units but was proportional only to the rotation angle performed by the gantry.

1.5 Discussion

Improved technologies enhance dose conformity, and avoiding dose delivery to critical structures has opened ways to treat complex oncological situations, such as MPM after EPP [10, 11]. The RT treatment of MPM patients is commonly performed with IMRT, with improved dose conformity and homogeneity to the targets in comparison with 3D conformal radiotherapy (3D CRT) [5]. However, a major drawback of IMRT is the treatment time. Treatment delivery is time-consuming due to the large number of fields which are usually doubled due to split field technologies. Furthermore, a large number of MUs is needed (2080 ± 414 MU). The introduction of VMAT reduced the number of MUs by a factor of 4.2, reducing the treatment time from 10 minutes to 4 minutes. As reported previously [10], the decrease in treatment time reduces patient motion during the treatment delivery and thus results in greater agreement between the dose planned and dose delivered. This reduction in treatment time will decrease the time in which the patient has to stay in an uncomfortable position on the back with arms above the head.

Concerning the dose to the OAR, no major differences were seen between IMRT and VMAT, except for the lung. However, a reduction by a factor of 1.8 and 2.8 for V13 and V20, respectively, for the lung was observed for VMAT. This reduction of lung dose could decrease the risk of complication, such as radiation-induced pneumonitis, where rates larger than 40 % have been reported [11].

The dose conformity and homogeneity were not statistically different for IMRT and VMAT. This is in agreement with previously published data [10]. Nevertheless, the small difference between IMRT and VMAT concerning the target coverage and dose homogeneity on the planning CT does not imply an identical delivery of dose to the target during all treatment sessions. Indeed, air cavities remain in the chest after EPP. The air volume change during RT can be considerable [3] This will have a direct impact on DVH parameters for IMRT and VMAT plans. Indeed, when reduction > 311 cm^3 of

the air cavity occurs, V95-V105, D1, and D99 are drastically modified. The decrease of dose to the target can even reach 100 % for IMRT for V100 and 72 % for VMAT. The reason comes from the fact that the air cavity volumes are always located on the ventral part of the resected lung. When the lung cavity is replaced by serofibrous tissue during treatment, dose distribution delivered with photons coming from the anterior direction will be most affected, and the proportion of photons coming from the anterior direction is more pronounced for IMRT than for VMAT. Therefore, a larger decrease of dose for IMRT in the target occurs when the air cavities disappear than for VMAT.

The overall decrease of dose coverage with decrease of air cavity is not a monotonic function, as observed on Fig. 1.3. These data are displayed for six MPM patients with air cavity larger than 100 cm^3. The change of PTV1 dose coverage will be strongly influenced by the location of the PTV1. Indeed, the higher the proportion of photons depositing energy in the PTV1 going through air cavity before the PTV1, the higher the PTV1 will be affected by a change of air cavity.

A special concern comes with the decrease of air cavity volumes >200 cm^3 reducing dose homogeneity of target volumes (Fig. 1.3 b). Small air cavity decrease (<200 cm^3) will impact only on the high dose in the PTV (V105 and V100). The minimal dose and V95 will decrease by less than 2 %.

If the air cavity volume decreases > 200 cm^3 compared to the planning situation, cold spots will appear in the target volume. Monitoring of air cavities can be achieved with two orthogonal kV images taken prior RT or with a CBCT. When an air cavity volume decrease larger than 200 cm^3 is observed, a control planning CT might be helpful in order to assess the impact on the dose variation and the need for an eventual new treatment plan.

The dose distribution can be affected by the number of beams. Regarding VMAT, an improvement of the dose distribution was observed when two arcs are used instead of one arc. However, increasing the number of arcs from two to three did not lead to any further improvement for partial- or full-arc rotation. When two arcs are chosen, partial-arc techniques harbor the advantage to avoid dose delivery to the remaining lung, and the beam-on time can further be reduced by more than 40 % compared with the full-arc rotation. Therefore, two partial arcs seem to be most suitable in respect to treatment time and dose distribution.

1.6 Conclusion

VMAT using multiple partial arcs enhances the treatment quality with photons when compared to IMRT by reducing the dose of ionizing radiation to the remaining lung while saving treatment time and integral dose. VMAT dose distributions are less susceptible to changing air cavities than IMRT. It is recommended that patients having air cavity variation exceeding 200 cm^3 be monitored attentively in order to consider adaptive replanning in case of structural changes during treatment.

Bibliography

[1] D J Sugarbaker, R M Flores, M T Jaklitsch, W G Richards, G M Strauss, J M Corson, M M DeCamp, S J Swanson, R Bueno, J M Lukanich, E H Baldini, and S J Mentzer. *Resection margins, extrapleural nodal status, and cell type determine postoperative long-term survival in trimodality therapy of malignant pleural mesothelioma: results in 183 patients.* J Thorac Cardiovasc Surg **117**(1), 54–63 (1999)

[2] S Yajnik, K E Rosenzweig, B Mychalczak, L Krug, R Flores, L Hong, and V W Rusch. *Hemithoracic radiation after extrapleural pneumonectomy for malignant pleural mesothelioma.* Int J Radiat Oncol Biol Phys **56**(5), 1319–1326 (2003)

[3] J Krayenbuehl, M Hartmann, A J Lomax, S Kloeck, E B Hug, and I F Ciernik. *Proton therapy for malignant pleural mesothelioma after extrapleural pleuropneumonectomy.* Int J Radiat Oncol Biol Phys **78**(2), 628–634 (2010)

[4] Baldini. *Patterns of failure after trimodality therapy for malignant pleural mesothelioma.* Ann Thorac Surg **63**, 334–338 (1997)

[5] J Krayenbuehl, O Susann, J B Davis, and I F Ciernik. *Combined Photon and Electron 3D-Conformal versus Intensity Modulated Radiotherapy with an Integrated Boost for Adjuvant Treatment of Malignant Pleural Mesothelioma following Pleuropneumonectomy.* Int J Radiat Oncol Biol Phys **69**(5), 1593–1599 (2007)

[6] A M Allen, D Schofield, F Hacker, L E Court, and M Czerminska. *Restricted field IMRT dramatically enhances IMRT planning for mesothelioma.* Int J Radiat Oncol Biol Phys **69**(5), 1587–1592 (2007)

[7] D Lovelock, S Lim, E Yorke, and et al. *Comparison of Dose Distributions Calculated Using Different Planning Systems with Radiochromic Film Measurements in an Inhomogeneous Phantom.* Med Phys **39**, 3828 (2012)

[8] E D York, A Jackson, and K E Rosenzweig. *Correlation of dosimetric factors and radiation pneumonitis for non-small-cell lung cancer patients in a recently completed dose escalation study.* Int J Radiat Oncol Biol Phys **63**, 692–699 (2005)

[9] S L Wang, Z Liao, and A A Vaporciyan. *Investigation of clinical and dosimetric factors associated with postoperative pulmonary complications in esophageal cancer patients treated with concurrent chemoradiotherapy followed by surgery.* Int J Radiat Oncol Biol Phys **64**, 692–699 (2006)

[10] M Scorsetti, M Bignardi, A Clivio, L Cozzi, A Fogliata, P Lattuada, P Mancosu, P Navarria, G Nicolini, G Urso, E Vanetti, S Vigorito, and A Santoro. *Volumetric modulation arc radiotherapy compared with static gantry intensity-modulated radiotherapy for malignant pleural mesothelioma tumor: a feasibility study.* Int J Radiat Oncol Biol Phys **77**(3), 942–949 (2010)

[11] A M Allen, M Czerminska, P A Janne, D J Sugarbaker, R Bueno, J R Harris, L Court, and E H Baldini. *Fatal pneumonitis associated with intensity-modulated radiation therapy for mesothelioma.* Int J Radiat Oncol Biol Phys **65**(3), 640–645 (2006)

1 Clinical Outcome of Postoperative Highly Conformal versus 3D Conformal Radiotherapy in Patients with Malignant Pleural Mesothelioma

J. Krayenbuehl[1], P. Dimmerling[1], I.F. Ciernik[2, 3], O. Riesterer[1]

[1] Department of Radiation Oncology, Zurich University Hospital, Zurich, Switzerland
[2] Center for Clinical Research, University of Zurich, Zurich, Switzerland
[3] Department of Radiotherapy and Oncology, Dessau Municipal Hospital, Dessau, Germany

Status of the manuscript: in press (2014) in the *Radiation Oncology* journal.

Author contribution J. Krayenbuehl: planning, data analysis and interpretation, manuscript drafting. Patient data collection was performed in collaboration with *P. Dimmerling*.

1.1 Abstract

Radiotherapy (RT) is currently under investigation as part of a trimodality treatment of malignant pleural mesothelioma (MPM). The introduction of highly conformal radiotherapy (HCRT) technique improved dose delivery and target coverage in comparison to 3-dimensional conformal radiotherapy (3DCRT). The following study was undertaken to investigate the clinical outcome of both radiation techniques.

Thirty-nine MPM patients were treated with neoadjuvant chemotherapy, extrapleural pneumonectomy (EPP) and adjuvant RT. Twenty-five patients were treated with 3DCRT, and 14 with HCRT (Intensity modulated radiotherapy or volumetric modulated arc therapy). Overall survival, disease free survival, locoregional recurrence and pattern of recurrence were assessed. A matched pair analysis was performed including 11 patients of each group.

After matching for gender, age, histology, tumour stage and resection status, HCRT seemed superior to 3DCRT with a local relapse rate of 27.3 % compared to 72.7 % after 3DCRT (p=0.06). The median time to local relapse was increased by 49 % with HCRT in comparison to 3DCRT from 10.9 $\pm$ 5.4 months to 16.2 $\pm$ 3.1 months (p=0.06). The median overall survival was 22.3 $\pm$ 15.3 months for HCRT and 21.2 $\pm$ 9.2 months for 3DCRT (p=0.57). Recurrence analysis showed that in-field local relapses occurred in previously underdosed regions of the tumor bed in 16 % of patients treated with 3DCRT and in 0 % of HCRT patients.

The use of HCRT increases the probability of local control as compared to 3DCRT by improving target volume coverage. HCRT does not improve overall survival due to high rates of distant recurrences.

1.2 Introduction

Malignant pleural mesothelioma (MPM) is a rare and aggressive malignancy associated with poor prognosis. Although MPM is often initially confined to the hemithorax, it has a high potential for metastatic spread in the course of disease [1]. The mainstay of treatment is surgery consisting of either pleurectomy/decortication (PD) or radical extrapleural pneumonectomy (EPP) in combination with cisplatin/pemetrexed and, in selected cases, postoperative radiotherapy [2–5]. The rationale to apply postoperative radiotherapy after EPP has been the high rate of local recurrence after EPP alone of about 40 % [6].

The pattern of pleural dissemination, infiltrative growth and the manipulations within the chest cavity during surgery place the entire ipsilateral

chest wall at high risk for post-surgical relapse, especially at the diaphragm insertion, the pericardium, mediastinum and bronchial stump. Technically, hemithoracic radiotherapy is challenging due to various reasons. Firstly, the size of the volume to be treated is large, and may cover up to six liters. Secondly, the target lies in close proximity to various organs at risk (OAR) such as the heart, ipsilateral kidney, liver, remaining lung, esophagus and/or spinal cord. Thirdly, the thoracic cavity has a complex shape with its costodiaphragmatic recess extending around the liver and the kidney. Previous publications showed that highly conformal radiotherapy (HCRT) such as intensity modulated radiotherapy (IMRT) or volumetric modulated arc therapy (VMAT) can improve the dose distribution in respect to target coverage and dose to OAR [7, 8]. However to our knowledge there is no clinical study published that investigated and compared clinical outcome after both radiation techniques. In order to verify if the technical improvements introduced with IMRT or VMAT have translated into a clinical benefit, we evaluated the clinical outcome of MPM patients treated with chemotherapy, surgery and 3DCRT or HCRT at our institution.

1.3 Material and methods

We reviewed the clinical outcome of 39 consecutive patients treated either with 3DCRT (25 patients) or HCRT (11 IMRT patients and 3 VMAT patients). Patient staging was established using FDG-PET/CT and/or conventional thoraco-abdominal CT. The patients with clinical stage T1-T3, N0-2, M0, R0-2 were treated with 3 cycles of preoperative chemotherapy (pemetrexed and cisplatin) followed by EPP and RT [7]. All histological subtypes were accepted for RT. Patients were not selected for this review if they had metastatic disease or a local relapse before the start of RT. The study was approved by the local ethics committee.

1.3.1 Radiation techniques

The 3DCRT group was treated between 1999 and 2005. These patients were treated with 25 x 1.8 Gy = 45 Gy to the hemithorax and subsequently, in a second series, a boost of 7 x 1.8 Gy = 12.6 Gy was given to the incompletely resected area (total dose 57.6 Gy). Dose calculation was performed on Pinnacle planning system (Philips Medical Systems) for a linear accelerator (Clinac 2100C, Varian Medical Systems). Details of the treatment technique have previously been published [7].

HCRT has been used at our institution since 2005 for the treatment of

MPM patients. Of the 14 patients treated with HCRT, 11 were treated with conventional static field IMRT and 3 patients with rotational IMRT (volumetric arc radiotherapy, i.e. Rapid Arc®in the present series).

IMRT and VMAT plans achieved similar dose distributions [9, 10]. In the case of HCRT only one series was applied with 26 x 1.75 Gy = 45.5 Gy delivered to the hemithorax with a simultaneous integrated boost of 26 x 2.15 Gy = 55.9 Gy delivered to the R1/R2 region. Planning and dose calculation was performed on the Eclipse planning system (Varian Medical Systems, Palo Alto, CA) for a linear accelerator (Clinac 6EX or Trilogy, Varian Medical Systems). The treatment technique and dose-volume constraints have been previously published [7, 9, 11].

1.3.2 Follow-Up and recurrence

Patients were followed up every three to four months with clinical examinations and CT or PET/CT scans. Local tumor progression or recurrence was defined as an increasing radiographic abnormality within or partially within the irradiation field. Recurrence adjacent to the field border but not in-field was defined as marginal miss recurrence. Regional recurrence was defined as recurrence in close proximity but not within the irradiated field. Tumor recurrence in the contralateral hemithorax or abdominal cavity was classified as a distant recurrence [12]. All in-field recurrences were carefully analyzed by 2 of the authors (JK, PD), in order to assess if they occurred in previously underdosed areas by comparing the respective diagnostic image with the radiation therapy treatment plan.

1.3.3 Statistics

All survival endpoints as well as tumor recurrence were measured from the date of treatment start (neoadjuvant chemotherapy) and were evaluated using the Kaplan Meier Method. In a subset of the cohort, a matched pair analysis was performed in order to compare outcome after 3DCRT and HCRT. For this analysis, the patients were matched for age, preoperative TNM, R and histology, and sex (except one pair).

1.4 Results

Between 1999 and 2011, 39 patients were treated with neoadjuvant chemotherapy and EPP followed by RT. All follow up patients were deceased at the time of this study.

1.4.1 Matched pair analysis

In the matched pair analysis, 11 HCRT and 11 3DCRT patients were matched based on tumor staging, resection status, tumor histology, age and gender (except one pair were the gender was not matched). In each group 3 patients had a tumor stage T1N0M0 with resection R0 and 8 patients, tumor stage T2N0M0 with resection R1. Tumor histology was epithelioid for 6 patients and biphasic for 5 patients in each group. The mean age was 59.6 years and 59.8 years for patient,Äôs in the HCRT and 3DCRT group.

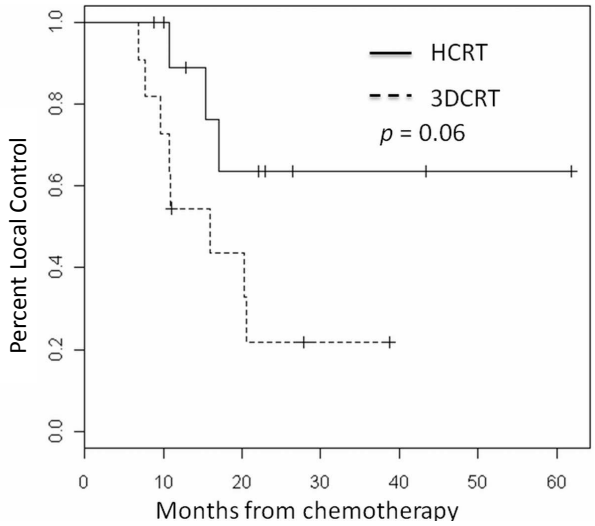

Figure 1.1: Local control for 11 matched modulated radiotherapy (HCRT) patients and 11 3-dimensional conformal radiotherapy (3DCRT) patients.

The median time to local relapse was increased by 49 % with HCRT in comparison to 3DCRT from 10.9 ± 5.4 months to 16.2 ± 3.1 months ($p = 0.06$) as displayed in Figure 1. Three (27.3 %) and eight patients (72.7 %) had a local relapse after HCRT and 3DCRT respectively. Nine HCRT (81.8 %) and nine 3DCRT (81.8 %) patients developed metastases within a median time of 18.4 ± 10.7 months and 10.9 ± 8.6 months ($p = 0.21$). The difference in disease free survival between HCRT and 3DCRT was not significant ($p = 0.72$). The median overall survivals were 22.3 ± 15.3 months for HCRT and 21.2 ± 9.2 months for 3DCRT and are displayed in Figure 2 ($p = 0.57$).

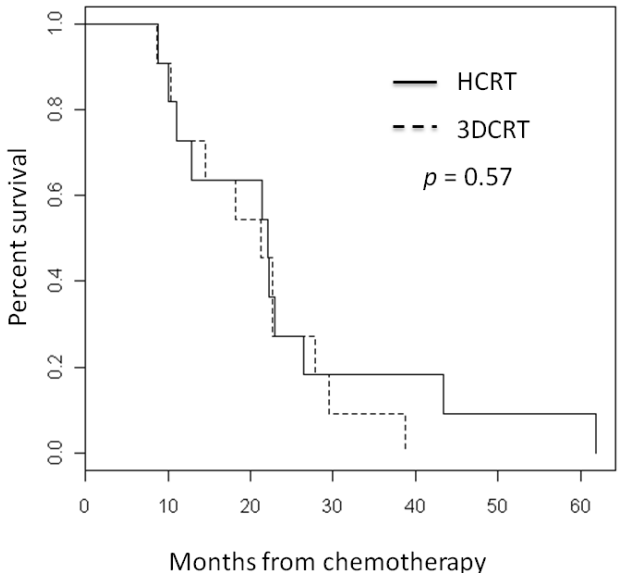

Figure 1.2: Overall survival for 11 matched modulated radiotherapy (HCRT) patients and 11 3-dimensional conformal radiotherapy (3DCRT) patients.

1.4.2 Outcome of the entire cohort

Fourteen HCRT and 25 3DCRT patients were treated and reviewed. Patient's sex, age, tumor characteristics and resection are displayed on Table 1.1.

The median overall survival was 20.8 ± 14.4 months for the HCRT group, and 26.9 ± 11.8 months for the 3DCRT group ($p = 0.48$). In the HCRT group, 10 patients (71 %) died of progressive disease and 4 patients (29 %) due to intercurrent disease:, one patient died of septic shock, one of acute myocardial infarction, one of progressive biventricular heart failure and another patient, who was well and without evidence of disease at two days before his sudden death, most likely also died due to a cardiac event. In the 3DCRT group 24 patients (96 %) died of progressive disease and one of septic shock (4 %).

The local control rates were improved after HCRT ($p = 0.30$). Four HCRT patients (28.6 %) suffered from locoregional relapse in comparison to 15 patients (60 %) treated with 3DCRT.

Characteristic	HCRT n = 14	3DCRT n = 25
Male	13	22
Female	1	3
Mean age (years)	61	61
Right sidded tumor	9	15
Left sidded tumor	5	10
Tumor histology epithelioid	8	17
Tumor histology biphasic	6	8
Initial tumor stage T1	3	15
Initial tumor stage T2	10	10
Initial tumor stage T3	1	0
Initial nodal stage N0	14	22
Initial nodal stage N1	0	1
Initial nodal stage N2	0	2
Resection R0	4	8
Resection R1	9	15

Table 1.1: Patient demographics and tumor characteristics of 39 patients who underwent neoadjuvant chemotherapy, extrapleural pneumonectomy and radiotherapy. *Abbreviations*: HCRT: Highly conformal modulated radiotherapy, 3DCRT: 3 dimensional conformal radiotherapy

Localization	Age	Sex	Histology	Time to recurrence (months)	Dose in recurrence region (Gy)
In-field recurrence	67	M	Epithelioid	10	54
In-field recurrence	62	M	Biphasic	15	56-59
In-field recurrence	64	M	Epithelioid	10	43-50
Marginal miss recurrence	65	M	biphasic	17	13

Table 1.2: Locoregional recurrences in patients who underwent modulated radiotherapy

1.4.3 Analysis of tumor recurrence

For patients treated with HCRT, local relapse occurred in-field in 3 patients (21.4 %), all within areas that had been treated with doses between 43 Gy to 59 Gy (according to our treatment planning protocol 95 % of the prescribed 45 Gy (=43 Gy) should enclose the target volume, which in this case is the tumor bed of the hemithorax, Table 1.2) and none in a clearly underdosed region. One patient (7.1 %) had a marginal miss recurrence at the field border (13 Gy). In the 3DCRT group, twelve patients (48 %) had in-field recurrences in regions treated with doses between 30 Gy and 56 Gy (Table 1.3). Notably, in 16 % of patients treated with 3DCRT (4/25) in-field recurrences occurred in regions that were covered with doses of only 30 to 43 Gy, instead of the prescribed $>$ 45 Gy. One patient (4.0 %) had a marginal miss recurrence (18 Gy). In one patient with a regional recurrence (4.0 %) the delivered dose was not possible to define because no diagnostic CT was available. In one patient (4.0 %) the site of recurrence could not be determined because of missing radiographs during follow-up

Localization	Age	Sex	Histology	Time to recurrence (months)	Dose in recurrence region (Gy)
In-field recurrence	61	M	Epithelioid	21	50
In-field recurrence	68	M	Biphasic	16	36
In-field recurrence	68	M	Epithelioid	13	30
In-field recurrence	65	M	Biphasic	19	56
In-field recurrence	65	M	Biphasic	16	50
In-field recurrence	50	M	Epithelioid	29	48
In-field recurrence	55	M	Biphasic	8	50
In-field recurrence	66	M	Biphasic	20	36, 50
In-field recurrence	68	M	Epithelioid	11	32-43, 46-50
In-field recurrence	58	M	Epithelioid	9	50
In-field recurrence	58	M	Epithelioid	11	50
In-field recurrence	56	M	Epithelioid	19	30
Marginal miss recurrence	55	M	epithelioid	19	18
Regional recurrence	62	M	epithelioid	13	N/A
Unknown	56	M	epithelioid	13	N/A

Table 1.3: Locoregional recurrences in patients who underwent 3D-conformal radiotherapy

Distant recurrences occurred in ten patients (71.4 %) treated with HCRT and in twenty 3DCRT patients (80 %). The median time to distant metastases was 18.4 ± 10.7 months in HCRT group and 16.7 ± 7.7 months in 3DCRT group ($p = 0.7$). In the HCRT group, distant metastases involved only the contralateral chest in three patients (30 %) and only the abdominal cavity in three patients (30 %). Both sites were affected by distant metastases in four further patients (40 %).

1.5 Discussion

We demonstrate in a retrospective analysis of patients with MPM and treated at our institution with trimodality therapy that the use of postoperative highly conformal radiation techniques (HCRT) reduces local recurrence in comparison to 3DCRT. A recurrence analysis showed that in the case of 3DCRT 4 of 25 patients (16 %) had a local recurrence in regions that were clearly underdosed according to current radiation protocols (doses > 45 Gy are recommended, e.g. SAKK 17/04) in contrast to 0 % of patients treated with HCRT. This supports the hypothesis that HCRT should improve local control in comparison to 3DCRT by improving target volume coverage. In our study patients treated with HCRT showed a tendency for improved progression free survival and local relapse free survival but did not benefit in terms of overall survival due to the high rates of distant relapses.

Local control is important in patients with MPM for symptom control, but also because some patients might benefit in terms of improved overall survival. Better local control after HCRT did not translate into improved overall survival in our patient series. Remarkably, the rate of death due to intercurrent disease, most often cardiac events, was higher after HCRT (29 %) in comparison to 3DCRT (4 %). Since cardiac sparing is rather improved with HCRT the most likely explanation for this difference is patient selection. The urgent research question, if postoperative radiotherapy impacts on overall survival after EPP, is addressed by a randomized study currently conducted in Switzerland, SAKK 1704. Patient accrual for this study was terminated in 2012 and the results are awaited.

Even after trimodality treatment local recurrence remains high in some patient series. In a retrospective series of 49 patients treated with 3D-conformal RT after EPP and chemotherapy 67 % of all recurrences included the ipsilateral hemithorax and 25 % of all recurrences were local only [12]. Therefore improvement of radiotherapy is mandatory. In recent years radiotherapy has made enormous technical advances. More sophisticated highly conformal radiation techniques (HCRT) such as IMRT or rotational RT

(VMAT) have become available and substituted for the older 3DCRT technique. The use of HCRT enables improvement in the dose distribution and target volume coverage. This is because with HCRT even complex target volumes such as the tumor bed of the costodiaphragmatic recess or the pericardium can be treated without or with little dose compromise and at the same time with optimal sparing of the normal tissue due to a steeper dose fall-off. Thus, the use of HCRT should intuitively improve treatment outcome in terms of local tumor control. Our data suggest indeed, that the use of HCRT bears considerable potential to improve on hemi-thoracic tumor control rates most likely due to improved target volume coverage.

The poor local control rates and high rates of in-field recurrences following 3DCRT in our cohort may be due to suboptimal dose coverage or the restriction of the target volume to avoid critical organs, both limitations inherent to the technique. After 3DCRT 4/24 (16.6 %) in-field recurrences occurred in regions covered with only 30-43 Gy. In the case of 3DCRT mixed beams of photons and electrons were used to optimize dose coverage. The match of these beams often causes cold and hot spots of dose coverage. Poor matching during daily treatment can result in $>$ 20 % dose inhomogeneity in the junction area [7]. In addition, as the spinal cord is blocked when the tolerance dose of 45 Gy is reached, insufficient dose delivery to parts of the mediastinum has been observed, resulting in underdosage to the tumor bed [7].

Favorable tumor control after IMRT as part of a trimodality therapy has previously been reported by Rice et al. [13]. The median overall survival of their 61 patients treated was 14.2 months with a locoregional recurrence rate of 13 % and only 5 % local in-field recurrences reported. The median dose prescribed was only 45 Gy, and half of all patients received doses even less than 45 Gy. The reason for the comparatively higher local control rate reported by Rice et al. in comparison to our study remains unclear. It may be explained by patient selection and the comparatively short median overall survival of 14.2 months in comparison to 20.8 months in the present series and by the retrospective study design. The shorter median overall survival reported by Rice et al. could be caused by more advanced tumor stages (40 T3, 8 T4, 26 N2), more aggressive subtypes (14 biphasic, 4 sarcomatoid) and the fact that neoadjuvant chemotherapy was not routinely administered.

With regard to toxicity the major dose limiting organ for postoperative radiotherapy of MPM is the contralateral lung. Lung complications such as radiation pneumonitis are likely to be higher with multi-field techniques such as IMRT or VMAT in comparison to 3DCRT, where opposed beams from 0 and 180 degrees are usually used, thereby optimally sparing the contralateral lung. With regard to dose escalation and lung sparing surgery,

protons might prove superior to IMRT/VMAT. Severe complications of the lung with grade 4 and 5 pneumonitis after IMRT have been reported [7, 12]. Since then, special attention to the contralateral lung dose has been given during the treatment planning process and pneumonitis rates should be lower today. Intuitively, the use of HCRT should reduce toxicity and complication probabilities of esophagus, heart, liver and kidney, however no data with regard to these toxicity endpoints comparing both treatment techniques are available.

In recent years, the need for extensive surgery has been questioned, and less radical surgery has been advocated such as pleurectomy/decortication. In the context of reduced surgery, the anatomical situation makes it difficult for RT to be applied to the entire pleural space, however, it can still be considered as a targeted local postoperative option in case of incomplete resection. Future clinical studies are required to define the role of radiotherapy in combination with lung sparing surgery.

1.6 Conclusions

In summary, the use of HCRT for treatment of patients with MPM after EPP is likely to improve local control rates. The local control improvement did not improve the overall survival due to the high rates of distant relapses in this series. Further improvement of trimodal or systemic therapy is required to tackle the high risk of distant recurrences.

Bibliography

[1] AS Tsao, I Wistuba, JA Roth, and HL Kindler. *Malignant pleural mesothelioma.* J Clin Oncol **27**, 2081–2090 (2009)

[2] VW Rusch, K Rosenzweig, E Venkatraman, L Leon, A Raben, L Harrison, MS Bains, RJ Downey, and RJ Ginsberg. *A phase II trial of surgical resection and adjuvant high-dose hemithoracic radiation for malignant pleural mesothelioma.* J Thorac Cardiovasc Surg **122**, 788–795 (2001)

[3] N J Vogelzang, J J Rusthoven, J Symanowski, C Denham, E Kaukel, P Ruffie, U Gatzemeier, M Boyer, S Emri, C Manegold, C Niyikiza, and P Paoletti. *Phase III study of pemetrexed in combination with cisplatin versus cisplatin alone in patients with malignant pleural mesothelioma.* J Clin Oncol **21**(14), 2636–2644 (2003)

[4] W Weder, R Stahel, J Bernhard, S Bodis, P Vogt, P Ballabeni, D Lardinois, D Betticher, R Schmid, R Stupp, H Ris, M Jermann, W Mingrone, A Roth, and A Spiliopoulos. *Multicenter trial of neo-adjuvant chemotherapy followed by extrapleural pneumonectomy in malignant pleural mesothelioma.* Ann Oncol **18**(7), 1196–1202 (2007)

[5] T Treasure, L Lang-Lazdunski, D Waller, JM Bliss, C Tan, M Snee, M O Brien, G Thomas, S Senan, and K O Byrne. *Extra-pleural pneumonectomy versus no extra-pleural pneumonectomy for patients with malignant pleural mesothelioma: clinical outcomes of the Mesothelioma and Radical Surgery (MARS) randomised feasibility study.* Lancet Oncol **12**, 763–772 (2011)

[6] PA Janne and E Baldini. *Patterns of failure following surgical resection for malignant pleural mesothelioma.* Thorac Surg Clin **14**, 567–573 (2004)

[7] J Krayenbuehl, O Susann, J B Davis, and I F Ciernik. *Combined Photon and Electron 3D-Conformal versus Intensity Modulated Radiotherapy with an Integrated Boost for Adjuvant Treatment of Malignant Pleural Mesothelioma following Pleuropneumonectomy.* Int J Radiat Oncol Biol Phys **69**(5), 1593–1599 (2007)

[8] A M Allen, D Schofield, F Hacker, L E Court, and M Czerminska. *Restricted field IMRT dramatically enhances IMRT planning for mesothelioma.* Int J Radiat Oncol Biol Phys **69**(5), 1587–1592 (2007)

[9] J Krayenbuehl, M Hartmann, A J Lomax, S Kloeck, E B Hug, and I F Ciernik. *Proton therapy for malignant pleural mesothelioma after extrapleural pleuropneumonectomy.* Int J Radiat Oncol Biol Phys **78**(2), 628–634 (2010)

[10] J Krayenbuehl, P Dimmerling, IF Ciernik, and O Riesterer. *Clinical Outcome of Postoperative Highly Conformal versus 3D Conformal Radiotherapy in Patients with Malignant Pleural Mesothelioma.* Radiation Oncology **submitted** (2013)

[11] J Krayenbuehl, O Riesterer, S Graydon, P Diemerling, S Kloeck, and I F Ciernik. *Volumetric modulated arc therapy for malignant pleural mesothelioma after extrapleural pneumonectomy.* J Appl Clin Med Phys **14**(4) (2013)

[12] Baldini. *Patterns of failure after trimodality therapy for malignant pleural mesothelioma.* Ann Thorac Surg **63**, 334–338 (1997)

[13] D C Rice, W R Smythe, Z Liao, T Guerrero, J Y Chang, M F McAleer, M D Jeter, A Correa, A A Vaporciyan, H H Liu, R Komaki, K M Forster, and C W Stevens. *Dose-Dependent Pulmonary Toxicity After Postoperative Intensity-Modulated Radiotherapy for Malignant Pleural Mesothelioma.* Int J Radiat Oncol Biol Phys , 350–357 (2007)

1 Hierarchical enhanced non-rigid registration for target volume correction and propagation for adaptive external beam radiotherapy of carcinoma of the prostate

A. Andronache[1], J. Krayenbuehl[2], G. Szekely[1], I.F. Ciernik[3, 4],

[1] Computer Vision Laboratory, Federal Institute of Technology, Zurich, Switzerland
[2] Department of Radiation Oncology, Zurich University Hospital, Zurich, Switzerland
[2] Center for Clinical Research, University of Zurich, Zurich, Switzerland
[3] Department of Radiotherapy and Oncology, Dessau Municipal Hospital, Dessau, Germany

Status of the manuscript: in press in *Journal of Applied Clinical Medical Physics*.

Author contribution J. Krayenbuehl: performed the data analysis and interpretation in colaboration with *A. Andronache*, manuscript drafting, revision and editing.

1.1 Abstract

Target volumes change during fractionated radiotherapy (RT). We investigate a tool based on the Hierarchical Enhanced Registration Algorithm (HERA) to project a 3D-segmentation set of the prostate into the subsequent imaging sets at any time point during RT by using intensity-based image registration techniques.

Sequential CT sets during RT at 15, 30, 45 and 60 Gy of two patients were used. Five expert clinicians outlined the prostate in a blinded fashion, defining intra-observer and inter-observer variability on a set of 35 and 25 scans, respectively. The observer variability and positioning for manual correction was compared to both affine and elastic image registration-based contour propagation.

The overall mean-error of the registration-based correction of the planning target volume was comparable to the inter-observer variability of manual target volume definition. The correction by affine image fusion was inferior to the results of elastic registration. The maximal deviation for the inter-observer segmentation was 15.4 mm, 10.5 mm for the affine and 8.0 mm for the elastic registration. The mean inter-observer variability was 1.5 ($\pm$ 1.4) mm, 2.8 ($\pm$ 2.3) mm for the affine and 2.2 ($\pm$ 1.9) mm for the elastic registration.

Intensity-based elastic registration of deformable anatomical structures with HERA is suitable for the assessment of changes of prostate volumes for the purpose of target propagation and adaptive radiotherapy.

1.2 Introduction

External beam radiotherapy of the prostate is generally performed over a larger number of fractions. Over this period, the volumes of the rectum and bladder can fluctuate causing displacement and may contribute to the deformation of the target volumes, as well. Therefore, anatomical and geometrical uncertainties must be taken into account by the planning target volume (PTV). The spatial plasticity of the prostate during the course of RT has been well documented, and the volume of the prostate may slightly increase during the first days of RT and shrink during the following weeks [1, 2]. In order to keep PTV margins minimal, daily target positioning verification before treatment can be beneficial [3]. Several techniques have been investigated to account for the inter-treatment positioning variability of the prostate. Before high-resolution in-room fluoroscopy or 3D-on-board imaging systems became available, the localization of the prostate mostly relied

on remote anatomical bony markers. Endorectal spacers help to predict the position of the prostate and could reduce internal target volume (ITV) margins [4]. Direct prostate localization is achieved with fiducial markers in the prostate [5, 6]. Other positioning systems rely on ultrasound technology or transponders [7, 8]. All these approaches, however, neglect the plasticity of the target structures and volumes over the treatment time.

Onboard CTs during RT provide a novel opportunity to redefine the volume of the prostate on a daily basis and if necessary, adapt the CTV. However, the reliability of CT-based prostate localization and volume assessment may be reduced by technical limitations, such as the typical low contrast soft tissue differentiation of the common on-board CT imaging systems, interfering with re-segmentation and automated target volume reconstruction.

In the present work we investigate the possibility of using image registration techniques as a tool for target volume propagation. Image registration is the process of transforming the different sets of data onto one coordinate system, such that the scene or the objects pictured from different views and/or at different time points are brought into alignment. Considering that the physician can make a detailed planning and contouring of the prostate onto an initial CT scan of a patient, we registered it to all the subsequent CTs acquired during the RT. By using non-rigid image registration techniques such as the Hierarchical Enhanced Registration Algorithm (HERA) [8], we studied the performance of both affine and non-rigid transformations to estimate the spatial changes and to compensate for the plasticity of the pelvic structures. The information from the positioning changes of the pelvis is applied to the prostate clinical target volume (CTV), allowing precise prostate localization during potentially each single treatment sessions. The ability of the physicians to manually define the prostate volume for the purpose of adaptive radiotherapy is compared to the performance of the proposed automated computer-based CTV registration. Routine adaptation of the prostate volume and on-line re-planning to account for volume changes during radiotherapy has not been introduced in routine treatment yet. One major requirement in implementation of adaptive image guided radiotherapy will rely on optimal iterative target volume assessment procedure. Using a method based on ray casting, hierarchical image registration , and manual segmentation is a novel approach in the context of adaptive radiotherapy. We hypothesize that the automated registration with HERA will improve the contouring of the prostate and eventually allow minimizing PTV margins for the purpose of adaptive radiotherapy, especially posteriorly avoiding underdosing the posterior lobes of the prostate.

1.3 Materails and Methods

1.3.1 Patient characteristics and CT acquisition

Sequential CTs were obtained from two prostate-cancer patients undergoing external beam radiotherapy. Patients were scanned and treated in a supine position with a rectal balloon with 40 cm^3 of air [4]. CTs were obtained before starting treatment and at 15 Gy, 30 Gy and 45 Gy for two patients, and, additionally, 60 Gy for one patient. All CTs have been performed on a helical single slice CT scanner. The slice thickness of the CT images was 5 mm for both patients. The in-plane resolution was 512 x 512 pixels of 0.9766 x 0.9766 mm^2 for the first patients, and 512 x 512 pixels of 0.8301 x 0.8301 mm^2 for the second patient.

1.3.2 Prostate contouring - inter-observer and intra-observer segmentation variability

The inter-observer variability of the manual prostate segmentation was defined by a group of five expert clinicians that, in a blinded fashion, manually contoured repeatedly the prostate in all 7 available CTs (0 Gy, 15 Gy, 30 Gy for two patients and 60 Gy for one patient). The manual segmentation was performed using Eclipse treatment planning system (Varian Medical Systems, Palo Alto, CA), and saved as DICOM-RT to be used in subsequent analysis. The long-term intra-observer variability was investigated by asking the same doctors to repeat the prostate segmentation in the available CT data. The average time interval between the delineation of the first and the second set of contours was about 6 months, in a blinded fashion. For both patients, the segmentation was done for the entire time-series of CT acquisitions (7 images) resulting in 35 CT sets for the inter-observer analysis. For the intra-observer analysis, the segmentation was repeated for the acquisition prior to the RT resulting in a set of 20 CTs.

1.3.3 Distance-based metrics

Each CT image had a series of 5 manual segmentations of the prostate, each of them furnished a set of 2D axial contour points defined on subsequent slices of the acquisition. The average center of mass of the prostate (CMP) was estimated from all the contour points of the 5 segmentations and each segmentation was reconstructed by using a simple tessellation procedure of the originally defined points. Then, the CMP was used as source point to radially cast 2048 rays, uniformly distributed using a constant angular step in

both elevation $0^{\circ} < \theta < 180^{\circ}$ and azimuth $0^{\circ} < \phi < 360^{\circ}$ directions. The average spatial location of the 5 intersection points between the segmented surfaces and each ray casted from the CMP was then used to estimate an average segmentation surface. At the same time, these intersection points, along each casted ray, define an estimate of the local inter-observer variability (within the analysed CT image). By putting together all these local estimates, we expressed globally the inter-observer segmentation variability in terms of standard deviations of contour displacements within the same CT image as delineated by the group of 5 clinicians.

In a similar local manner, the long-term intra-observer variability was expressed in terms of standard deviation of the contour displacements distribution estimated from the long-term repeated manual segmentations of the five clinicians on the two available CTs prior RT.

1.3.4 Image registration and contour propagation

HERA was used to estimate and to correct for the plasticity of the pelvic structures between subsequent CT scans [8]. HERA optimized an affine transformation (displacement, rotation, skew and scaling) and an elastic deformation field between the initial CT scan (prior to RT) and each subsequent CT scan (during RT) of each patient. These transformations (affine and elastic) were used eventually to propagate the prostate contour as defined on the initial CT scan of each patient, prior to RT. The registration procedure used image intensity cross-correlation as similarity measure, as all images were acquired in the same modality (i.e. CT). In addition, to limit the influence of out of interest pelvic tissues and structures, we restricted the registration process to the prostate surrounding region.

The propagated contours were characterized by using the same ray-casting strategy as for the evaluation of the intra- and inter-observer manual segmentation variability.

1.3.5 Evaluation of the contour propagation effectiveness

To evaluate the precision of image registration as a propagation tool, we compared the propagated contours of the prostate with the segmentations obtained manually. We used different measures to locally describe and quantify the precision of the registration for each of the 5 CT data acquired during the RT.

In a first step, the registration-based contour propagation was compared to the inter-observer variability of the prostate segmentation. Therefore,

a two-tailed Student t-test was used on the null hypothesis that the mean (average) of the propagated contours is inside the confidence interval of the mean of the manually segmented contours against the alternative hypothesis that the mean of the propagated contours is outside this confidence interval.

In a second step, the registration-based contour propagation was compared to the intra-observer variability. Having the CT data segmented twice by each doctor, one can compare the two populations of contour deviations originating from the same person - in one case, the contours have been generated by the same person on the same image, and in the other case, the contours have been generated by the same person on two different images and propagated over. Therefore, we compared the deviations in contouring the same image with deviations in contouring different images that are afterwards registered. If the first population describes only the reproducibility in contouring of the observers, the second population represents a complex variability that accumulates the reproducibility in contouring together with the registration/propagation error.

For all tests performed, the CT done at 0 Gy, prior to RT, was chosen as the floating image. The following CTs were considered as reference. As such, the initial contours are always propagated onto the following acquired images.

In all these statistical tests, each population was consisted of 2048 sets, each consisting of 5 points. A statistical t-test was performed locally on each sets of point, along each casted ray (the tests were performed 2048 times). For all tests, a p-value smaller than 0.05 was accepted as significant.

1.4 Results

1.4.1 Contour propagation versus inter-observer variability

First, we evaluated the performance of the propagation of the planning contours against the inter-observer variability of the prostate segmentation. Table 1.1 describes the inter-observer variability (the 1st row), together with the registration error of contour propagation while using the affine registration (the 2nd row), and while using the elastic registration (the 3rd row). Table 1.1 summarises the average of the descriptive statistics for the differences from the mean prostate contour: the mean, the standard deviation, and the maximal distance. The mean deviation was increased by 1.24 mm with the affine registration and 0.64 mm with the elastic registration in comparison to the segmented registration. But the maximum registration was reduced by

1.38 mm (respectively 2.76 mm) with the affine (respectively elastic) registration. The mean and maximum deviation was the largest in the Y-direction (superior-inferior direction) for affine and elastic registration due to the CT resolution in the Y-direction (5 mm). In the anterior-posterior direction, the mean deviation was small, bellow 1 mm for the manual, affine and elastic registrations. Nevertheless, the maximal deviation could be reduced by 3 mm with the affine registration and 3.7 mm with the elastic registration.

	X mean	X std	X max	Z mean	Z std	Z max	Y mean	Y std	Y max	mean	std	max
Segment	0.56	0.75	6.40	0.57	0.74	6.73	1.04	1.19	7.89	1.52	1.40	9.50
Affine	0.87	0.92	4.05	0.85	0.85	3.74	2.11	2.29	7.60	2.76	2.26	8.12
Elastic	0.64	0.64	3.31	0.64	0.62	2.97	1.69	1.91	6.52	2.16	1.86	6.74

Table 1.1: Segmentation variability. Mean segmentation variability averaged over all data along the X-axis (patient's right-left), Z-axis (patient's anterior-posterior) and Y-axis (patient's superior-inferior) and the resulting 3D distance showing the mean, the standard deviation and the maximum difference for inter-observer segmentation, affine and rigid registration. All measures are given in mm.

Fig. 1.1 depicts a box-plot for the local inter- and intra-observer variability distribution (along the 2048 rays) together with the contour propagation errors (by affine or elastic transformations) from one set of images that were thereafter registered. The inter- and intra-observer segmentation variability is represented on both images: the reference image (a follow-up image) and the floating image (the planning or initial image). The results showed a slight increase of the median deviation with the affine and elastic registration in comparison with the manual segmentation. A decrease of the maximum deviation is therefore achieved with the affine and elastic registration. The intra-observer deviation could be reduced by more than 3 mm with the affine registration and by more than 5 mm with the elastic registration. Fig. 1.2 depicts an example of distribution of the p-values over the entire surface of the prostate. The p-value represents the goodness of fit of two populations of contours formed on one side by the manual segmentations of the prostate in the currently analyzed image, and, on the other side, the affine and elastic segmentations propagated from the planning CT. The values $p < 0.05$ indicate a failure to propagate the planning contours, which is equivalent with a rejection of the null hypothesis that stated that the two populations are similar. In the present case, 95.5 % (respectively 97.4 %) of the 2048 sets of points had a $p > 0.05$ for the affine (elastic) registration.

Fig. 1.3 illustrates for the same set of images the distribution of various statistics over the segmented surface of the prostate. The inter-observer variability in the segmentation of the prostate is the largest in the superior part of the prostate. In this region, the standard deviation was larger than 1.8 mm in the reference images and larger than 2.5 mm on the floating images. The same variability was observed for the left part of the prostate. However, on the right side, the standard deviation was the smallest, under 0.6 mm. The 3rd and 4th rows depict the spatial distribution of the p-values of the contour propagation when using the affine and the elastic registration. The white patches represent those regions where the propagation of the planning contours failed ($p < 0.05$). These regions locate in the anterior direction for the affine and elastic registration and on the right direction for the affine registration. In these regions the inter-observer variability is small, less than 1 mm. Small mis-registrations had major influence on the statistical tests, were p values smaller than 0.05 were observed.

1.4.2 Contour propagation versus intra-observer variability

A next stage of our study was to examine the performance of the planning contours' propagation against the intra-observer variability. By using the

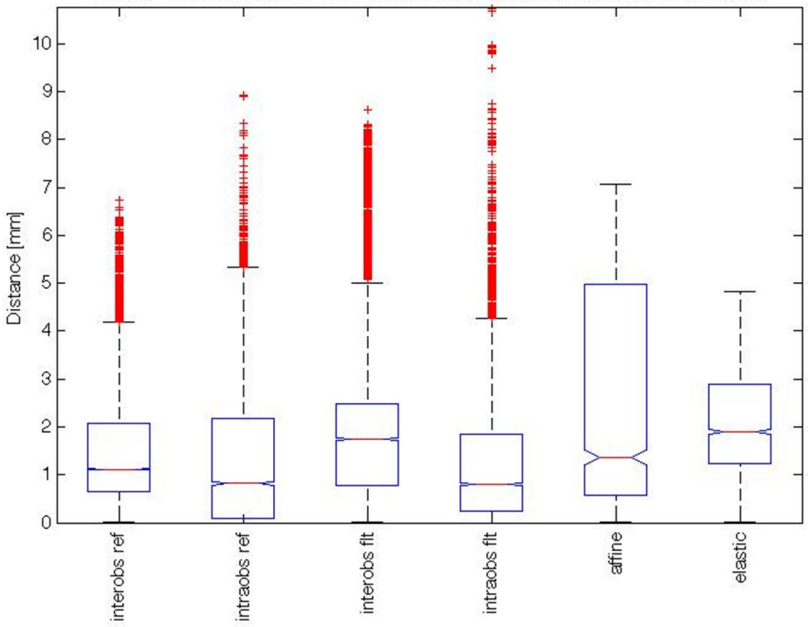

Figure 1.1: Deviation of inter- intra-individual segmentation and the registration errors. Summary of the intra- and inter-observer variability of the segmentation and the propagation errors for the target CT performed at 30 Gy. All the deviations are given in absolute values. The box-plots visualize the local inter- and intra-observer variability distribution (along the 2048 rays) together with the contour propagation errors (by affine or elastic transformations) from one set of images that were thereafter registered. The inter- and intra-observer segmentation variability is represented on both images: the reference image (a follow-up image, denoted by *ref*) and the floating image (the planning or initial image, denoted by *flt*).

same technique of showing the distribution of various statistics over the segmented surface of the prostate, Fig. 1.4 depicts the spatial distribution of the intra-observer variability over the reconstructed average surfaces of both planning and target CT on the first two rows. The intra-observer variability is large in the superior and inferior part of the prostate, with a standard deviation up to 4 mm. In the other regions the standard deviation is below 2.5 mm. The 3rd and 4th rows of Fig. 1.4 show the spatial distribution of the p-values on the prostate surface. The registrations are very good in the

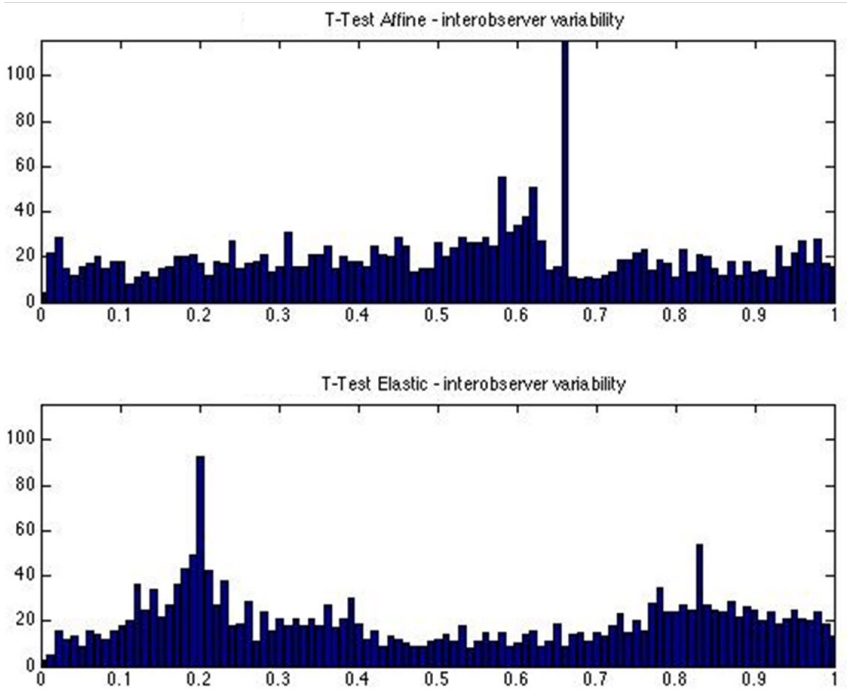

Figure 1.2: Distribution of the p-values over the entire surface (2048 points) of the prostate whilst evaluating the performance of contour propagation against the inter-observer variability of manual segmentation. The propagation of the planning CT was performed for the CT scan at 30 Gy. The p-values < 0.05 indicate significant differences and therefore propagation failure.

superior and inferior part of the prostate while in the right, left and posterior direction, the propagation failed (the white patches with $p < 0.05$). Here again, the registration failed in regions were intra-observer variability is smaller than 1mm.

1.5 Discussion

Inter-treatment target volume variability is a well recognized source of error in external beam radiotherapy [9]. Repeated 2D or 3D-imaging prior to dose

delivery has been used to ascertain target coverage and to spare neighbouring structures [10]. Currently clinical standards use rigid positioning verification approaches, basing mostly on 2D, and more recently on 3D structure matching techniques [11]. Adaptive treatment taking structure deformation into account improves dose distribution of photon-based treatments [12].

In the present study we show that, by using a registration algorithm as a propagation tool, an automated 3D computer-based target volume adaptation over a prolonged treatment compares favorably with expert-derived target reassessment for the purpose of adaptive planning. Target volume propagation using deformable imaging registration for adaptive RT bears several potential advantages, especially, the possibility to reduce the internal target margin to close to zero [13]. Imaging systems for target position verification systems, such the Calypso System (Calypso Medical Technologies, Seattle, USA) or the ExacTrac^{TM}(BrainLAB, Feldkirchen, Germany), allows reducing the irradiated target volume margins to 1 mm if imaging of the prostate localization is used every 15 seconds [14]. In the case of high dose applications, for example prostate, saving millimeters in the posterior margin could be clinically beneficial for the rectum , especially at dose levels exceeding 75 Gy [15]. The reduction of the posterior margin of the planning target volume results in a reduction of the dose applied to the rectum and makes dose escalation feasible. On the anterior direction, a reduction of the margin would also reduce the dose to the pubic symphysis, which is in close proximity to the PTV.

The inter- and intra-observer deviations were greater or similar to the variance of the population formed by deviations in contouring for the elastic region in a very large portion of the prostate. Furthermore, elastic registration based contour propagation performed better than manual re-contouring of the prostate in all three spatial directions in respect to the maximal deviation. The maximal deviation could be reduced using the elastic registration in comparison to the inter-observer variability. The largest deviation was observed in the superior-inferior direction. This is probably due to the CT resolution in the superior-inferior direction, which was 5 mm in comparison to 0.8301 mm and 0.9766 mm for the two patients in the left-right and anterior-posterior directions. By reducing the slice thickness, a decrease of the mean and maximal deviation could be achieved for the affine and elastic registration.

The affine and rigid registration failed in regions were inter and intra-observer variability was small ($<$1 mm). In these regions the standard deviation of the affine and rigid registration was larger by less than 0.3 mm (Table 1). This difference was significant but not clinically relevant since we are bellow the set-up accuracy.

The elastic registration performed better than the affine adjustment. This improvement will have a direct impact when on-line re-optimization is used [9]. Indeed, an improvement of the accuracy of the registration will have a direct impact on the margins for the target and therefore, on the dose to the organ at risks.

1.6 Conclusion

HERA-based non-rigid prostate volume reassessment using repetitive CT during radiotherapy for the purpose of position verification, target volume adjustment and on-line plane re-optimization allows the clinician to minimize PTV margins. Elastic target volume propagation is a feasible and attractive strategy which merits clinical implementation in the treatment workflow and verification of its utility for the purpose of adaptive RT planning.

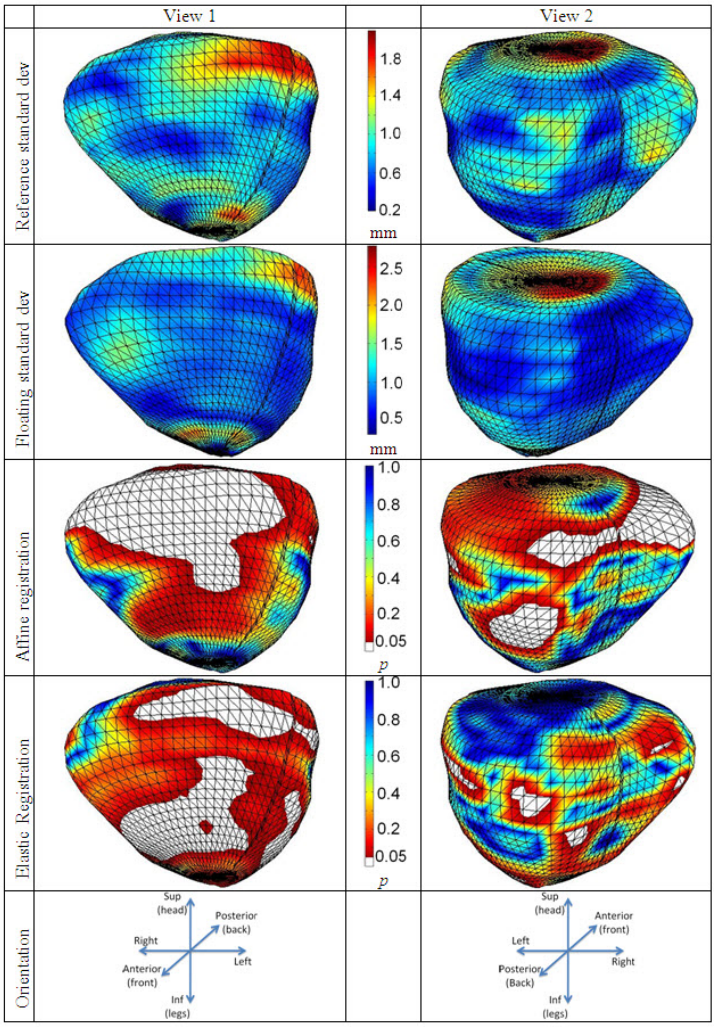

Figure 1.3: Contour propagation versus inter-observer variability. The surface distribution of the inter-observer variability, defined as standard deviation of the segmentations done by 5 doctors at 30 Gy (the first row) and on the floating data at the time prior to treatment (the second row). The distance are represented in mm. The distribution of the p-values onto the prostate after affine (the third row) and elastic (the fourth row). The white parts are marking the regions where the contour propagation failed.

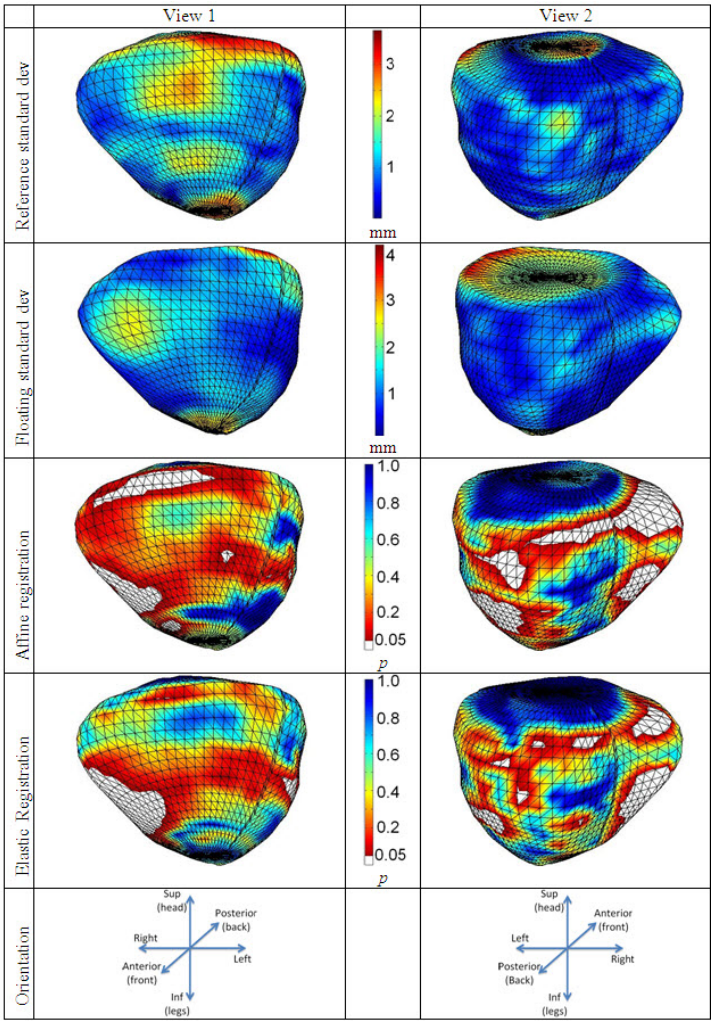

Figure 1.4: Contour propagation versus intra-observer variability. The first two rows depict the intra-observer variability onto the currently analyzed data (CT performed after 30 Gy) and onto the planning data (CT performed). The following two rows depict the p-values distributed on the average surface of the prostate. The white parts represent the regions where the standard deviations of the intra-observer variability is smaller than the propagated variability.

Bibliography

[1] Y Wang, JA Efstathiou, GC Sharp, HM Lu, IF Ciernik, and AV Trofimov. *Evaluation of the dosimetric impact of interfractional anatomical variations on prostate proton therapy using daily in-room CT images.* Med Phys **38**(8), 4623–4633 (2011)

[2] PA Kupelian, KM Langen, TR Willoughby, and et al. *Image-guided radiotherapy for localized prostate cancer: treating a moving target.* Semin Radiat Oncol **18**, 58–66 (2008)

[3] KM Langen, TR Willoughby, Meeks SL, and et al. *Observations on real-time prostate gland motion using electromagnetic tracking.* Int J Radiat Oncol Biol Phys **71**, 1084–1090 (2008)

[4] IF Ciernik, BG Baumert, P Egli, and et al. *On-line correction of beam portals in the treatment of prostate cancer using an endorectal balloon device.* Radiother Oncol **65**, 39–45 (2002)

[5] RA Linden, PR Weiner, LG Gomella, and et al. *Technique of outpatient placement of intraprostatic fiducial markers before external beam radiotherapy.* Urology **73**, 881–886 (2009)

[6] S Wachter, N Gerstner, D Dorner, and et al. *The influence of a rectal balloon tube as internal immobilization device on variations of volumes and dose-volume histograms during treatment course of conformal radiotherapy for prostate cancer.* Int J Radiat Oncol Biol Phys **52**, 91–100 (2002)

[7] DA Kuban, L Dong, R Cheung, and et al. *Ultrasound-based localization.* Semin Radiat Oncol **15**, 180–191 (2005)

[8] A Andronache, M von Siebenthal, G Szekely, and P Cattin. *Non-rigid registration of multi-modal images using both mutual information and cross-correlation.* Med Image Anal **12**(1), 3–15 (2008)

[9] QJ Wu, D Thongphiew, Z Wang, and et al. *On-line re-optimization of prostate IMRT plans for adaptive radiation therapy.* Phys Med Biol **53**, 673–691 (2008)

[10] Y Xie, M Chao, P Lee, and et al. *Feature-based rectal contour propagation from planning CT to cone beam CT.* Med Phys **35**, 4450–4459 (2008)

[11] H Wang, AS Garden, L Zhang, and et al. *Performance evaluation of automatic anatomy segmentation algorithm on repeat or four-dimensional computed tomography images using deformable image registration method.* Int J Radiat Oncol Biol Phys **72**, 210–219 (2008)

[12] WY Song, E Wong, GS Bauman, and et al. *Dosimetric evaluation of daily rigid and nonrigid geometric correction strategies during on-line image-guided radiation therapy (IGRT) of prostate cancer.* Med Phys **34**, 352–365 (2007)

[13] Q Wu, G Ivaldi, J Liang, and et al. *Geometric and dosimetric evaluations of an online image-guidance strategy for 3D-CRT of prostate cancer.* Int J Radiat Oncol Biol Phys **64**, 1596–1609 (2006)

[14] W Curtis, M Khan, Magnelli A, and et al. *Relationship of Imaging Frequency and Planning Margin to Account for Intrafraction Prostate Motion: Analysis Based on Real-Time Monitoring Data.* Int J Radiat Oncol Biol Phys **85**, 700–706 (2013)

[15] M Zhang, V Moiseenko, and M Liu. *PTV margin for dose escalated radiation therapy of prostate cancer with daily on-line realignment using internal fiducial markers: Monte Carlo approach and dose population histogram (DPH) analysis.* J Appl Clin Med Phys **7**(2), 38–49 (2006)